MINIMIZING RESIDUAL STRESSES IN MOLDED PARTS

by

MING JAW LIOU

B.S., Taiwan National University
(1978)
M.S., Massachusetts Institute of Technology
(1984)

SUBMITTED TO THE DEPARTMENT OF
MECHANICAL ENGINEERING IN PARTIAL
FULFILLMENT OF THE REQUIREMENTS FOR THE
DEGREE OF

DOCTOR OF PHILOSOPHY

IN MECHANICAL ENGINEERING

at the

MASSACHUSETTS INSTITUTE OF TECHNOLOGY

May 1987

Signature of Author _____
Department of Mechanical Engineering
May 1, 1987

Certified by _____
Prof. Nam P. Suh
Thesis Supervisor

Accepted by _____
Prof. A. A. Sonin
Chairman, Department Graduate Committee

MINIMIZING RESIDUAL STRESSES
IN MOLDED PARTS

by

MING JAW LIOU

Submitted to the Department of Mechanical Engineering on May 1, 1987 in partial fulfillment of the requirements for the degree of DOCTOR OF PHILOSOPHY IN MECHANICAL ENGINEERING.

Abstract

Means of minimizing the flow-induced and thermally-induced residual stresses in injection molded parts through optimization of the thermal history of the process are presented. Two approaches to residual stress minimization have been studied: the use of a passive insulation layer and the active control of the surface temperature. The passive insulation layer prevents the polymer melt from freezing during filling of the mold and allows the flow-induced stresses to relax after filling. The cavity surface attains high temperature during filling which subsequently cools down to low temperature due to heat transfer to the mold. The criteria for the optimal thermal properties and the required thickness of the layer are presented. A numerical simulation model of non-isothermal filling and cooling of viscoelastic materials has been developed to understand the molding process and evaluate this approach. This model predicts the stress development and relaxation in the molding cycle. Both simulation and experimental results show that the final stresses in the molded parts can be reduced by at least 40% with the use of insulation layer. The second approach, an active control of the surface temperature, is to find an optimal thermal history within a specified time period for minimizing residual thermal stresses in viscoelastic materials. Both free and constrained plates with temperature gradient across the thickness are investigated. The surface temperature of each plate is chosen as the control variable while the temperature at every node across the thickness is chosen as the state variable. Euler-Lagrange equations are solved with first gradient algorithm to iterate the solutions. Physical insights are provided for the optimal cooling paths predicted theoretically.

Thesis Supervisor: Prof. Nam P. Suh
Title: Professor of Mechanical Engineering

Acknowledgement

My thanks first go to Professor Nam P. Suh, my thesis advisor, for his support, encouragement and technical guidance through my stay at MIT. From him I learned the commitment to innovation. To him I give my highest appreciation for guiding me through my intellectual and professional development. I also appreciate his commitment to advising students on weekends while on leave from MIT as the Assistant Director of Engineering at National Science Foundation. I am indebted to other members of my thesis committee: Professor R. C. Armstrong and Professor T. G. Gutowski for their valuable suggestions which have been of great benefit to me.

This research was sponsored by the MIT-Industry Polymer Processing Program. The sponsors of the program are Boeing Commercial Aircraft Co., C. R. Industries, Hysol Division/Dexter Co., E. I. DuPont de Numour and Co., Eastman Kodak Co., Intelitec Co., Kraft Co., Lord Co., Norton Performance Plastics, Martin Marietta Co. and Xerox Co.. I am grateful for their support and interest. Special thanks go to Mr. Gordon Brown, Mr. Edward Morrison, Mr. Darryl Miller, Mr. Ernie Kirkpatrick, Mr. Robert Jones and Dr. Jehuda Greener, all of Eastman Kodak Co., for their interest in my research and support on the experiments.

I am also grateful to Dr. Archie Bice of DuPont Co. for his interest in this research. Mr. Ralph Cross, Mr. John Border and Mr. Russell Ford of Intelitec Co. deserve my appreciation for their support in the early stage of this research.

All of my colleagues around the laboratory should receive my thanks for sharing their ideas with me. Special thanks go to Hong Tian for the discussion on mathematics. Wesley Cobb, LMPVAX system manager, is always helpful in solving

the problems of data and word processing. I also want to thank Ken Wright, karl Seeler, Dae Eun Kim and Louis Bonhomme for proofreading this thesis. Avi Benatar, Neil Goldfine, Larry Oslund, Algis Plioplys, Karl Seeler and Ken Wright are always there to share the author's ups and downs throughout the course of this study. Thanks also go to Tony Rogowski and Wendy Soll for allowing the author to use their computer-controlled hot press.

I am forever indebted to my parents who are tireless supporters of all my endeavors. I wish they are always happy and healthy. My wife, Chilon, and son, Yihong, deserve my thanks for their patience, encouragement and love.

Table of Contents

List of Figures

List of Tables

Nomenclature

b	Half thickness of the flow channel
c	Specific heat
$\mathbf{c}_k$	Elastic strain tensor in the "k"th relaxation mode
$\overset{\nabla}{\mathbf{c}}_k$	Jaumann tensor derivative with respect to time
C'	Stress-optic coefficient
$\mathbf{e}$	Rate of strain tensor
e_{ij}	Deviatoric components of strain tensor
$\mathbf{e}_k^p$	Irreversible rate of strain tensor
G'	Storage modulus
G''	Loss modulus
$(i-1)$	The $(i-1)th$ iteration
$I_{k,1}$, $I_{k,2}$	$\mathbf{c}_k$'s basic invariants
k	Thermal conductivity
l	Half thickness of the plate
Δn_1	Birefringence in 1-2 plane
Δn_2	Birefringence in 2-3 plane
Δn_3	Birefringence in 1-3 plane
N	Number of relaxation modes
p	Isotropic pressure

Q	Volumeric flow rate
s $(0<s<1)$	Dimensionless rheological parameter
s_{ij}	Deviatoric components of stress tensor
t	Time
t_f	Final time
T	Temperature
T_c	Temperature of coolant
T_g	Glass transition temperature of polymer
T_o	Initial temperature
T_w	Surface temperature
u	Velocity in x direction
W	Elastic potential
W_k	Elastic potential in the "k"th relaxation mode
x,1	Coordinate in flow direction
y,2	Coordinate in gapwise direction
z,3	Coordinate in width direction
α	Thermal diffusivity
α_o	Coefficient of thermal expansion
$\dot{\gamma}$	Strain rate
δ	Unit tensor
δ_{ij}	Kronecker delta
ϵ	Strain tensor

ϵ_{ij}	Components of strain tensor
$\frac{1}{3}\epsilon_{kk}$	Dilatational strain
η_k	Viscosity in the "k" relaxation mode
η_o	Zero-shear-rate viscosity
θ	Temperature, $\theta = T - T_o$
θ_g	Glass transition temperature, $\theta_g = T_g - T_o$
θ_k	Relaxation time constant in the "k"th relaxation mode
θ_w	Surface temperature, $\theta_w = T_w - T_o$
μ_k	Shear modulus in the "k"th relaxation mode
ξ	Reduced time
ρ	Density
σ	Stress tensor
σ_{ij}	Components of stress tensor
$\frac{1}{3}\sigma_{kk}$	Hydrostatic or mean normal stress
ϕ	Time-temperature shift factor
ω	Frequency
ω	Vorticity tensor

Chapter 1

Introduction

1.1 Injection Molding Process

Injection molding is a process in which a polymer melt is forced into a closed mold where it solidifies under pressure in the shape of the mold cavity. Then the mold is opened and the molded part is ejected. The resulting parts are usually finished parts which require no further work before being used as final products. Although thermoplastic injection molding is the subject of this thesis, the techniques discussed can also be applied to other materials as well as other molding processes.

An injection molding machine consists of two parts: an injection unit to melt and inject polymer into the mold, and a clamp unit to hold the mold closed against the pressure of injection and subsequently open the mold for part removal. There are various distinct design approaches used in both the injection and clamp units. The mechanical design of the clamp unit is a major topic in itself. This thesis considers only the filling and cooling of the polymer in the mold. A comprehensive review on the design of an injection molding machine is given by Rubin [30].

1.2 Problem Statement

The flow of polymer during mold filling produces stresses in the parts. These stresses are greatest near the surface of the part where the polymer starts to freeze immediately after it comes in contact with the cavity surface and thus cannot relax. The relaxation time constant increases with decreasing temperature. For amorphous polymer, relaxation is almost impossible when the temperature is below

its glass transition point.

In addition to the flow-induced residual stresses, there are also thermally-induced stresses caused by non-uniform cooling. During the cooling process, a temperature gradient develops across the thickness of a part due to the heat conduction from the plastic to the mold. When the part has a varying thickness, a gradient also develops perpendicular to the thickness direction. The temperature gradient results in differential thermal contraction and stress relaxation, which in turn lead to thermal stresses inside the part [27, 23].

Both flow-induced and thermally-induced residual stresses inside a part result dimensional instability over the life time of the part. For high precision optical parts, dimensional accuracy and stability on the suface are particularly critical. Moreover, non-uniform stresses inside optical parts produce differential optical indices.

The ideal condition in injection molding is to have a hot mold during the filling stage and a cold mold for cooling. Hot mold during the filling can eliminate short shot and weld lines and minimize flow-induced stresses in molded parts. Subsequent to the complete filling of the mold, cold mold is required so that the parts can quickly pass through the glass transition temperature and be ejected from the mold. However, it takes a very long time for the whole mold to go through this thermal cycle because of its huge thermal inertia. This thermal cycling would also reduce the life of the mold.

1.3 Research Goal

The goal of the research presented in this thesis is to minimize flow-induced and thermally-induced residual stresses in injection molded parts through optimization of the thermal history of the process. Two different approaches to residual stress minimization are studied in this thesis.

The first approach is to apply a passive insulation layer with low thermal inertia on the cavity surface. The outermost surface of this layer reaches a high temperature during the filling satge, which subsequently cools down upon futher cooling. This layer provides a hot cavity surface during the filling and a cold cavity surface during the cooling without heating the mold. The criteria for the optimal thermal properties and the required thickness of the layer are presented. A numerical simulation model of non-isothermal filling and cooling is developed to evaluate this approach. Experiments are also done to compare the residual stresses and cooling times for two cases: with the passive layer and without the passive layer. The experimental results are also compared with the theoretical predictions.

The second approach, an active control of the surface temperature, is to find an optimal thermal history which minimize thermally-induced stresses in viscoelastic materials. Both free and constrained plates with temperature gradient across the thickness are studied. The surface temperature of each plate is chosen as the control variable while the temperature at every node across the thickness represents the state variable. Euler-Lagrange equations are solved with first gradient numerical iteration to obtain the optimal cooling profiles. Physical insights are provided for the optimal cooling paths predicted theoretically.

Chapter 2

Fundamentals of Injection Molding Process

2.1 Introduction

The injection molding process begins with feeding polymer pellets from the hopper to the screw for mixing, heating and transport to the mold. As the screw rotates to transport the polymer forward, the mechanical shear of this action provides viscous heating to further melt the polymer in addition to the electric heater surrounding the barrel. Mixing and heating occurs simultaneously between screw flights. The polymer melt finally passes through the screw tip non-return valve.

Accumulation of polymer melt in front of the rotating screw causes the screw to displace toward the rear. Rotation, accumulation and backward displacement continue until the desired quantity of melt is available for injection. Then the screw is hydraulically activated for forward injection, while the screw tip non-return valve closes to prevent material back-flow along the screw. The screw tip functions as an injection piston, forcing polymer melt into the mold through the nozzle.

The melt then flows through the mold sprue, runner and gate into the mold cavity. The sprue forms the overall entrance into the mold. It has a generous taper to facilitate removal of polymer, and a streamlined channel to minimize the resistance to flow.

The runner system is the connection between the sprue and the gate. It should be large enough to provide rapid filling with minimum pressure loss. Although the runners can be reground and reused, the length of the runner should

be kept to a minimum. A hot runner system, where the polymer in the runner is prevented from solidifying by employing a heating unit around them in the mold, can also be used to achieve material saving and faster cycle.

The gate controls the flow of polymer melt into the cavity. Its size should be small enough so that the runners can be separated from the molded parts easily, and the gate can solidify after the filling. However, a small gate creates large shear strains in the polymer melt, and consequently increases the residual stresses in molded parts. A fan gate can be used if the stress level in the molded parts is of concern. In molds with multiple cavities, gates and runners also serve to balance the flow so that all cavities fill simultaneously. The location of the gate is also important since it affects the formation of weld lines in molded parts.

2.2 Characteristics of Injection Molded Parts

One of the problems in the injection molding process is that the filling process is coupled with the cooling process [17]. The cooling of the injected polymer melt occurs before the filling is completed. Therefore, every point in the molded part experiences a different thermo-mechanical history. This variations combined the coupled nature of injection molding processes create anisotropic and nonhomogeneous characteristics in molded parts, which degrade the quality of the parts. These are caused by the non-uniform molecular orientation and residual stresses inside the parts.

The molecular orientation and residual stresses inside injection molded parts have become the focal point of many experimental and theoretical investigations. Tadmor [33] presented two major sources of orientation in injection molding: the elongational flow in the melt front and the shear flow behind it. He then proposed a semiquantitative model to determine the the distribution of molecular orientation in injection molded amorphous polymer. He also concluded that the orientation in

the surface skin is caused by the steady elongational flow in the advancing front, whereas the orientation in the core region is related to the shear flow behind the front, between two solidifying layers.

Dietz, White and Clark [6] developed a simplified model for the orientation development and relaxation in injection molding. They separated the state of the polymer melt in the cavity into an isothermal core region and two solidified layers on the walls. An isothermal power law model was used to calculate the shear stress in the core region. A linear viscoelastic Maxwell model was utilized to study the stress relaxation in the cooling stage.

Greener and Pearson [8] followed this model but used the viscoelastic constitutive equation of Marrucci [24] to predict the residual stresses in injection molded parts. He attributed the non-zero birefringence along the midplane of the molded part to thermal stresses, which were induced by non-uniform cooling.

A more rigorous model for predicting stress relaxation was developed by Isayev and Hieber [14] using Leonov constitutive equation. This work will be discussed in more detail in Chapter 3.

2.3 Processing Parameters

In the injection molding process, a hot polymer melt is injected into a cold cavity. The melt and cavity temperature as well as the flow rate and injection pressure determine the thermo-mechanical history of the molded part. The mechanical properties of injection molded parts are strongly affected by the thermo-mechanical history of the processes. Due to the complexity of the process, most of the studies in the effects of processing conditions on the final properties of the molded parts rely on empirical investigations.

Siegmann et al. [32] conducted a comprehensive study on the influence of

melt temperature, mold temperature, injection rate and injection pressure on the residual stresses of molded parts. They found that stress in the surface region decreases with increasing melt temperature in zones far away from the gate. This was attributed to the fact that the stress relaxation in polymer increases as the melt temperature increases. However, the polymer melt may degrade if the processing temperature is too high.

In that report, increasing mold temperature was found to decrease the magnitude for compressive stress on the surface. As the mold temperature approached T_g, very low value of residual stress was measured. The increasing mold temperature reduced the amount of frozen-in stresses and allowed the flow-induced stresses to relax. At one extreme, Johnson [15] reported that relatively strain-free parts could be obtained by heating the mold to the polymer melt temperature. It should be noted that if the mold temperature is above T_g, the parts will not solidify and their dimensions will not stabilize.

Menges and Wubken [25] reported similar findings in which frozen orientation was reduced by increasing melt and mold temperature since these have the same effects on relaxing the orientation. They also found that an increase in injection rate led to slightly higher surface orientation while the internal orientation was significantly reduced. In terms of the thickness of the oriented layer, Isayev [13] found that increasing the flow rate substantially decreased the thickness of the oriented layer. These findings agree with each other because high flow rate reduces the filling time, and therefore reduces the thickness of solidified layer during the filling process. Furthermore, higher strains which resulted from higher injection rate, led to faster relaxation since the stress relaxation is also strain-dependent.

In order to mold a high quality part with minimum orientation, the processing parameters may be adjusted to achieve the goal. However, there are

limits to the adjustable ranges of processing parameters. Moreover, the compromise among minimum orientation, cycle time and dimensional stability should also be considered. An optimal processing condition should be developed to improve the part quality without reducing productivity.

2.4 Process Simulation

The process of injection molding involves flow, heat transfer and the mechanics of viscoelastic materials. The complexity of the process has made analytical solutions so difficult that numerical simulations of the process have been used to understand the details of the process.

Extensive studies [10, 16, 37, 35, 19] have focused on the filling process to calculate the thermal and flow fields of this unsteady flow as well as to predict the positions of melt front and the required injection pressure. The power law model was the most commonly used constitutive equation. This model is strain-rate and temperature dependent but cannot account for the viscoelastic characteristics of polymer.

The Cornell group [5] developed a two dimensional mold filling program which utilized the generalized Hele-Shaw flow model. The position of the melt front was presented as function of time, and therefore the location of weld lines, if any, could be predicted. They employed the finite element method in the planar coordinates and the finite difference method in the gapwise direction. The power law material model was also used. The advance of melt front in each time step, however, required the user's judgement and correction.

Kim [18] contributed to that program with a automatic melt front mesh generation feature which used a so called boundary-pressure-reflection scheme to determine the moving melt front automatically.

Few researchers have attempted modeling of the packing and cooling processes. This could be attributed to the complexity of considering the state equation and viscoelastic material model. However, these processes are important if the properties of molded parts are to be predicted. Unfortunately, the studies that have been conducted [16, 4, 19, 7] are primarily concerned with the pressure field in the packing and cooling stages. To the best of the author's knowledge, the effects of packing on the final stress distributions in the molded parts have not been studied. This is probably because of the complexity of the phenomena, which include the state equation, the viscoelastic material model and solidification.

The effects of cooling on the residual stresses have been investigated using the quenching of viscoelastic materials per se [27, 23, 22] instead of the cooling process in injection molding. Nevertheless stress relaxation models in the cooling have been reported [14, 17] which considered the cooling only as a stress relaxation process by neglecting the thermally-induced stresses. Thermally-induced stresses are caused by temperature gradient during the cooling. Others [5, 8] approximated the quenching as the cooling process in injection molding.

Chapter 3

Passive Insulation Layer for Stress Relaxation

3.1 Introduction

The flow of polymer during mold filling in injection molding produces stresses in the parts. The stresses near the surface of the part, where the polymer starts to freeze immediately after it comes in contact with the cavity surface, cannot relax. The filling and the cooling processes are coupled. The relaxation time constant increases with decreasing temperature. For amorphous polymer, relaxation is nearly impossible when the temperature is below its glass transition point.

The ideal condition in injection molding is to have a hot mold during filling and a cold mold during cooling in order to decouple the filling and the cooling processes. High mold temperature during the filling eliminates short shots, weld lines and flow-induced residual stresses in molded parts. Low mold temperature during cooling is required so that the parts can quickly pass through glass transition temperature before they can be ejected from the mold. However, if the entire mold is to be heated and cooled, it will take tens of minutes for the thermal cycle to complete and the life of mold would also be reduced.

A low thermal inertia mold, which could provide rapid change of temperature on the cavity surface by a heated layer on the cavity surface without changing the temperature of the whole mold, was developed in MIT-Industry Polymer Processing Program [17] and Intelitec Corporation. The flow-induced stresses relax if the cavity surface is heated to the same temperature as the entering polymer melt during the filling process. However, one of the difficulties in that technique was the thermal stresses introduced at the interface between the heated layer and the mold due to the large temperature gradient. Furthermore, uniform heating of the layer

was hard to achieve in 3-D complex cavity surface.

Another technique for reducing flow-induced and thermally-induced residual stresses without external heating is to apply a passive insulation layer with low thermal inertia on the cavity surface. The interface temperature between the incoming polymer melt and the mold during filling will rise according to the particular thermal properties of this layer. The heat conduction from the polymer to the mold is delayed for few seconds which are long enough for filling and subsequent stress relaxation. Therefore, polymer does not freeze during the filling, allowing the flow-induced stresses to relax prior to solidification.

The thermally-induced stresses can also be reduced since the temperature gradient in the polymer will be lowered by this layer. This layer provides a hot cavity surface during filling and a cold cavity surface during cooling without having to heat or cool the whole mold.

Two simple criteria for the optimal thermal properties and required thickness of the layer are presented. A numerical simulation model of non-isothermal filling and cooling was developed. This model predicts the stress development and relaxation in the molding cycle. The effects of this layer on the residual stresses of the molded parts can also be evaluated with this model. Experimental results showed that the birefringence in the molded parts was reduced by 40% with this layer.

3.2 Thermal Criteria

Two criteria have been identified, based on the fundamental principles of heat conduction, for the optimal thermal properties and the required thickness of the layer that give the best performance. They give guidelines for selecting the materials and thickness of the layer.

3.2.1 Thermal Properties of the Layer

In order to raise the interface temperature between the polymer flow and the cavity surface above the glass transition temperature for a few seconds after the filling process, the thermal properties of the layer should be selected as follows.

When two semi-infinite parts with different initial temperatures T_1 and T_2 come into contact, the temperature T_0 at the interface is governed by

$$\frac{T_1-T_0}{T_0-T_2}=\left(\frac{(k\rho c)_2}{(k\rho c)_1}\right)^{1/2}, \tag{3.1}$$

where

$k =$ *thermal conductivity,*
$\rho =$ *density,*
$c =$ *specific heat.*

The interface temperature increases with decreasing ($k\rho c$) of the insulation layer. T_0 is not a function of time for two semi-infinite parts. The derivation of equation (3.1) is shown in Appendix B.

In situations where the plastic part and the insulation layer have finite thicknesses, Equation (3.1) is still valid as long as the outside surface temperatures of the two parts are not affected by the contact. This fact will be used as the second criterion to estimate the required thickness of the layer. From equation (3.1), the value of ($k\rho c$) for the insulation layer can be determined if T_0 is specified, since T_1, T_2 and ($k\rho c$) of the polymer are known.

3.2.2 Thickness of the Layer

For equation (3.1) to be valid, the insulation layer should be thick enough so that the heat does not penetrate the layer within a specified time period. The

temperature history of a semi-infinite solid with step change in surface temperature from T_2 to T_o is given [12] by

$$\frac{T - T_2}{T_o - T_2} = erfc\left(\frac{z}{2\sqrt{\alpha t}}\right), \tag{3.2}$$

where
$erfc(u) = 1 - erf(u)$ *is the complementary error function,*
$z =$ *distance from surface,*
$\alpha = \dfrac{k}{\rho c} =$ *thermal diffusivity,*
$t =$ *time.*

By knowing the thermal properties of the layer from equation (3.1), the required thickness of the layer can be calculated if the time to keep the interface temperature well above T_g after filling for stress relaxation is specified.

3.3 Thermal Analyses

After calculating the required thermal properties and thickness of the layer based on the thermal criteria, it is necessary to check if the increase of cycle time is within the acceptable range.

It is expected that the subsequent cooling would take longer than when the insulation layer is excluded. However, the percent of increase should not be large for two reasons. First, since the thermal conductivity of polymer is much lower than those of the layer and the mold, the cooling time must be dominated by the heat conduction inside the polymer.

Second, a steep temperature gradient develops within the layer for the first few seconds while the surface temperature of the part is kept well above T_g. Although the thermal conductivity of the layer is lower than that of the mold, the

heat flux through the layer should not decrease due to this high temperature gradient since heat flux is the product of thermal conductivity and temperature gradient. Therefore, the subsequent cooling would not be delayed too much.

Table 3-1 gives the values of interface temperature for different materials in contact with polystyrene. These values are obtained from equation (3.1). It is clear that the material which has the smallest $k\rho c$ gives the highest interface temperature. The values in Table 3-1 are the interface temperatures right after the contact occurs, and before heat has penetrated through the layer. A simple numerical simulation of conduction can give us the transient temperature profile even after heat has penetrated through the layer.

Figure 3-1 shows the transient temperature profile after hot polystyrene (240 ^{o}C) comes in contact with a cold steel mold (70 ^{o}C). It should be noted that the thicknesses of the different materials are not in scale in the figure. The surface temperature of the polystyrene drops to 89 ^{o}C, which is below its T_g of 100 ^{o}C, immediately after contacting with the steel mold. Therefore, the flow-induced orientation near the surface cannot relax. The total cooling time, defined as when the highest temperature inside the part passes through T_g, is 11 seconds.

The results for the case where a Teflon layer is applied on the cavity surface are shown in Figure 3-2. The surface temperature of the polystyrene drops to 123 ^{o}C after the polymer and the layer come in contact, as predicted from the first thermal criterion and shown in Table 3-1. A typical filling time in injection molding process is about 0.5 seconds, at which the interface temperature is still kept at about 123 ^{o}C. Therefore, the flow-induced orientation will relax after the filling process.

In about 13 seconds, the highest temperature inside the part reaches T_g and the interface temperature is at 87 ^{o}C. This layer provides a hot cavity for the

	$(k\rho c)$ (CGS)	T_0 (°C)
Steel	3.73×10^{13}	89
Al_2O_3	9.01×10^{12}	105
Teflon	2.88×10^{12}	123
Styrene	6.10×10^{11}	155

Table 3-I: Interface Temperature for Different Materials in Contact with Styrene, $T_1 = 240$ °C, $T_2 = 70$ °C.

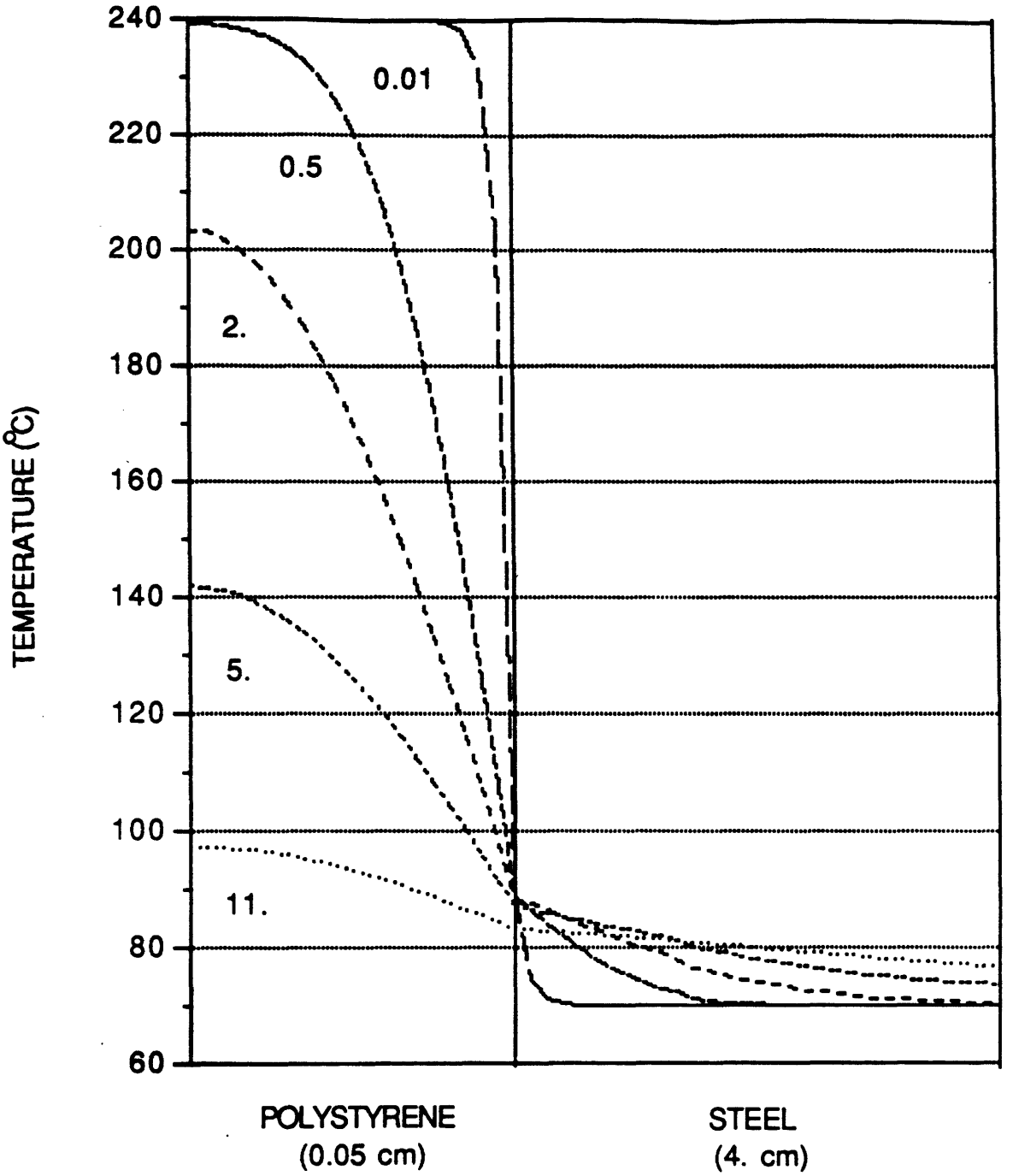

Figure 3-1: Transient Temperature Profile after a Hot Polystyrene Contacts with a Cold Steel Mold, 0.01 to 11 Seconds.

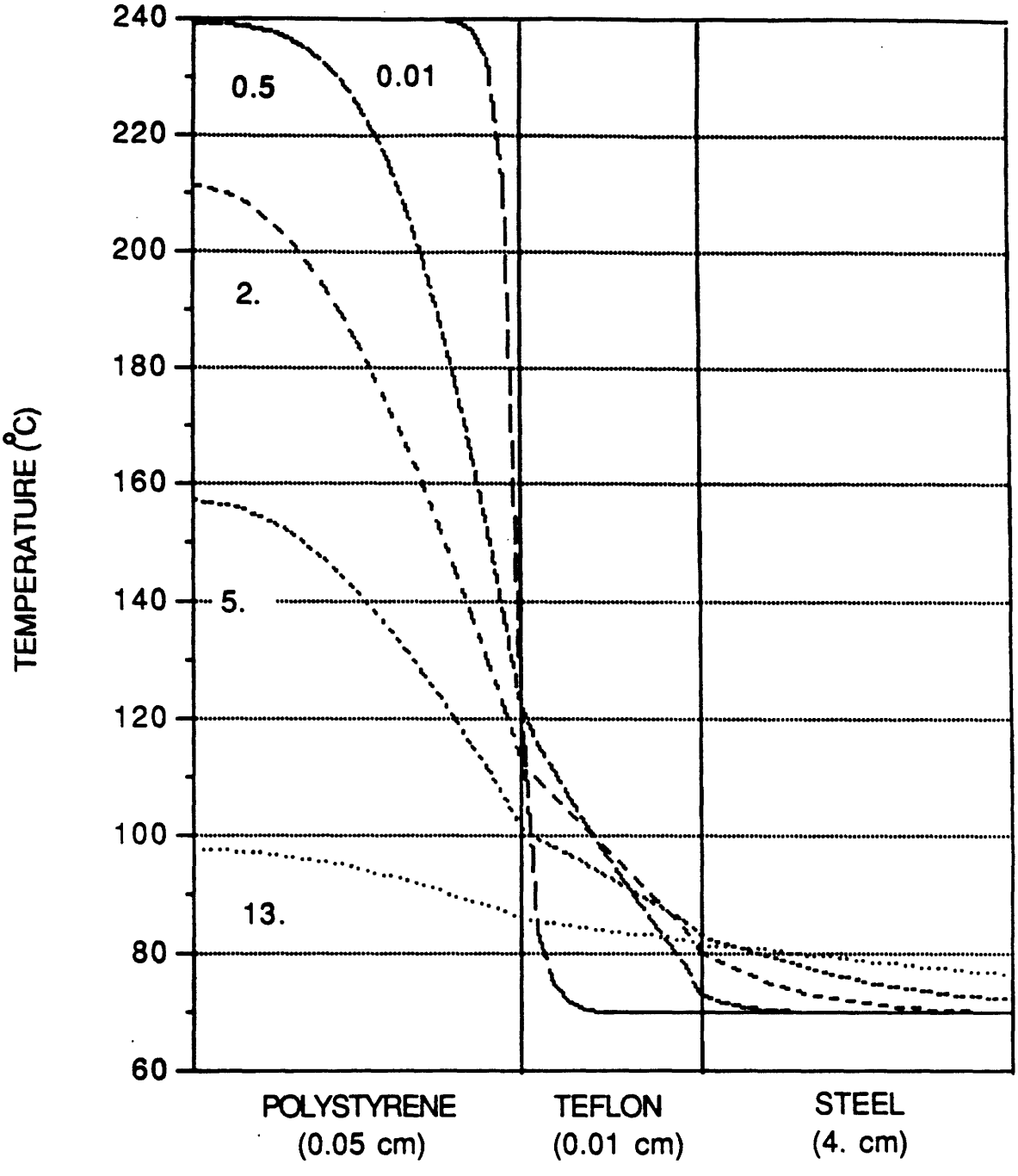

Figure 3-2: Transient Temperature Profile after a Hot Polystyrene Contacts with a Cold Teflon Layer on a Steel Cavity, 0.01 to 13 Seconds.

filling and a cold cavity for the cooling without having to heat or cool the whole mold. The polymer sees the mold temperature only at their interface. If the interface temperature is high, the polymer behaves as though subjected to a hot mold regardless of the temperature in the rest of the mold.

The objective of having an insulation layer with small $k\rho c$ on the cavity surface is to keep the polymer above T_g for a few seconds after the filling so that the flow-induced stresses can relax. The cooling time for this case is 13 seconds as compared to 11 seconds in the former case. The increase of cooling time is less than 20%, which is expected from the two reasons explained previously.

3.4 Stress Development and Relaxation

The thermal analyses in the last section were based on conduction only, which gave us an approximation of the transient temperature profile during the molding cycle. The influence of convection and viscous heating in polymer flow should also be considered since polymer melts, in general, have high viscosities. Moreover, a model to predict the stress development and relaxation in the molding cycle should also be developed in order to gain insights into the processes and evaluate the effects of this passive layer on the final stresses of molded parts. Filling and cooling in the injection molding process were simulated in order to understand how the stresses develop and relax in the molding cycle.

3.4.1 Constitutive Equations

A viscoelastic material model must be used in order to account for the stress relaxation in the polymer. The Leonov constitutive equations [21, 20], which were obtained from the methods of irreversible thermodynamics to describe the behavior of polymer in an arbitrary elastic state, were used. The constitutive equation may be expressed as

$$\sigma + p\,\delta = 2\,\eta_o\,s\,\mathbf{e} + 2\sum_{k=1}^{N}\,(W_{k,1}\mathbf{c}_k - \mathbf{c}_k^{-1}W_{k,2}),$$

(3.3)

$$\overset{\nabla}{\mathbf{c}_k} - \mathbf{c}_k(\mathbf{e} - \mathbf{e}_k^p) - (\mathbf{e} - \mathbf{e}_k^p)\,\mathbf{c}_k = 0,$$

(3.4)

where

$$\overset{\nabla}{\mathbf{c}_k} \equiv \dot{\mathbf{c}}_k = \omega\,\mathbf{c}_k - \mathbf{c}_k\,\omega,$$

(3.5)

$$\mathbf{e}_k^p = \frac{1}{2\mu_k\theta_k}\left[\left(\mathbf{c}_k - \frac{I_{k,1}}{3}\delta\right)W_{k,1}^s - \left(\mathbf{c}_k^{-1} - \frac{I_{k,2}}{3}\delta\right)W_{k,2}^s\right],$$

(3.6)

$$2W_k^s = W_k(I_{k,1},I_{k,2}) + W_k(I_{k,2},I_{k,1}),$$

(3.7)

$$W_{k,j} = \frac{\partial W_k}{\partial I_{k,j}}.$$

(3.8)

In these equations, σ is the stress tensor, p is the isotropic pressure, δ is the unit tensor, η_o is the zero-shear-rate viscosity, s $(0<s<1)$ is the dimensionless rheological parameter, $\mathbf{e}$ is the rate of strain tensor, $\mathbf{c}_k$ is the elastic strain tensor (the Finger measure) in the "k"th relaxation mode, $I_{k,1}$ and $I_{k,2}$ are $\mathbf{c}_k$'s basic invariants, $\overset{\nabla}{\mathbf{c}_k}$ is the Jaumann tensor derivative with respect to time, W is the elastic potential, W_k is the elastic potential in the "k"th relaxation mode, $\mathbf{e}_k^p$ is the irreversible rate of strain tensor, θ_k and η_k are relaxation time and viscosity in the

"k"th relaxation mode respectively. The shear modulus in the "k"th relaxation mode μ_k can be given as $2\mu_k = \eta_k/\theta_k$.

The rheological parameters θ_k and η_k can be determined by standard rheological measurements for a linear case. If not very large elastic deformation is considered, the classic statistic potential of the high-elasticity theory can be taken as the elastic potential W_k.

$$W_k = \mu_k(I_{k,1} - 3), \tag{3.9}$$

$$W_k^s = \frac{\mu_k}{2}(I_{k,1} + I_{k,2} - 6).$$

This material model with the considerations of temperature-dependent modulus, viscosity and relaxation time makes it possible to predict the stress development in unsteady, non-isothermal flow during filling and the non-isothermal stress relaxation during cooling.

3.4.2 Model Formulation

Isayev and Hieber [14] employed this constitutive equation for modelling both the filling and cooling in injection molding. They idealized the problem by considering a fully-developed Poiseuille-type polymer flow of uniform initial temperature. The wall temperature is then abruptly lowered to room temperature. The temperature field is determined by transient one-dimensional conduction. The flow field is subsequently calculated under constant flow rate with temperature-dependent viscoelastic properties.

They applied this idealized problem to the filling process of injection molding by assuming that the fields at t=0 correspond to the fields at the end of the channel while the fields at $t=t_{fill}$ is equivalent to the fields at the gate. They neglected the elongational flow and assumed a constant temperature in the

advancing melt front. Despite the simplifications, the prediction seemed to correlate with the experimental results very well.

In the present model, convection and viscous heating are included. The thermal aspect of the fountain flow is considered; the initial temperature assigned to the new melt front at every time step is based on the fountain flow field. As such, the initial temperature of the advancing melt front comes from the equilibrium temperature in the core region of previous melt front. The initial temperature of the melt front, from which the thermal field of the flow is calculated, plays an important role in the simulation because the stress field is affected strongly by the temperature-dependent viscoelastic properties. The objective of this filling and cooling model is to evaluate the idea of using the insulation layer for stress relaxation.

We consider here a model for the injection molding of a plate (Figure 3-3). The flow direction is shown by x or 1 while z or 2 represents the thickness direction. The polymer melt is initially at a uniform temperature T_o and is injected under constant flow rate into a mold cavity with the mold temperature at T_m. A thin insulation layer, also at T_m initially, on the cavity surface is used to control the thermal history of the molded parts for stress relaxation. A cooling channel inside the mold with constant coolant temperature draws the heat out of the mold continuously.

The kinematic matrices for the case of simple shear have the forms,

$$\mathbf{e} = \dot{\gamma}/2\begin{pmatrix} 0 & 1 & 0 \\ 1 & 0 & 0 \\ 0 & 0 & 0 \end{pmatrix}, \quad \omega = \dot{\gamma}/2\begin{pmatrix} 0 & -1 & 0 \\ 1 & 0 & 0 \\ 0 & 0 & 0 \end{pmatrix}, \tag{3.10}$$

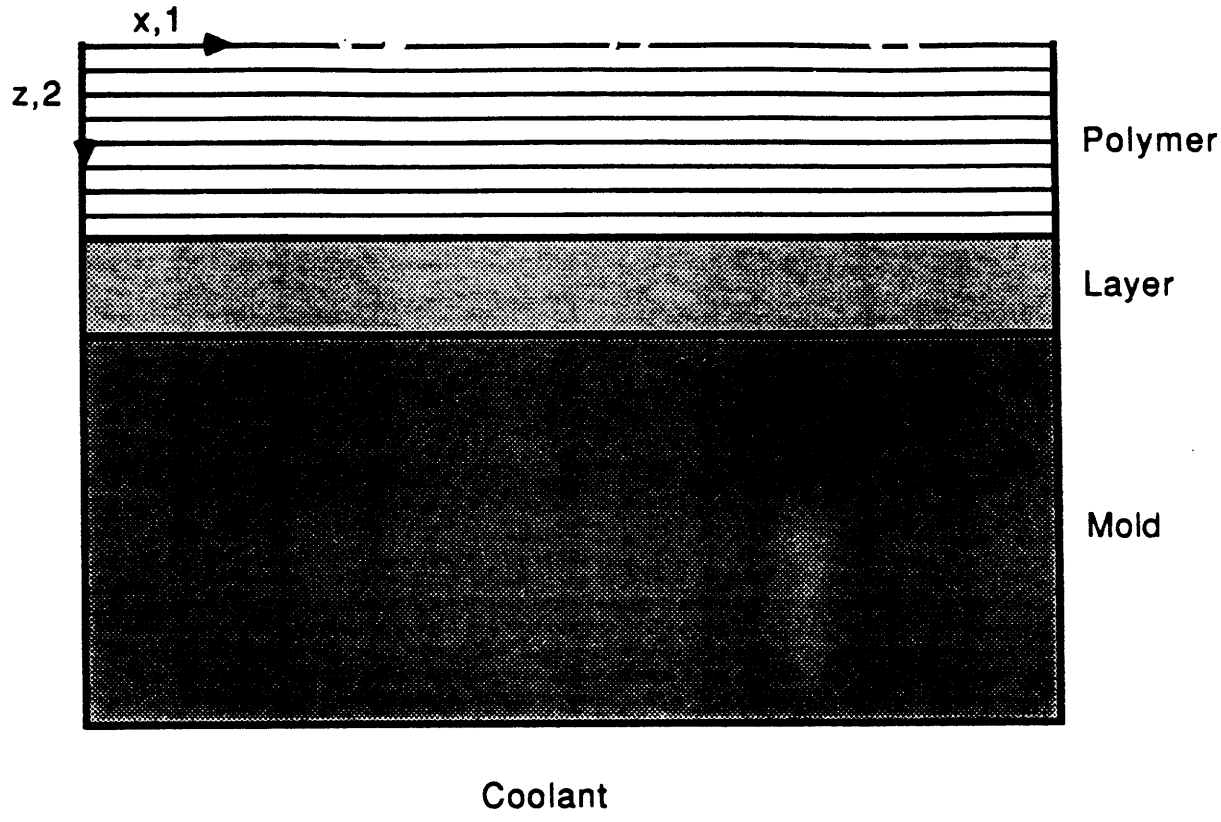

Figure 3-3: Schematic Diagram of the Injection Flow.

$$\mathbf{c}_k = \begin{pmatrix} c_{11}^{(k)} & c_{12}^{(k)} & 0 \\ c_{12}^{(k)} & c_{22}^{(k)} & 0 \\ 0 & 0 & 1 \end{pmatrix}, \quad \mathbf{c}_k^{-1} = \begin{pmatrix} c_{22}^{(k)} & -c_{12}^{(k)} & 0 \\ -c_{12}^{(k)} & c_{11}^{(k)} & 0 \\ 0 & 0 & 1 \end{pmatrix}. \tag{3.11}$$

and the basic invariants of c_k are given by

$$I_{k.1} = I_{k.2} = c_{11}^{(k)} + c_{22}^{(k)} + 1. \tag{3.12}$$

The incompressibility condition $det\ c_k = 1$ takes the following form,

$$c_{11}^{(k)} c_{22}^{(k)} = 1 + c_{12}^{(k)^2}. \tag{3.13}$$

In this particular case, equation (3.4) can then be shown as

$$\begin{aligned} &2\,\theta_k \frac{\partial c_{11}^{(k)}}{\partial t} + c_{11}^{(k)}\,(\,1 - c_{22}^{(k)}\,) + 2\,c_{12}^{(k)}\,(\,c_{12}^{(k)} - 2\,\dot{\gamma}\theta_k\,) = 0, \\ &2\,\theta_k \frac{\partial c_{12}^{(k)}}{\partial t} + c_{12}^{(k)}\,(\,c_{11}^{(k)} + c_{22}^{(k)}\,) - 2\,\dot{\gamma}\theta_k\,c_{22}^{(k)} = 0. \end{aligned} \tag{3.14}$$

The governing equations for flow and heat transfer are

$$\frac{\partial \sigma_{12}}{\partial z} - \frac{\partial p}{\partial x} = 0, \tag{3.15}$$

$$2\int_0^b u\,dz = Q, \tag{3.16}$$

$$\rho C_p \left(\frac{\partial T}{\partial t} + u\frac{\partial T}{\partial x}\right) = K\frac{\partial^2 T}{\partial z^2} + \sigma_{12}\,\dot{\gamma}. \tag{3.17}$$

The inertial terms are assumed to be very small and have been neglected from equation (3.15). However, the convection and viscous heating are taken into account in equation (3.17), which can also be used to calculate the heat conduction in the insulation layer and in the steel mold with $u = 0$ and $\dot{\gamma} = 0$. The boundary conditions of the velocity are

$$u = 0, \quad at\ z = b, \tag{3.18}$$

$$\frac{\partial u}{\partial z} = 0, \quad at\ z = 0. \tag{3.19}$$

The conditions of temperature are given by

$$\frac{\partial T}{\partial z} = 0, \quad at\ z = 0, \tag{3.20}$$

$$T = T_c, \quad at\ the\ cooling\ channel. \tag{3.21}$$

A cooling channel (Figure 3-3) inside the mold with constant coolant temperature draws the heat out of the mold continuously. It should be noted that the temperature on the cavity surface is not fixed, but is determined by the thermal properties $k\rho c$ of the material on the cavity surface. For this simple shear flow, equation (3.3) can be represented as

$$\sigma + p\,\delta = 2\,\eta_o\,s\,\mathbf{e} + 2\sum_{k=1}^{N} \mu_k\,\mathbf{c}_k. \tag{3.22}$$

where η_o is the zero-shear-rate viscosity which can be given as

$$\eta_o = \sum_{k=1}^{N} \frac{\eta_k}{(1-s)}, \quad (0 < s < 1). \tag{3.23}$$

and s is the dimensionless rheological parameter. Integrating equation (3.15) and using the fact that $\sigma_{12} = 0$, at $z = 0$, we arrive at

$$\sigma_{12} = \frac{\partial p}{\partial x} z. \tag{3.24}$$

From the shear component of equation (3.22) we can get

$$\frac{\partial p}{\partial x} z = 2 \sum_{k=1}^{N} \mu_k c_{12}^{(k)} + \eta_o s \dot{\gamma}. \tag{3.25}$$

In addition, integrating equation (3.16) by parts and making use of equation (3.18) give

$$-2 \int_0^b \dot{\gamma} z \, dz = Q. \tag{3.26}$$

As suggested by Isayev and Hieber [14], equations (3.13), (3.14), (3.26) and (3.25) are a system of 3N+2 equations for 3N+2 unknowns, which are $c_{11}^{(k)}$, $c_{12}^{(k)}$, $c_{22}^{(k)}$, $\dot{\gamma}$ and $\frac{\partial p}{\partial x}$. This is a set of nonlinear equations which can be solved by numerical iteration.

3.4.3 Numerical Procedure

Newton-Raphson iteration was used to solve this set of nonlinear equations [2]. The general form of nonlinear equations can be expressed as

$$\mathbf{F}(\mathbf{U}^*) = \mathbf{0}. \tag{3.27}$$

where $\mathbf{U}^*$ is the solution of the set of equations. Both $\mathbf{F}$ and $\mathbf{U}^*$ are in vector forms. Assume that the solution $\mathbf{U}_{t+\Delta t}^{(i-1)}$ of the (i-1)th iteration has been evaluated; then a Taylor series expansion gives

$$\mathbf{F}(\mathbf{U}^*) = \mathbf{F}(\mathbf{U}_{t+\Delta t}^{(i-1)}) + \left[\frac{\partial \mathbf{F}}{\partial \mathbf{U}}\right]_{\mathbf{U}_{t+\Delta t}^{(i-1)}} (\mathbf{U}^* - \mathbf{U}_{t+\Delta t}^{(i-1)}). \tag{3.28}$$

where higher-order terms are neglected. Equations (3.27) and (3.28) give

$$\left[\frac{\partial \mathbf{F}}{\partial \mathbf{U}}\right]_{\mathbf{U}_{t+\Delta t}^{(i-1)}} (\mathbf{U}^* - \mathbf{U}_{t+\Delta t}^{(i-1)}) = -\mathbf{F}(\mathbf{U}_{t+\Delta t}^{(i-1)}). \tag{3.29}$$

If we define

$$\begin{aligned} \Delta \mathbf{U}^{(i)} &\equiv (\mathbf{U}^* - \mathbf{U}_{t+\Delta t}^{(i-1)}), \\ \mathbf{K}_{t+\Delta t}^{(i-1)} &\equiv \left[\frac{\partial \mathbf{F}}{\partial \mathbf{U}}\right]_{\mathbf{U}_{t+\Delta t}^{(i-1)}}, \end{aligned} \tag{3.30}$$

where $\mathbf{K}_{t+\Delta t}^{(i-1)}$ is defined as the tangent matrix in iteration $(i-1)$, which is assumed to be nonsingular. Thus equation (3.29) can be rewritten as

$$\mathbf{K}_{t+\Delta t}^{(i-1)} \Delta \mathbf{U}^{(i)} = -\mathbf{F}(\mathbf{U}_{t+\Delta t}^{(i-1)}). \tag{3.31}$$

$\Delta \mathbf{U}^{(i)}$ can then be calculated from equation (3.31) by the algorithm based on Gauss elimination and is used to obtain the next approximate solution by

$${}^{t+\Delta t}\mathbf{U}^{(i)} = {}^{t+\Delta t}\mathbf{U}^{(i-1)} + \Delta \mathbf{U}^{(i)}. \tag{3.32}$$

Since an incremental analysis is performed with time step of size Δt, the initial conditions in this iteration are

$$\begin{aligned} \mathbf{K}_{t+\Delta t}^{(0)} &= \mathbf{K}_t, \\ \mathbf{F}_{t+\Delta t}^{(0)} &= \mathbf{F}_t, \\ \mathbf{U}_{t+\Delta t}^{(0)} &= \mathbf{U}_t. \end{aligned} \tag{3.33}$$

The iteration is continued until appropriate convergence criteria are satisfied.

The numerical procedure used in this model begins with the initial meshes at the entry of the cavity, representing the entering polymer melt. The initial conditions are the solutions of isothermal, steady-state, fully-developed flow between two parallel plates. The temperature distribution is first calculated by converting equation (3.17) into finite difference scheme. Subsequently, the values of θ_k, μ_k and λ_k are obtained from the temperature at every node.

The system of 3N+2 equations is then solved simultaneously for every node by Newton-Raphson numerical iteration. Since those equations involve integration across the thickness, iterations are needed not only at the solution of every node but also across the thickness direction as well. Iteration between solving equation (3.17) and the system of 3N+2 equations should also be performed because they are supposed to be solved simultaneously.

After the equilibrium conditions have been reached at every time step, the melt front marches forward one step in the x direction. The size of the step is determined by the flow rate. The initial temperature of the new melt front is taken from the core region of previous melt front at the last time step, which is suggested by the fountain flow phenomena [33].

The above procedure continues until the filling process is finished. The polymer then enters cooling period for stress relaxation. During this stage, equations (3.13) and (3.14) are simultaneously solved with $\dot{\gamma}=0$ for 3N unknown $c_{11}^{(k)}$, $c_{12}^{(k)}$ and $c_{22}^{(k)}$. The shear stress is then calculated by [14]

$$\sigma_{12} = 2 \sum_{k=1}^{N} \mu_k c_{12}^{(k)}. \tag{3.34}$$

The simulation is continued until the highest temperature in the polymer reaches

T_g assuming that no relaxation occurs at $T < T_g$.

The temperature dependence of θ_k is based on the W.L.F. equation [36],

$$\log(\phi(T)) = log\left(\frac{\theta_k(T)}{\theta_k(T_g)}\right) = \frac{-17.44\,(T-T_g)}{51.6+(T-T_g)}. \tag{3.35}$$

An amorphous polymer above T_g is in a rubber state. Rubber elasticity is distinguished by two basic characteristics: very large elastic strains and elastic moduli that increase with increasing temperature. The latter response is opposite to that found in other materials, including polymer below T_g.

Elastic moduli μ_k of amorphous polymers in the rubber state have a linear dependence of absolute temperature. This can be demonstrated [11] by simple application of the first and second laws of thermodynamics, which is presented in Appendix C. After determining the values of θ_k and μ_k, the value of viscosity can then be obtained through $\eta_k = 2\,\mu_k\,\theta_k$.

The rheological parameters η_k, θ_k and s are determined by standard dynamic measurements for a linear case. For small amplitude oscillation, the functions $G'(\omega)$ and $G''(\omega)$ in the Leonov model can be presented as [20]

$$G'(\omega) = \sum_{k=1}^{N} \frac{\eta_k \theta_k \omega^2}{1+\theta_k{}^2\omega^2},$$
$$G''(\omega) = \eta_o s\omega + \sum_{k=1}^{N} \frac{\eta_k \omega}{1+\theta_k{}^2\omega^2}. \tag{3.36}$$

The model constants have been evaluated [14] for polystyrene (Styron 678) with $N = 2$ as

$$\theta_1 = 0.80\ sec, \quad \eta_1 = 5.44 \cdot 10^4 \frac{gm}{cm\ sec},$$
$$s = 0.09, \tag{3.37}$$
$$\theta_2 = 0.027\ sec, \quad \eta_2 = 1.5 \cdot 10^4 \frac{gm}{cm\ sec}.$$

After all the unknowns are determined for every node at every time step, other variables can be calculated from the following formulae.

$$u = -\int_z^b \dot{\gamma} dz\ ,$$
$$\sigma_{12} = 2 \sum_{k=1}^{N} \mu_k c_{12}^{(k)} + \eta_o s \dot{\gamma},$$
$$\sigma_{11} - \sigma_{22} = 2 \sum_{k=1}^{N} \mu_k [\, c_{11}^{(k)} - c_{22}^{(k)} \,],$$
$$\sigma_{22} - \sigma_{33} = 2 \sum_{k=1}^{N} \mu_k [\, c_{22}^{(k)} - 1 \,], \tag{3.38}$$
$$\sigma_{11} - \sigma_{33} = 2 \sum_{k=1}^{N} \mu_k [\, c_{11}^{(k)} - 1 \,],$$
$$\Delta n_1 = C(T) [\, (\sigma_{11} - \sigma_{22})^2 + 4\sigma_{12}^2]^{1/2},$$
$$\Delta n_2 = C(T) [\, \sigma_{22} - \sigma_{33} \,],$$
$$\Delta n_3 = C(T) [\, \sigma_{11} - \sigma_{33} \,],$$

where C(T) is the stress-optic coefficient, and Δn_1, Δn_2 and Δn_3 are the birefringences in the 1-2, 2-3 and 1-3 planes respectively. White and coworkers [29, 6, 34] found that the stress-optic law is valid in polymer melt and the molecular orientation in polymeric parts is related to the level of principle stress difference at the time of vitrification. Therefore, a stress-optic coefficient with the appropriate value at the molten state near T_g should be used since the coefficient varies with temperature.

The Cornell group [5] suggested that frozen-in birefringence in injection molded parts of polystyrene is due to the effect of flow. However, the frozen-in stresses are due to both filling and cooling. This is because the stress-optic coefficient depends strongly on temperature. For polystyrene, the coefficient is large in the melt and decreases by an order of magnitude as the temperature passes through T_g.

3.4.4 Simulation Results

Figure 3-4 compares the temperature on the cavity surface along the flow channel at the end of filling with and without Teflon layer on the cavity surface. The Teflon layer prevents the polymer from freezing during filling by raising the cavity temperature to 125 ^{o}C. The flow-induced stresses can, therefore, relax after the filling. If the incoming polymer melt is to contact steel instead, the interface temperature decreases to 89 ^{o}C at which the flow-induced stresses near the surface cannot relax. These values are close to those calculated from the first thermal criterion shown in Table 3-1. The small deviations are the result of viscous heating, which can be clearly seen from the gapwise temperature distribution in Figure 3-5.

The gapwise temperature distributions for these two cases are presented in Figure 3-5. The polymer temperature near the surface are increased by the insulation layer to allow the stress relaxation after the filling. The effect of viscous heating creates a maximum temperature at a location away from the midplane. Indeed, the insulation layer promotes more viscous heating than the steel cavity since there is no viscous heating in the frozen region. The viscous heating therefore raises the interface temperature even higher, in addition to the contribution from the first thermal criterion.

Pressure distribution along the flow channel is given in Figure 3-6. Due to the higher temperature, and consequently lower viscosity, in the polymer melt of coated cavity, the pressure at the gate is significantly lower. This is advantageous

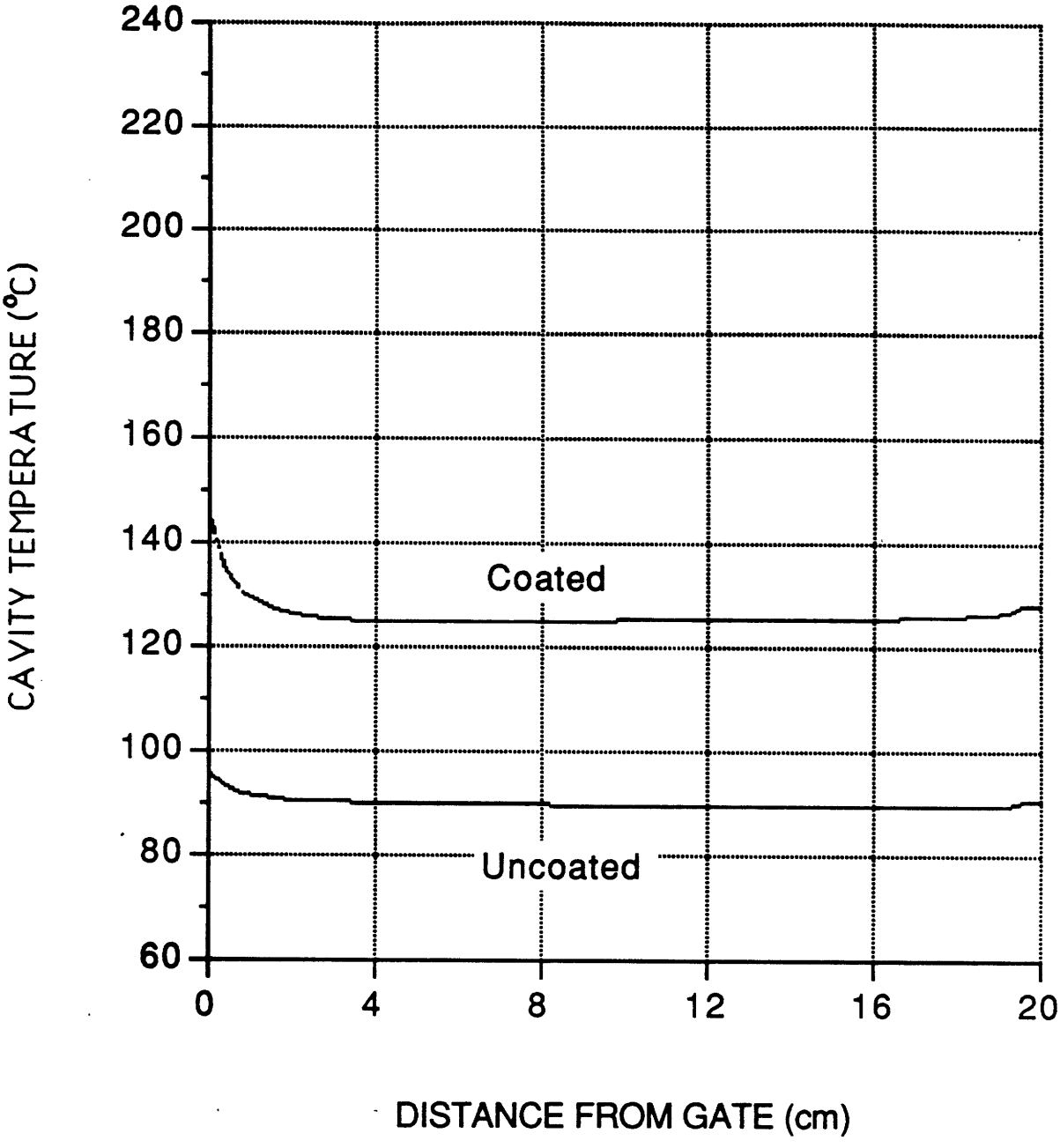

Figure 3-4: Interface Temperature along the Flow Channel at the End of Filling.

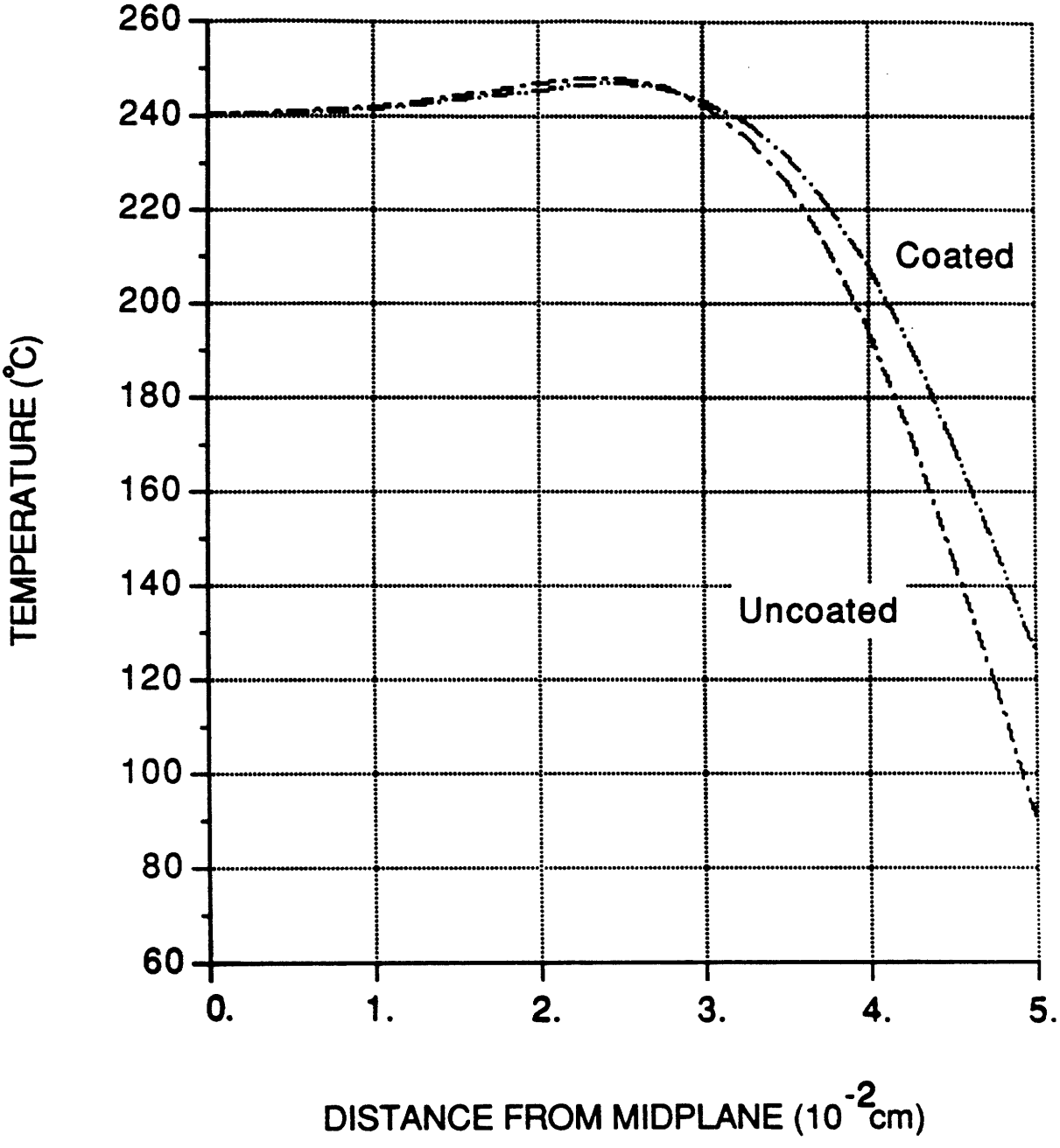

Figure 3-5: Gapwise Temperature Distribution at the End of Filling.

because a smaller injection pressure, and therefore a smaller machine, is required to inject the same shot size. However, because a pressure drop exists between the hydraulic system and the gate, the reduction of the pressure in the hydraulic system may not be as significant as the pressure reduction in the gate region shown in Figure 3-6. Experimental results (Table 3-II shown in the next section) have given a reduction of 15% for hydraulic pressure in the ram as compared to the reduction of gate pressure by 21% in Figure 3-6.

The velocity profile across the thickness immediately before the end of filling is presented in Figure 3-7. The region of the frozen layer, where the velocity is zero, can be identified in the uncoated cavity. The coated cavity, as was expected, eliminates the frozen layer during the filling by raising the cavity temperature well above T_g. Since the flow rates are the same in both cases, the frozen layer near the surface results in higher velocity in the center. Flow in a narrower channel leads to higher strain rate in the polymer melt as shown in Figure 3-8. A higher strain rate produces larger strains and stresses in molded parts.

The shear stress developed at the end of filling and its relaxation during the subsequent cooling, is shown in Figure 3-9. The abrupt decrease of shear stress following the filling is due to the disappearance of the strain rate in equation (3.22) for the cooling. The curves of 0.5- and 0.5+ correspond to the shear stress distributions at 0.5 second immediately before and after the filling is complete. The strain rate is zero right after the filling is complete. Most of the shear stress relaxes in the first half second after the filling. The stress inside the plate relaxes completely while that near the surface does not. The insulation layer has allowed more stress relaxation on the surface as compared with the part injected from the coated cavity (Figure 3-10).

The relaxation of the primary normal stress difference $\sigma_{11}-\sigma_{22}$ after the filling is shown in Figure 3-11. The stresses inside the polymer relaxes almost

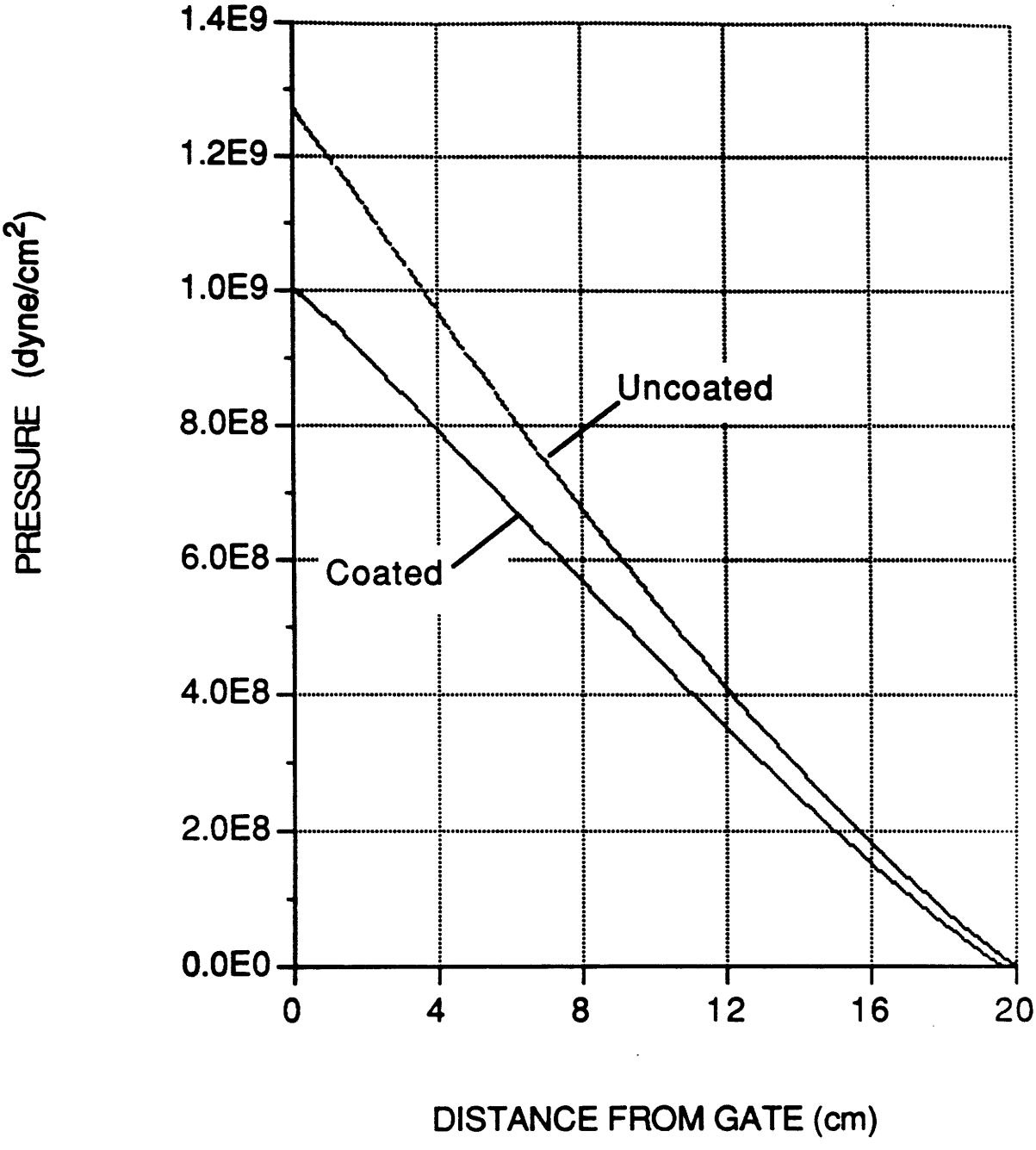

Figure 3-6: Pressure Distribution along the Flow Channel at the End of Filling.

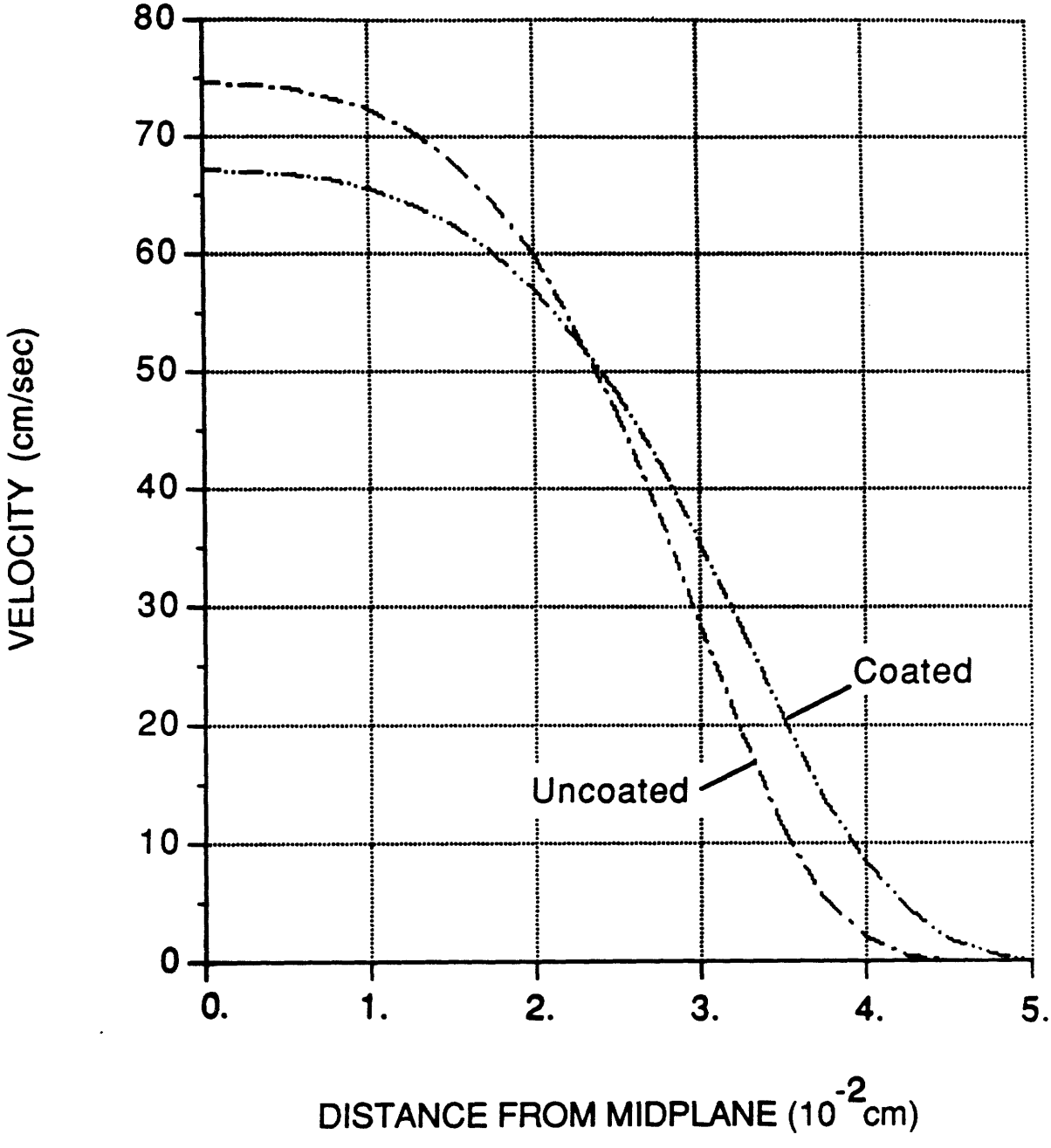

Figure 3-7: Gapwise Velocity Distribution at the End of Filling.

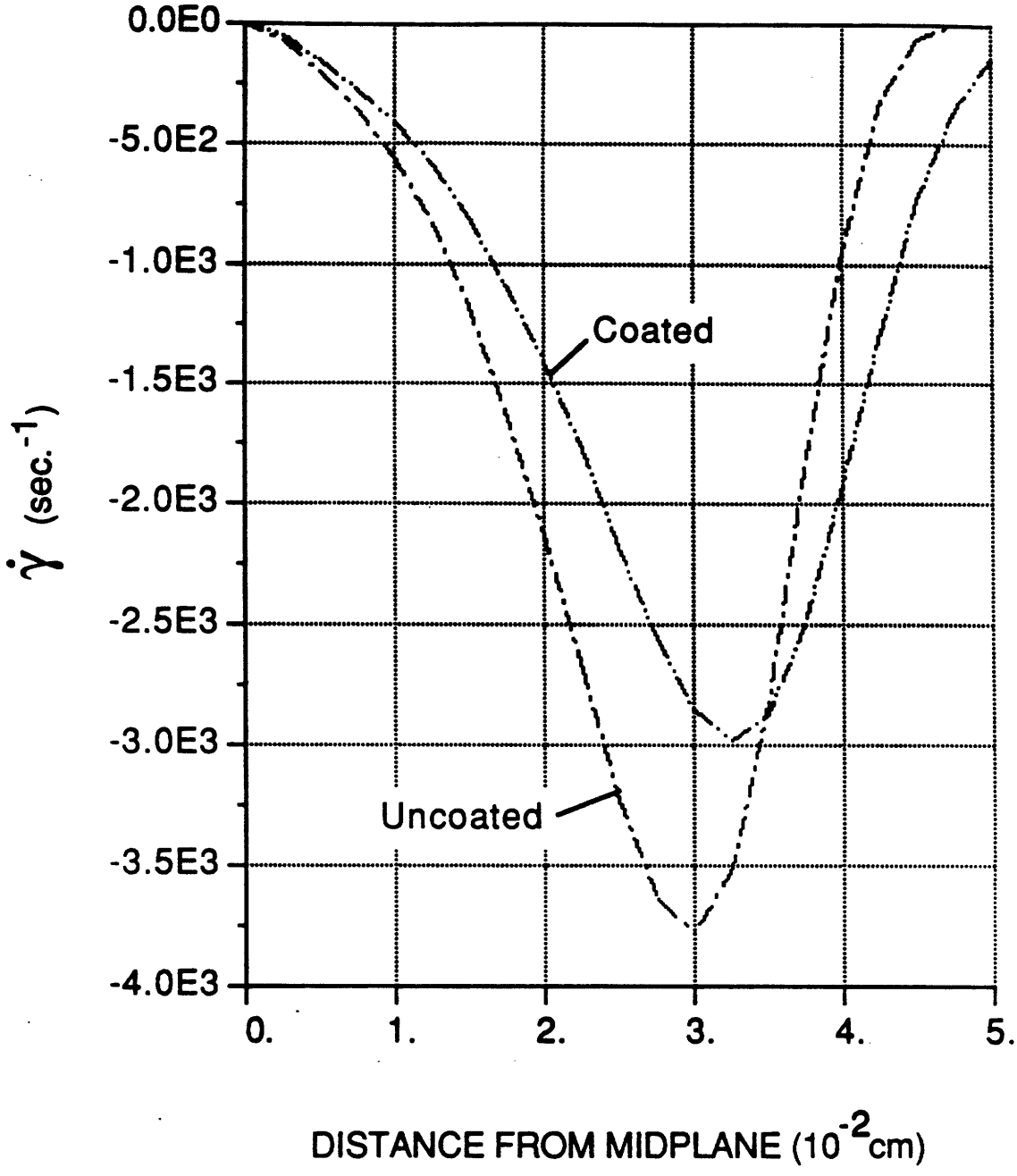

Figure 3-8: Gapwise Strain Rate Distribution at the End of Filling

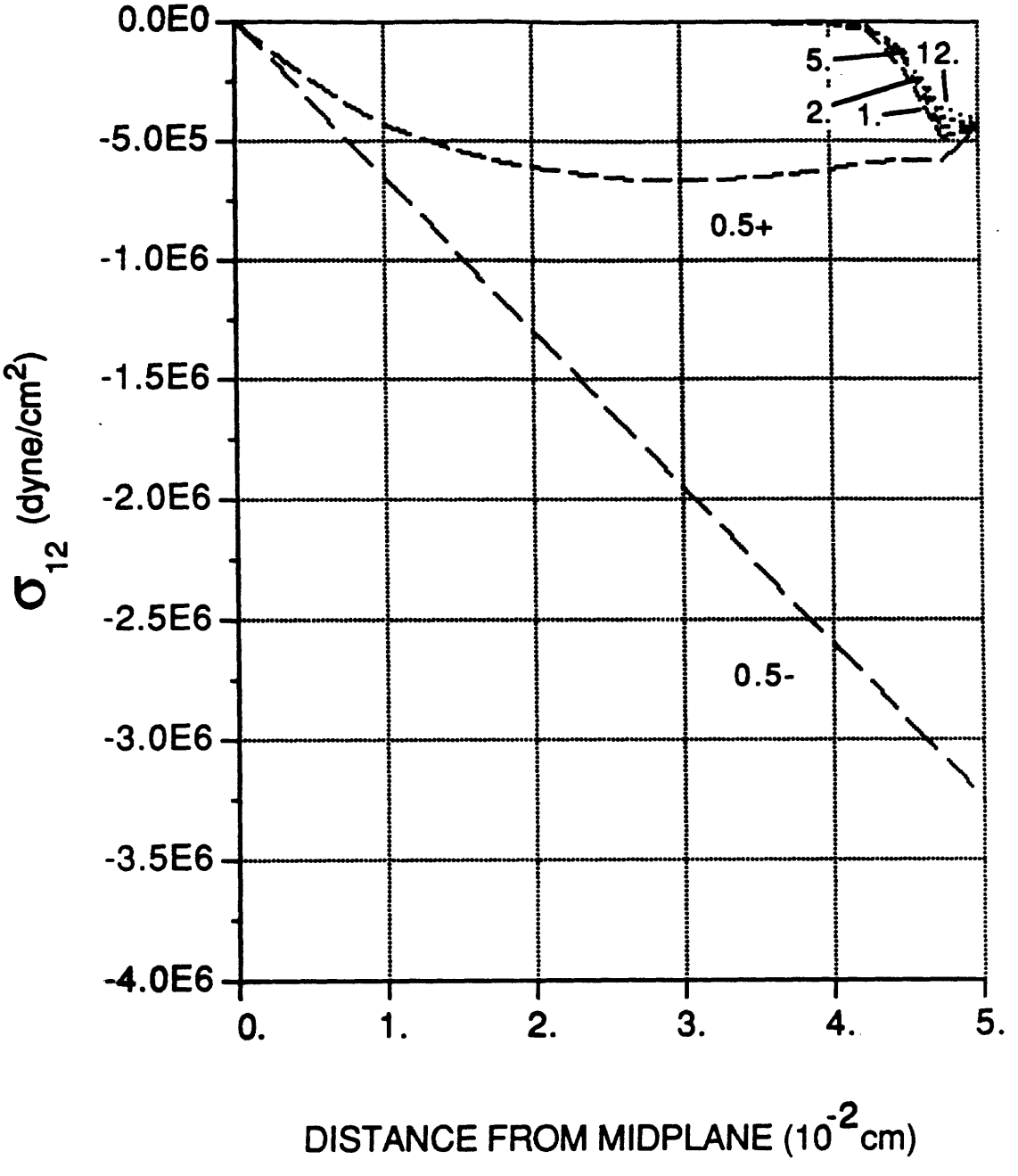

Figure 3-9: Relaxation of Shear Stress after the Filling of Uncoated Cavity, 0.5 sec. (end of fillng) - 12 sec. (end of cooling).

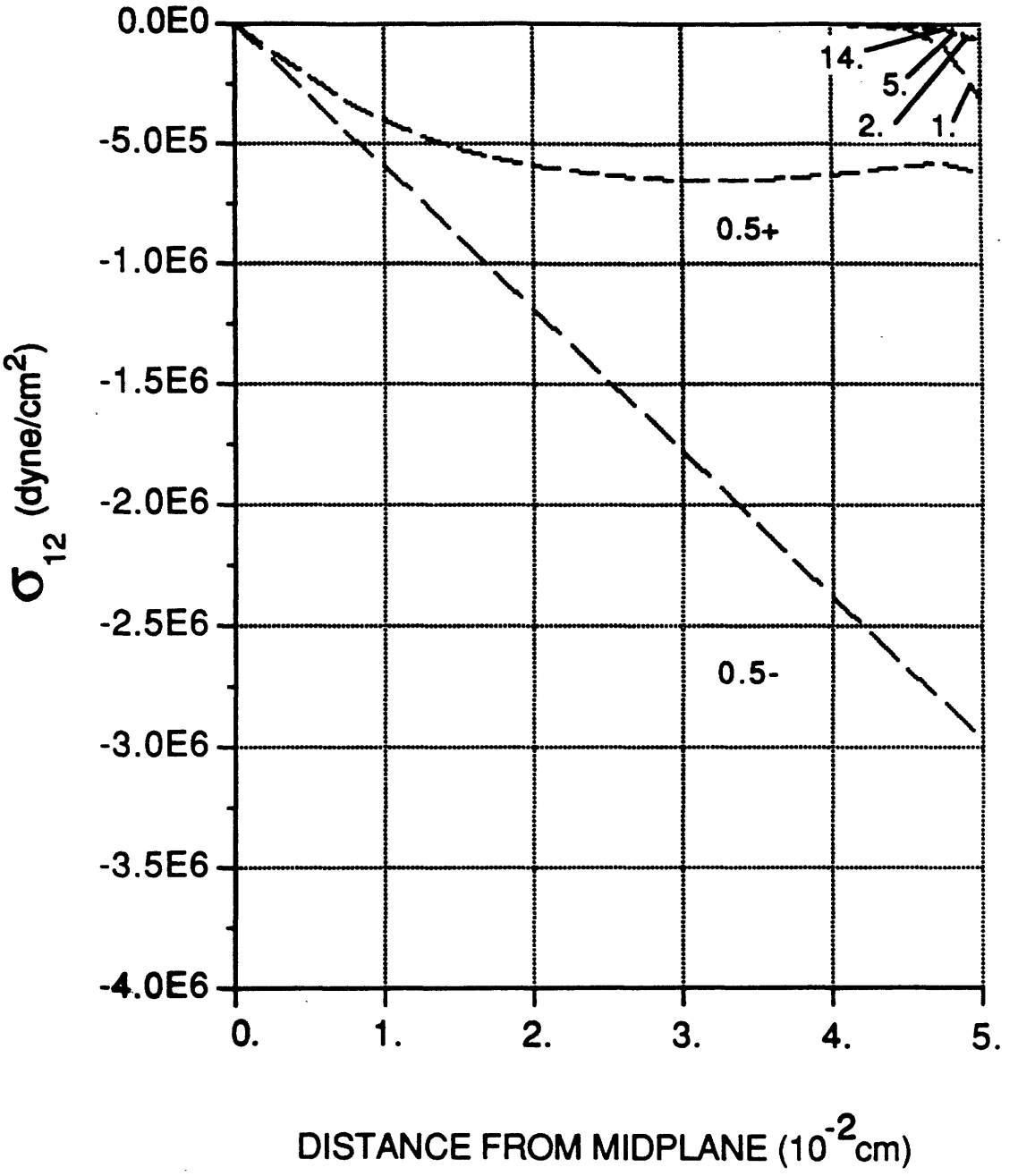

Figure 3-10: Relaxation of Shear Stress after the Filling of Coated Cavity, 0.5 sec. (end of fillng) - 14 sec. (end of cooling).

completely while the stresses near the surface relaxes only partially or not at all. Most of the relaxation occurs in the first half second after filling. The stress state does not change much in the remaining cooling stage. Comparing the coated with the uncoated cavities (Figure 3-12), the stress distributions do not show much difference immediately after the filling. However, the insulation layer has allowed more stress relaxation, especially near the surface.

The maximum value of $\sigma_{11}-\sigma_{22}$ occurs not on the surface but near the surface. This is because the polymer on the surface freezes immediately after it contacts the steel cavity, and it does not accumulate any more strain because the strain rate is zero in this frozen layer. Nor does it relax any strain because it is frozen. On the other hand, the polymer near the surface, which is not totally frozen, accumulates more strain as the filling progresses since maximum strain rate exists in this region. Only small amount of strain can relax after the filling because the temperature is close to T_g. For the polymer far away from the surface, the strain rate is small and the temperature is high. Only a small amount of strain accumulates and quickly relaxes.

The relaxation of secondary normal stress difference $\sigma_{22}-\sigma_{33}$, which is presented in Figures 3-13 and 3-14, show the characteristics similar to those of $\sigma_{11}-\sigma_{22}$. The coated cavity also allows more stress relaxation than the uncoated cavity. Figures 3-15 and 3-16 show the relaxations of $\sigma_{11}-\sigma_{33}$ in a similar manner to the relaxation of $\sigma_{11}-\sigma_{22}$. The coated cavity results in more stress relaxation after the filling.

The relaxations of birefringence, which are defined in equation (3.38), is given in Figures 3-17 and 3-18. The curves of 0.5- and 0.5+ correspond to the birefringence at 0.5 second (end of filling) immediately before and after the filling finishes respectively. The instantaneous change of birefringence at 0.5 second is due to the abrupt change in shear stress resulting from the sudden change of strain rate

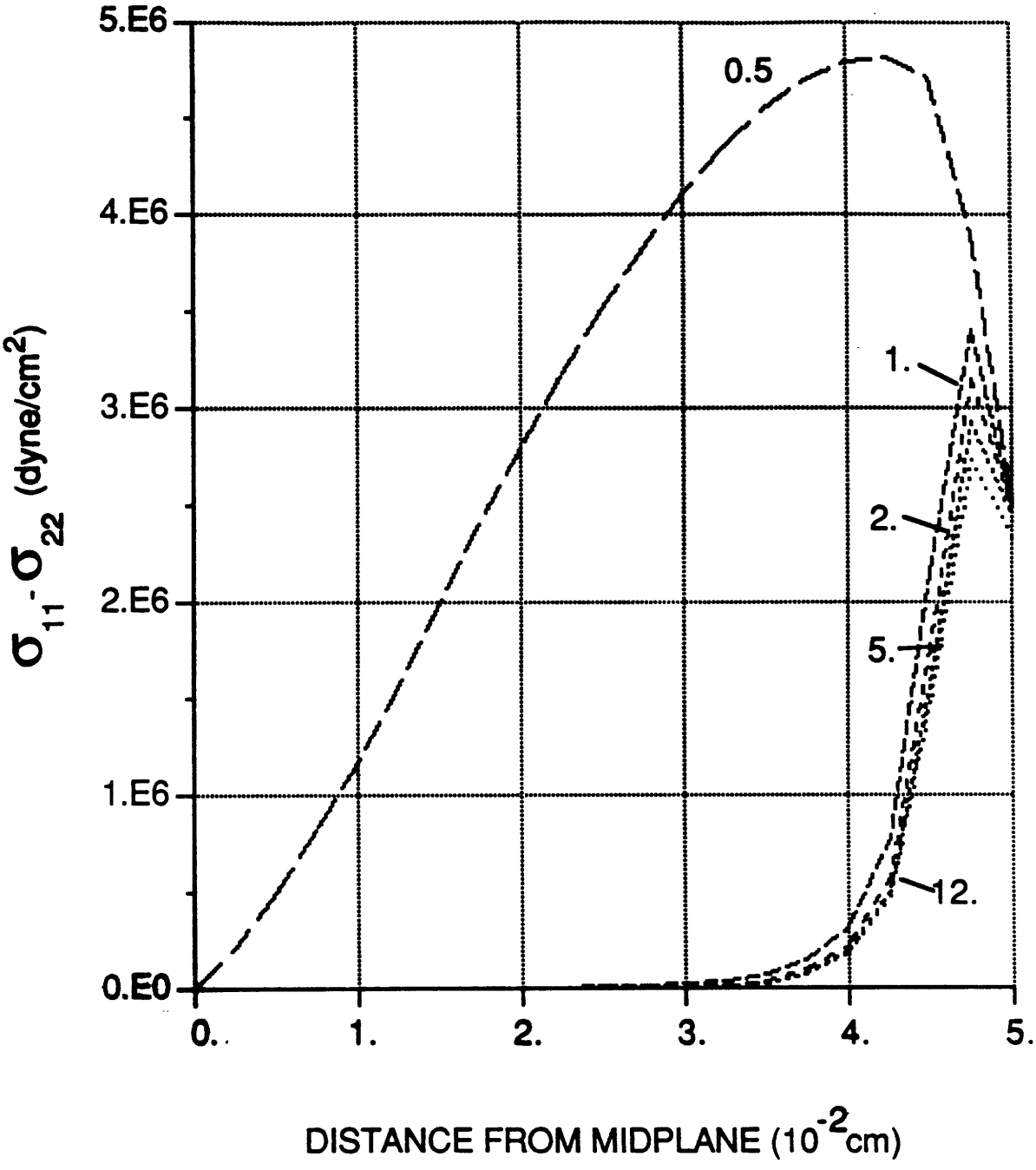

Figure 3-11: Relaxation of $\sigma_{11} - \sigma_{22}$ after the Filling of Uncoated Cavity, 0.5 sec. (end of fillng) - 12 sec. (end of cooling).

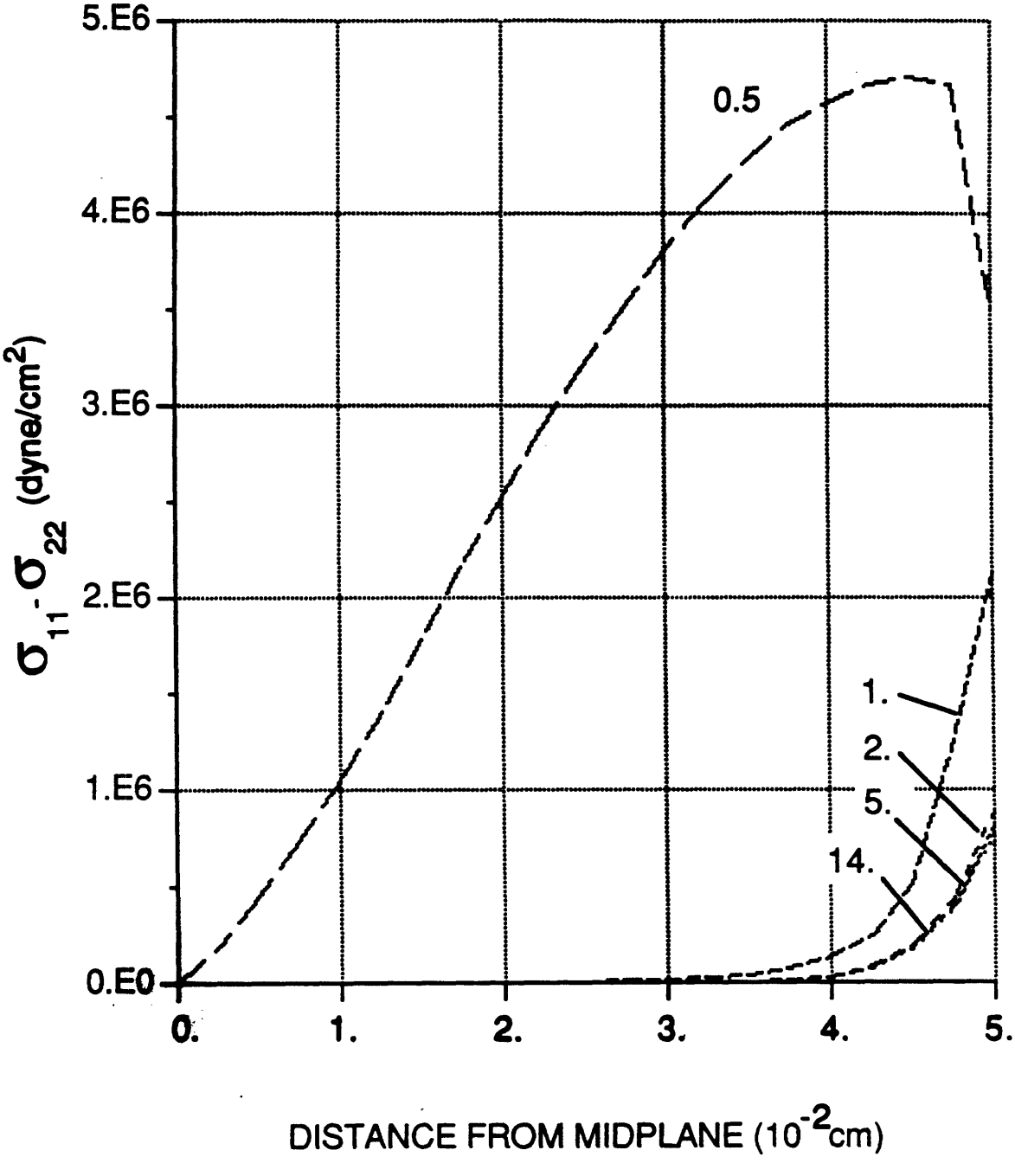

Figure 3-12: Relaxation of $\sigma_{11} - \sigma_{22}$ after the Filling of Coated Cavity, 0.5 sec. (end of filling) - 14 sec. (end of cooling).

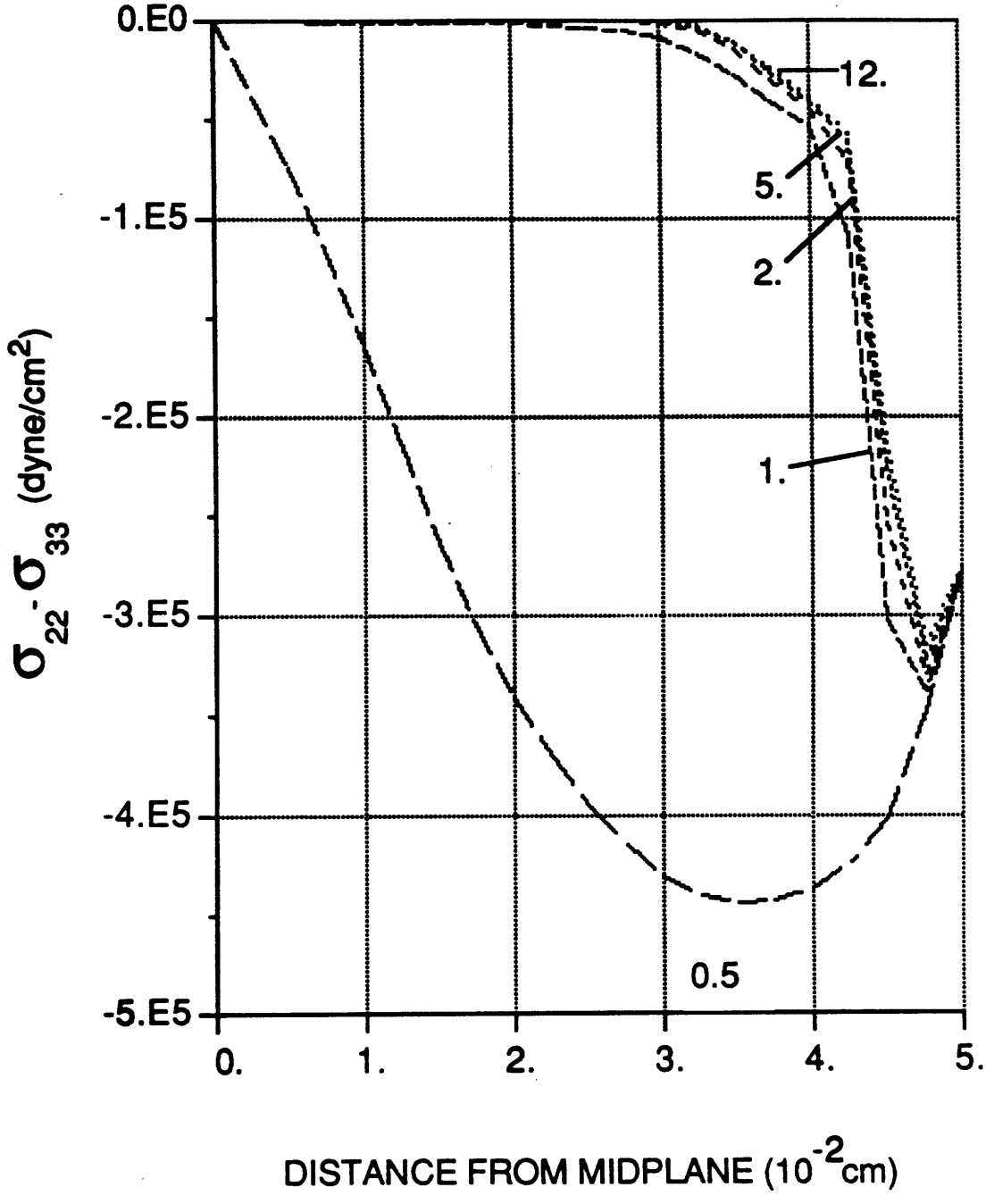

Figure 3-13: Relaxation of $\sigma_{22}-\sigma_{33}$ after the Filling of Uncoated Cavity, 0.5 sec. (end of fillng) - 12 sec. (end of cooling).

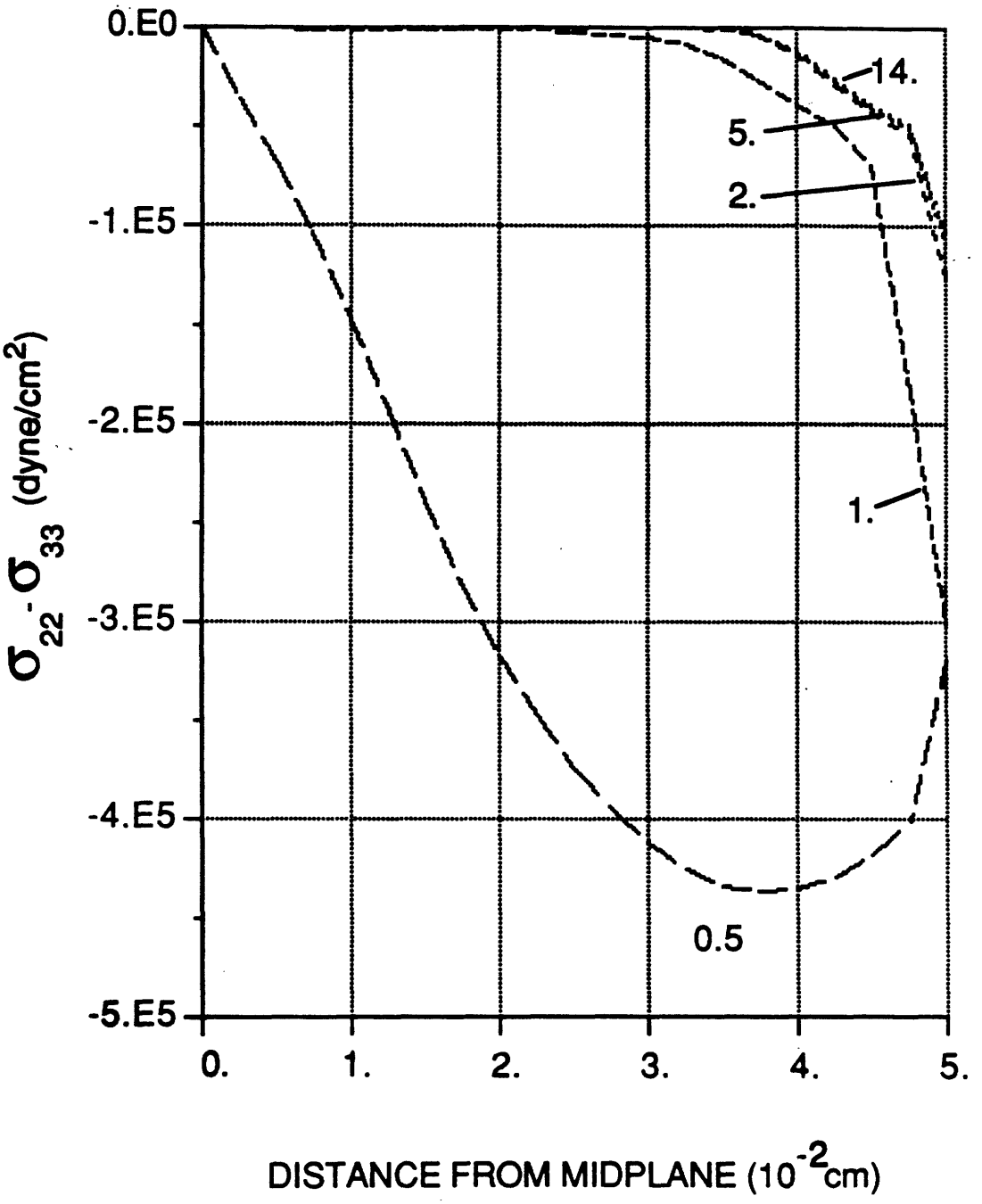

Figure 3-14: Relaxation of $\sigma_{22}-\sigma_{33}$ after the Filling of Coated Cavity, 0.5 sec. (end of filling) - 14 sec. (end of cooling).

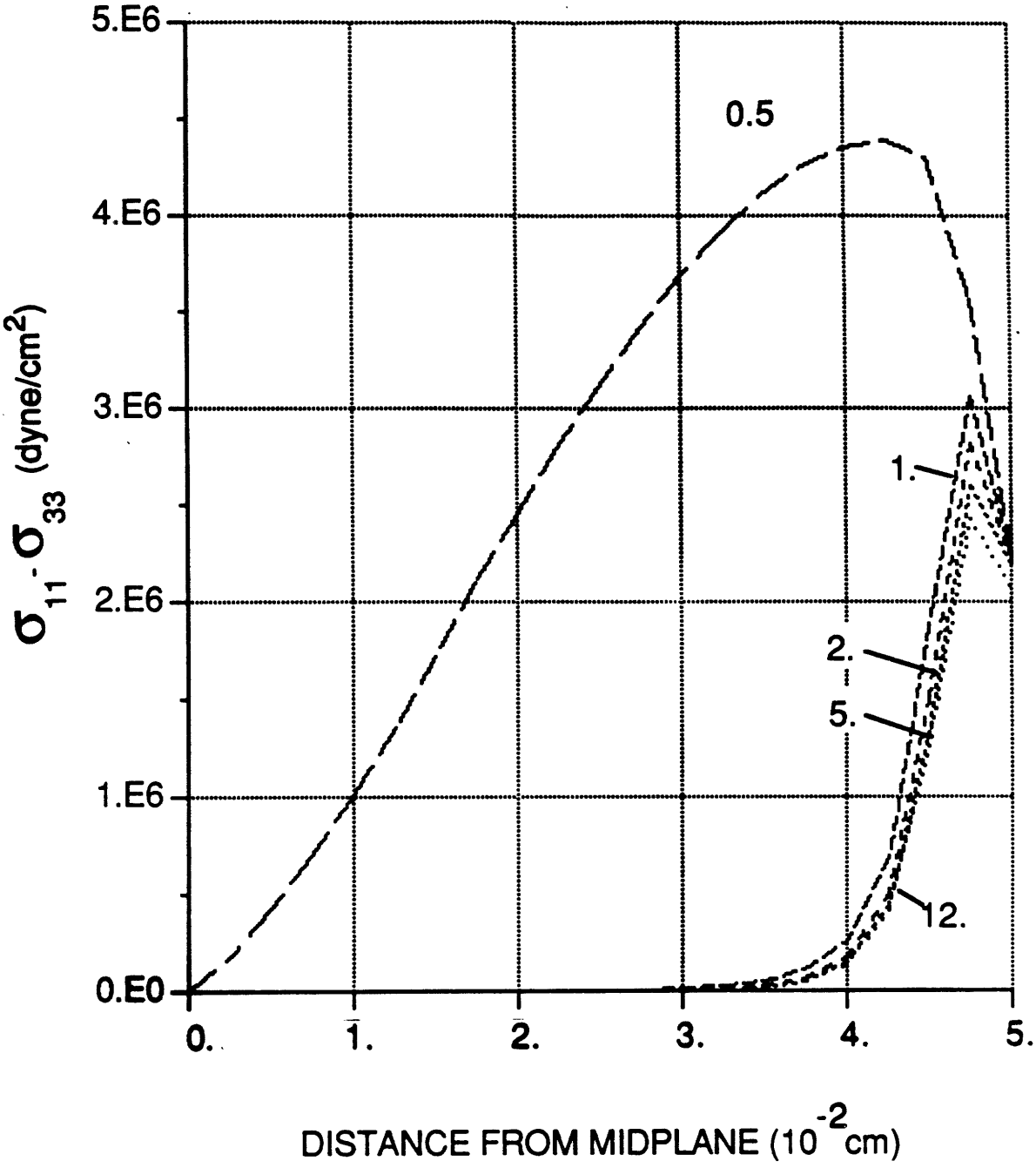

Figure 3-15: Relaxation of $\sigma_{11}-\sigma_{33}$ after the Filling of Uncoated Cavity. 0.5 sec. (end of fillng) - 12 sec. (end of cooling).

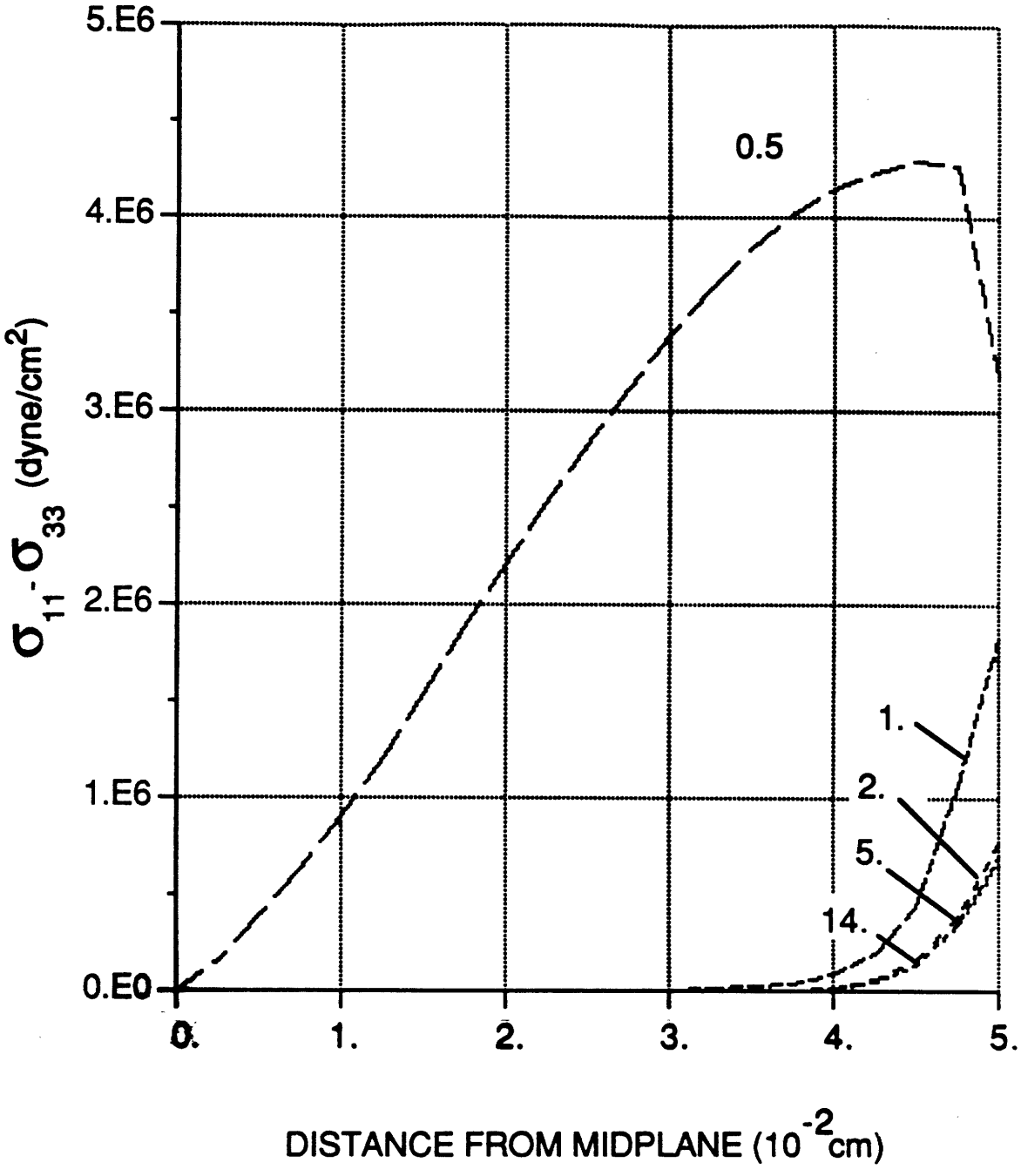

Figure 3-16: Relaxation of $\sigma_{11}-\sigma_{33}$ after the Filling of Coated Cavity, 0.5 sec. (end of filling) - 14 sec. (end of cooling).

when the filling is completed. Most of the birefringence relaxation occurs in the first half second following the filling. It relaxes completely in the core region and not at all near the surface. Figure 3-18 shows the coated cavity has allowed the relaxation of birefringence not only in the core region but also near the surface.

3.5 Experiments

Two identical molds were fabricated with and without Teflon coatings on the cavity surfaces to mold a plate with a thickness of 0.1 cm. The plate was 20 cm long and 6 cm width. The cavities were fan-gated at one end so that the conditions of the entering polymer melt was close to the assumptions of isothermal fully-developed flow in the simulation. Teflon-S with a thickness of 0.01 cm was applied to one of the two molds.

Dow Styron 685-D polystyrene was injection-molded using a Van Dorn 150 ton injection molding machine in Eastman Kodak Co.. The processing conditions are given in Table 3-II. The injection temperature was 240 ^{o}C while the mold temperature was 70 ^{o}C. The same conditions were used in both the coated and uncoated molds. The required injection pressure to completely fill the coated cavity was 1130 psi while that in the uncoated cavity was 1310 psi.

A reduction of 15% was gained in the injection pressure of the coated cavity beacuse of the higher average temperature and consequently lower viscosity in the polymer melt. This would enable a smaller machine to inject the same shot size with the coated cavity. A reduction of 21% in gate pressure resulting from the simulation was achieved as shown in Figure 3-6. The difference between 21% and 15% is due to the pressure drop between the hydraulic system and the gate.

The birefringence Δn_3 of the molded parts in the 1-3 plane was measured using a Polariscope System (Model 051) manufactured by Photolastic Inc.. The

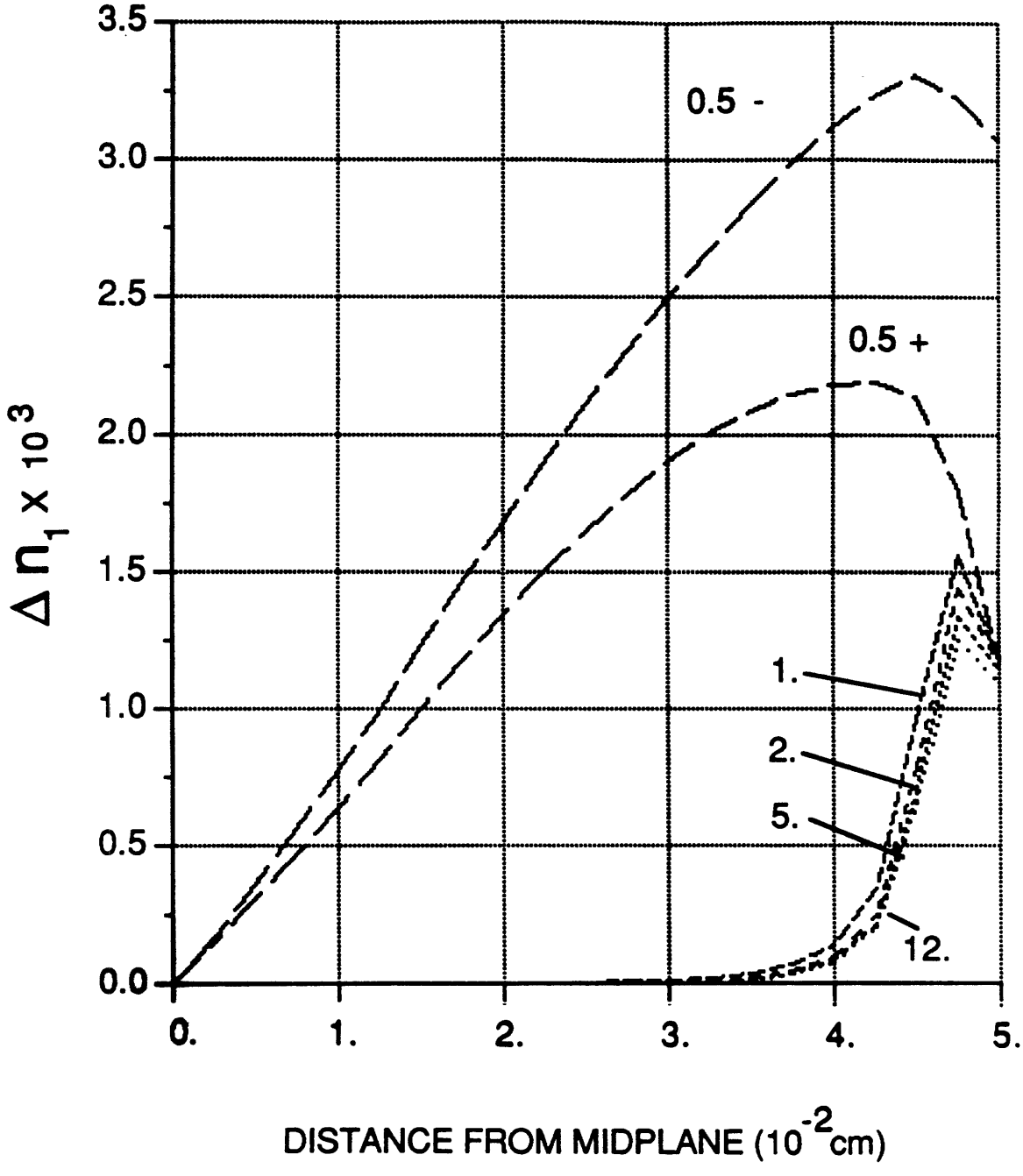

Figure 3-17: Relaxation of Birefringence after the Filling of Uncoated Cavity, 0.5 sec. (end of filling) - 12 sec. (end of cooling).

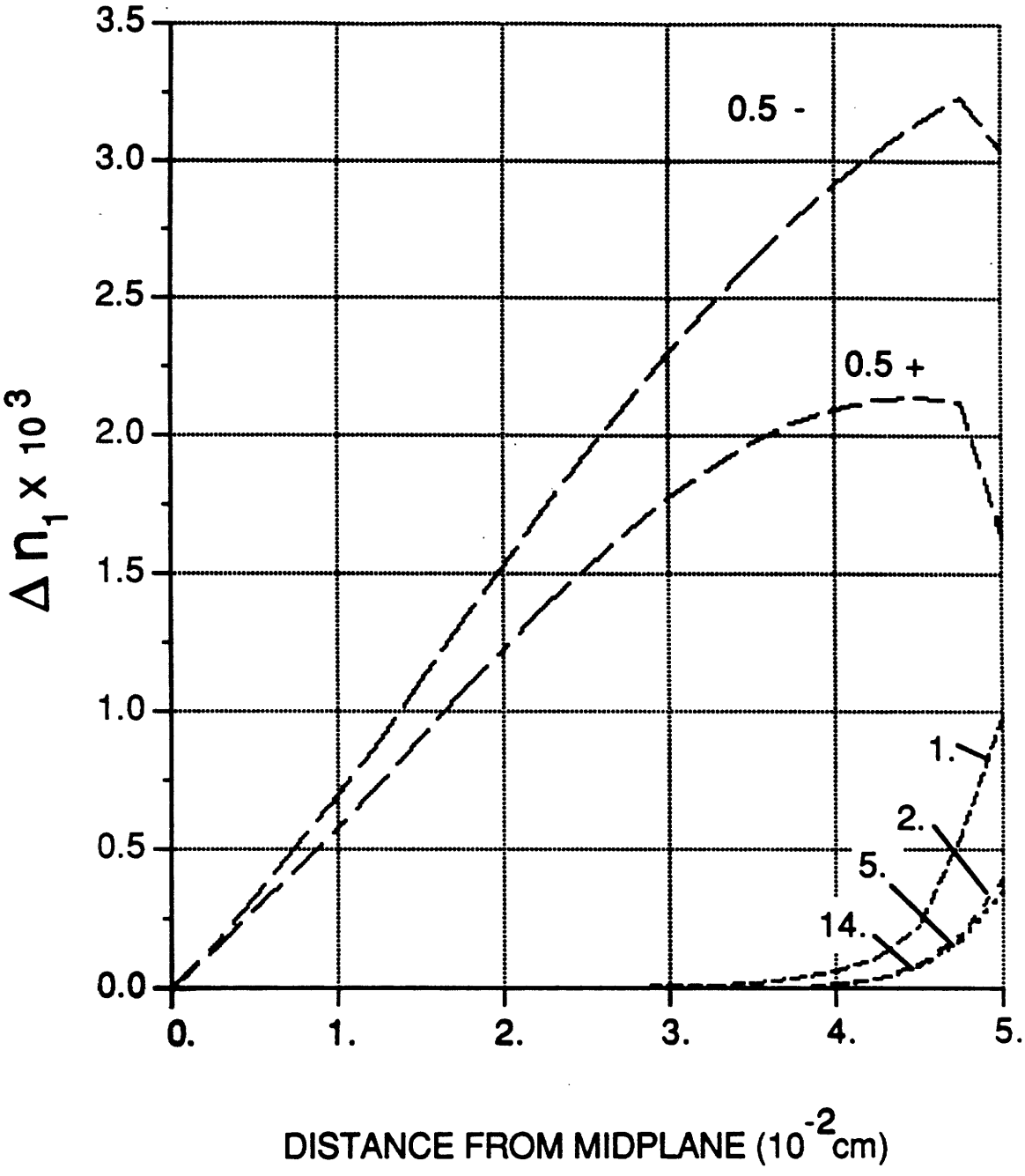

Figure 3-18: Relaxation of Birefringence after the Filling of Coated Cavity, 0.5 sec. (end of filling) - 14 sec. (end of cooling).

	Coated Cavity	Uncoated Cavity
Injection Temp.	240 °C	240 °C
Mold Temp.	70 °C	70 °C
Injection Pressure	1130 psi	1310 psi

Table 3-II: Processing Conditions in Experiments.

circular polariscope was used to obtain the isochromatic fringe pattern. The fringe order at every isochromatic fringe could then be identified with N=0 at the end of flow direction. Tardy Compensation was also used to quantify the value of birefringence at every point along the flow direction. The values of $\sigma_{11} - \sigma_{33}$ were then determined by

$$\sigma_{11} - \sigma_{33} = \Delta n_3 \frac{1}{C} \tag{3.39}$$

where C = *stress–optic coefficient*

The value of C is taken as $1.5 \times 10^{-10}\ cm^2/dyne$ from reference [6]. The experimental values of $\sigma_{11} - \sigma_{33}$ along the flow direction computed from equation (3.39) are presented in Figure 3-19. The values decrease with increasing distance from the gate. The coated cavity allows more stress relaxation following the filling and therefore reduces the values of $\sigma_{11} - \sigma_{33}$ in the molded parts.

The average values of $\sigma_{11} - \sigma_{33}$ in 1-3 plane from the simulation can be obtained by integrating $\sigma_{11} - \sigma_{33}$ in Figures 3-15 and 3-16 across the thickness and dividing the result by the thickness. The distributions along the flow direction is given in Figure 3-20. The values decrease, as in the experimental results, with increasing distance from the gate. The coated cavity has resulted in smaller $\sigma_{11} - \sigma_{33}$ in the molded parts because it allowed stress relaxation near the surface.

The discrepancy between the predicted and measured values comes from the value of stress-optic coefficient used to calculate the normal stress difference. The stress-optic coefficient of polystyrene decreases by an order of magnitude from the melt to glass transition temperatures [5]. It also varies between different manufacturers and with different molecular weights. White et al. [29, 6, 34] suggested that a stress-optic coefficient with the appropriate value near T_g should be used because the molecular orientation in plastic parts is related to the level of

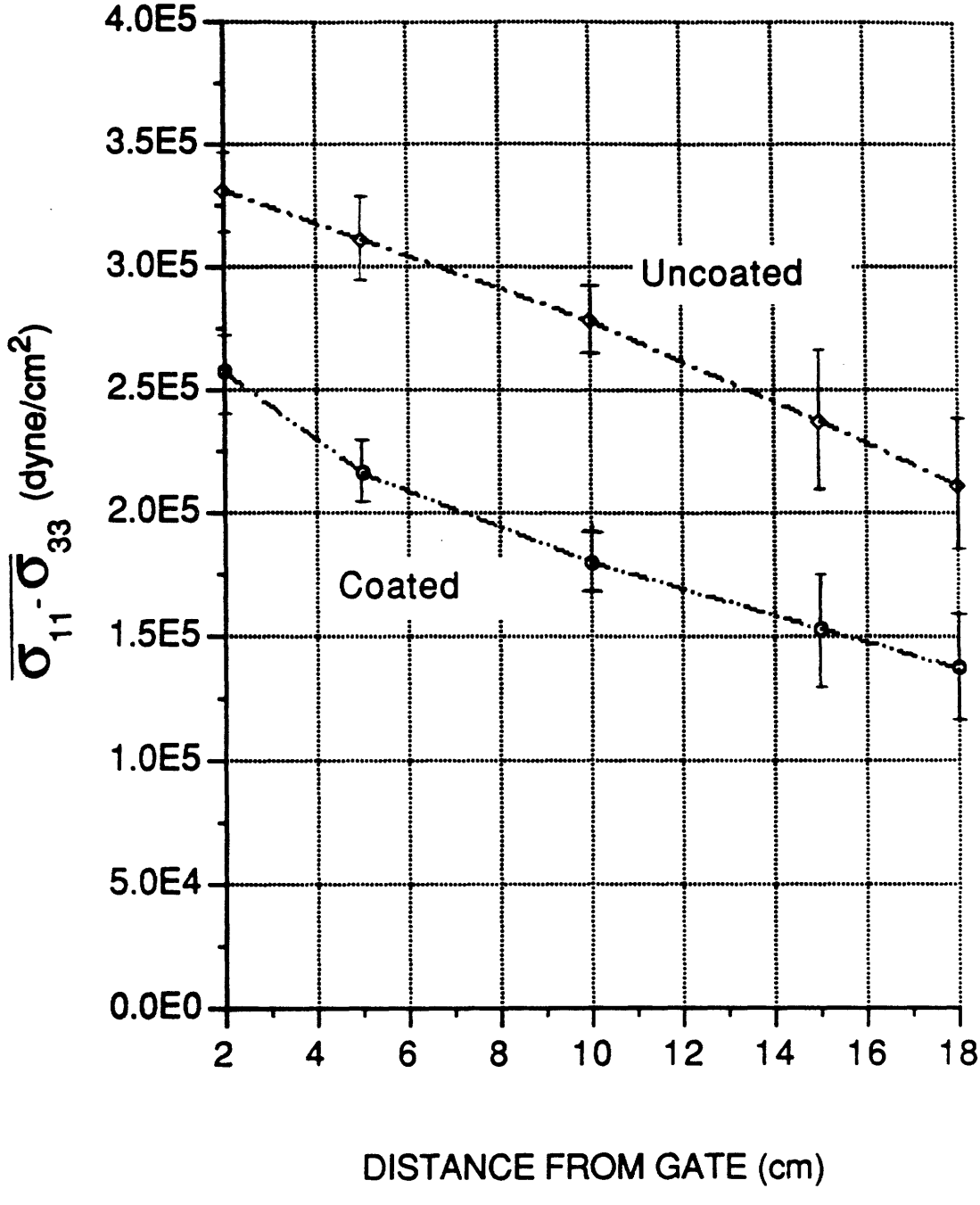

Figure 3-19: Experimental Results of Average $\sigma_{11} - \sigma_{33}$ along the Flow Direction.

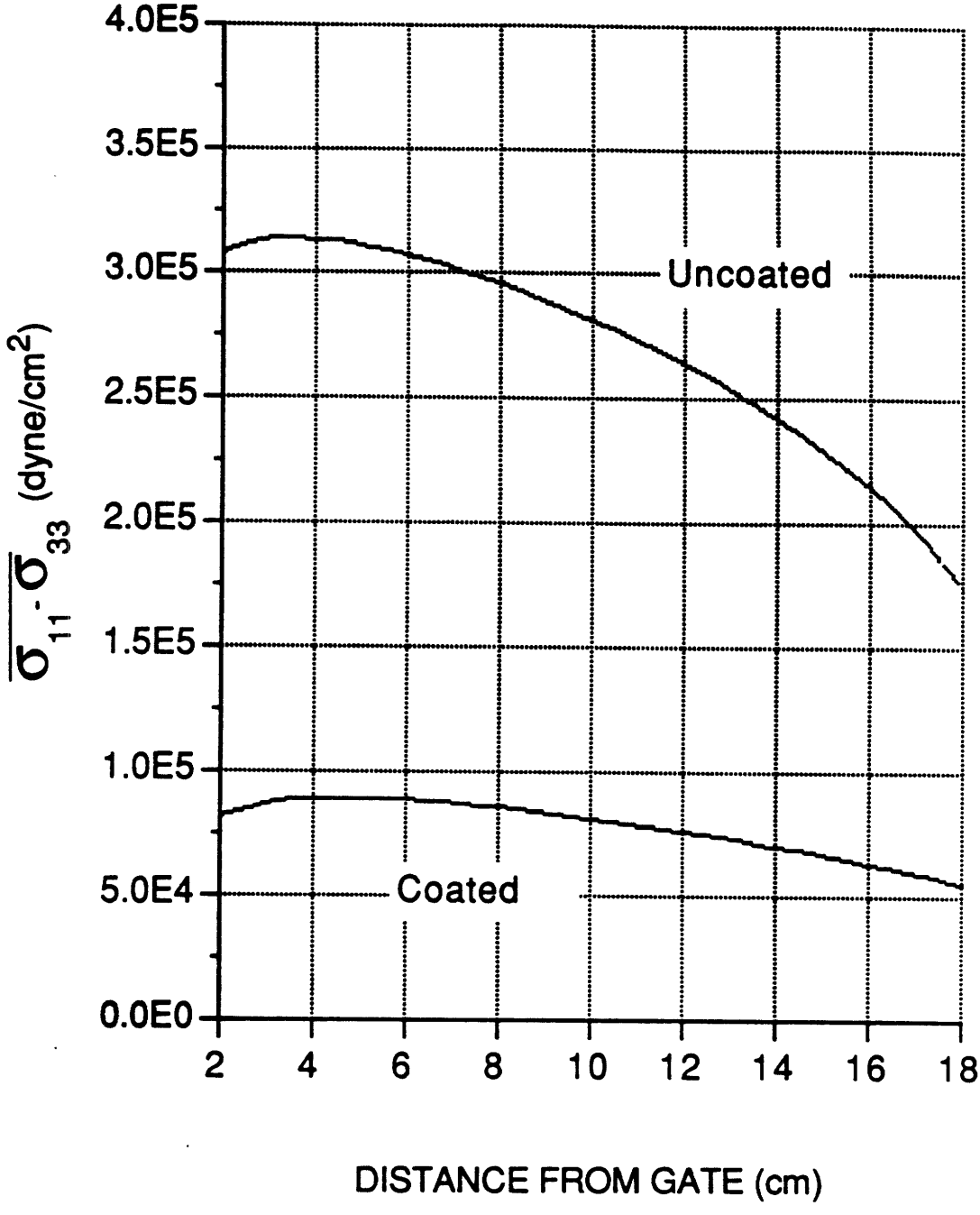

Figure 3-20: Simulation Results of Average $\sigma_{11} - \sigma_{33}$ along the Flow Direction.

principle stress difference at the time of vitrification. It is not related to the stress state in the final parts which should be determined from direct stress measurement.

3.6 Summary

One of the problems in injection molding is that filling and cooling are coupled, which means the cooling begins before the filling is completed. Therefore, flow-induced stresses cannot relax in the surface region. The dimensions of the parts may change over the life time of the parts if the residual stresses are too high. Therefore, the ideal condition in injection molding is to have a hot mold during the filling and a cold mold during the cooling in order to decouple these two processes. However, it takes tens of minutes to have the whole mold go through this ideal thermal cycle. Not only does the cycle time increases drastically, but also the life of the mold decreases.

The approach presented in this chapter solved this problem by using a passive insulation layer with low thermal inertia on the cavity surface. This layer raised the temperature on the cavity surface during the filling without heating the whole mold. Consequently, it provided a hot cavity surface during the filling and a cold cavity surface during the cooling.

Two simple criteria for the optimal thermal properties and required thickness of the layer have been presented. The first criterion tells us that the smaller the $k\rho c$ of the layer, the higher the interface temperature. The second criterion allows us to calculate the required minimum thickness for the layer so that the flow-induced stress can relax after the filling and the increase of subsequent cooling time is kept to a minimum.

In addition to the optimal thermal properties of the layer, the material used for the layer should also satisfy the following conditions. Good wear resistance is

required in order to extend the life of cavity. The melting point of the layer should be much higher than that of the polymer. The bonding strength of the layer to the mold must also be high enough to avoid delamination as the processing pressure is tremendously high in molding processes and the thermal stresses in the layer should not be ignored. A good surface finish is, of course, a must if high precision optical parts are to be molded. A material for the layer which meets all these requirements is yet to be developed.

A numerical simulation model for the molding cycle has been developed to understand the stress development and relaxation during the molding cycle and to evaluate this approach. This model utilizes the Leonov constitutive equation to represent the time- and temperature-dependent stress relaxation. The results show that the stresses inside the parts relax completely while those near the surface relax partially or not at all. Most of the relaxation occurs in the first half second after the filling when the polymer is still at a relatively high temperature. The maximum stresses exist not on the surface but near the surface due to the fact that the frozen layer on the surface does not accumulate any more strains during the filling because the strain rate is zero in the frozen layer.

By comparing the results from the coated and uncoated cavities, the insulation layer raises the cavity temperature during the filling, which subsequently allows the flow-induced stresses to relax after the filling. The final residual stresses are significantly reduced. The cooling time is increased by less than 20% and the total cycle time should be increased by even less percent because the cooling time is only a portion of the total cycle time. The required injection pressure is also reduced because the polymer has higher temperature and therefore lower viscosity during the filling. A smaller injection molding machine can be used to inject the same shot size.

A typical molding process includes both material flow and cooling processes.

A part will start to cool before the process of material flow is completed. The technique presented in this chapter decouples the processes of material flow and cooling and allows the flow-induced stresses to relax after the flow. This idea can be applied not only to the injection molding processes but also to all molding processes, including the molding of metals. Its effects are particularly significant in the molding of metals because the values of $k\rho c$ of metals are much larger than those of polymer. An insulation layer like ceramic can easily raise the interface temperature to a higher level when molding metals.

Chapter 4

Optimal Cooling for Minimum Residual Stresses

4.1 Introduction

A molding process, in general, is a process in which a heated malleable material is forced to flow or deform into the shape of the mold cavity. The material then solidifies and retains the shape of the cavity. The molding process is capable of producing complex three dimensional parts in a single molding operation. The material starts to cool before the process of material flow or deformation is completed. The flow-induced stresses in the material near the surface cannot relax after the flow and result in residual stresses in the molded parts. In addition to the flow-induced residual stresses, non-uniform cooling also causes thermally-induced residual stresses.

For large structural molded parts, annealing is usually necessary in order to relax the residual stresses so that their dimensions will not change over the life time of the parts. Although the heating in the annealing process relaxes the residual stresses, the cooling process may reintroduce thermally-induced residual stresses if it is non-uniform. The temperature gradient developed during the cooling results in differential thermal contraction and stress relaxation, which consequently create thermal stresses in the parts.

In order to reduce thermally-induced stresses which result from annealing, the cooling process must be very slow, usually requiring days, to keep the temperature gradient very small so that the part cools uniformly. Not only is energy input wasted during such a long operation, but productivity is also reduced. The objective of this study is to find an optimal cooling path within a specified time

period for minimum residual thermal stresses.

A low thermal inertia mold, which has a heating element on the cavity surface and can provide rapid change of cavity temperature, was developed in MIT-Industry Polymer Processing Program and Intelitec Corporation. To utilize the potential of this new technology, an optimal thermal history during the molding cycle to minimize residual stresses in the molded parts needs to be established.

This chapter first analyzes the development of the residual thermal stresses caused by the temperature gradient during the cooling. The stresses are then minimized through optimization of the thermal history in the cooling cycle.

4.2 Thermal Stress Analyses

The analysis of thermal stresses in viscoelastic materials must take into consideration the temperature dependent properties. However, some analyses [1] have idealized these properties by assuming inviscid behavior above and elastic behavior below the critical temperature referred to as the glass transition temperature of an amorphous polymer. Such models neglect the important stress relaxation property of viscoelastic materials.

A material model termed [31] "thermorheologically simple" was also investigated [26, 27]. This model exhibits a pure shift in relaxation function plotted against the logarithm of time when there is a temperature change. The relaxation functions measured at two temperatures, T_1 and T_2, are related simply by a change in the time scale with a factor $\phi(T_2)$, which reduces the time scale as the temperature increases. Therefore, it is convenient to define a reduced time ψ which includes the varying scale factor $\phi(T)$ so that the viscoelastic stress-strain relation under a continuously varying temperature has the same form as the

isothermal relation.

Based on this shift hypothesis, Morland and Lee [26] introduced the generalized relaxation integral law

$$s_{ij}(z,\psi) = \int_0^{\psi} G_1(\psi-\psi')\frac{\partial}{\partial\psi'}[e_{ij}(z,\psi')]\,d\psi',$$

$$\sigma_{kk}(z,\psi) = \int_0^{\psi} G_2(\psi-\psi')\frac{\partial}{\partial\psi'}[\epsilon_{kk}(z,\psi') - 3\alpha_o\theta(z,\psi')]\,d\psi', \tag{4.1}$$

where

$$s_{ij} = \sigma_{ij} - \frac{1}{3}\delta_{ij}\sigma_{kk},$$

$$e_{ij} = \epsilon_{ij} - \frac{1}{3}\delta_{ij}\epsilon_{kk},$$

$$\sigma_{kk} = \sum \sigma_{ii},$$

$$\epsilon_{kk} = \sum \epsilon_{ii},$$

$\delta_{ij} = Kronecker\ delta,$

$\psi = \int_0^t \phi(\theta(z,s))\,ds, \quad \phi = time\text{-}temperature\ shift\ factor,$

$$G_1 = 2G = \frac{E}{(1+\nu)}, \quad G_2 = 3K = \frac{E}{(1-2\nu)},$$

$G = shear\ modulus, \quad K = bulk\ modulus$

$\alpha_o = coefficient\ of\ thermal\ expansion,$

$\theta = T - T_o.$

The deviatoric components of the stress s_{ij} and strain e_{ij} are introduced to separate

the shear and dilatational responses of a homogeneous and isotropic viscoelastic solid. Thermal contraction is taken into account in the dilatational response of the materials. The temperature effect on the response is considered in the reduced time ψ which is a function of the shift factor ϕ. The shift factor, in turn, depends on the temperature.

4.2.1 A free plate

Lee, Rogers and Woo [23] used equation (4.1) to calculate the residual thermal stresses in a free glass plate (Figure 4-1) cooled symmetrically from both surfaces. The strain fields in the plate can be expressed as

$$\epsilon_{xy} = \epsilon_{yz} = \epsilon_{zx} = 0, \quad \epsilon_{xx} = \epsilon_{yy}, \quad \epsilon_{zz} = \epsilon_{zz}, \tag{4.2}$$

where the z-axis is perpendicular to the surfaces of the plate. It is assumed that the lateral dimensions of the plate are large compared with its thickness, so that edge effects can be neglected.

In the absence of body and inertia forces, the equilibrium equations give

$$\frac{\partial}{\partial z}\sigma_{zz} = 0. \tag{4.3}$$

The free surface tractions require that

$$\sigma_{zz} = 0 \quad at \quad z=0,\ 2l. \tag{4.4}$$

By Equations (4.3) and (4.4),

$$\sigma_{zz} = 0. \tag{4.5}$$

Therefore, the stress components are

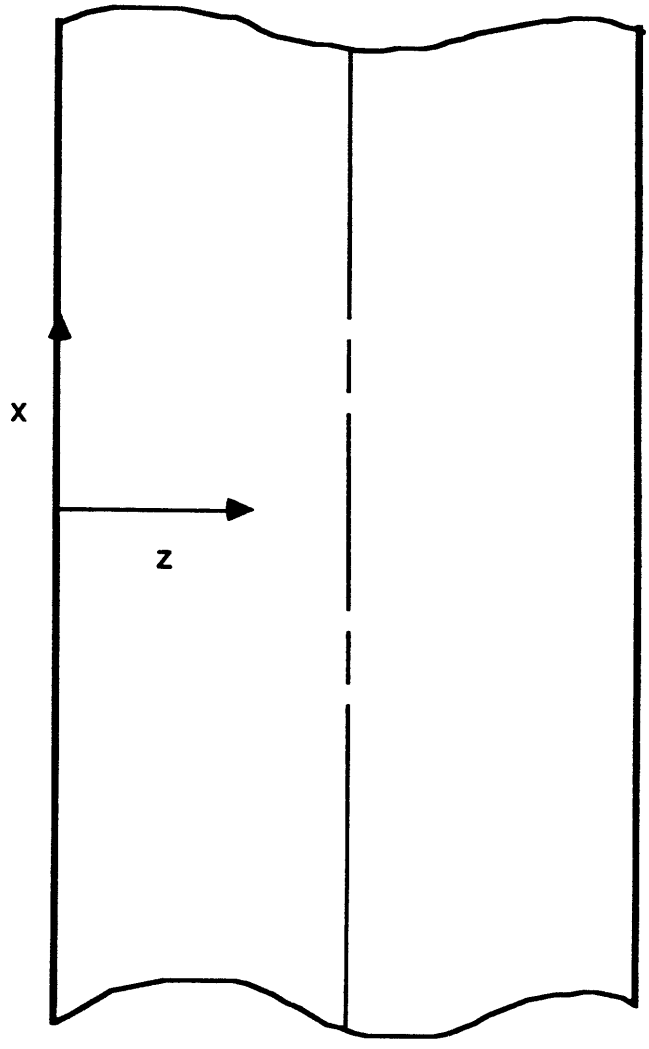

Figure 4-1: Schematic Diagram of a Free Plate.

$$\sigma_{zz} = \sigma_{xy} = \sigma_{yz} = \sigma_{zx} = 0, \quad \sigma_{xx} = \sigma_{yy}. \tag{4.6}$$

Symmetry and no surface tractions have led to zero shear stresses. The deviatoric strains can be obtained as

$$\begin{aligned} &e_{xy} = e_{yz} = e_{zx} = 0, \\ &e_{xx} = e_{yy} = \frac{1}{3}(\epsilon_{xx} - \epsilon_{zz}), \quad e_{zz} = -\frac{2}{3}(\epsilon_{xx} - \epsilon_{zz}), \end{aligned} \tag{4.7}$$

while the deviatoric stresses are

$$\begin{aligned} &s_{xy} = s_{yz} = s_{zx} = 0, \\ &s_{xx} = s_{yy} = \frac{1}{3}\sigma_{xx}, \quad s_{zz} = -\frac{2}{3}\sigma_{xx}. \end{aligned} \tag{4.8}$$

By using Equation (4.1), the following integral equations are obtained.

$$\begin{aligned} \sigma_{xx}(z,\psi) &= \int_0^{\psi} G_1(\psi-\psi')\frac{\partial}{\partial\psi'}[\epsilon_{xx}(z,\psi') - \epsilon_{zz}(z,\psi')]\, d\psi', \\ 2\sigma_{xx}(z,\psi) &= \int_0^{\psi} G_2(\psi-\psi')\frac{\partial}{\partial\psi'}[2\epsilon_{xx}(z,\psi') + \epsilon_{zz}(z,\psi') \\ &\qquad - 3\alpha_o\theta(z,\psi')]\, d\psi'. \end{aligned} \tag{4.9}$$

Applying the Laplace transform to equation (4.9) and making use of the convolution theorem, one arrives at

$$\begin{aligned} &\sigma_{xx}(z,s) = sG_1(s)[\epsilon_{xx}(z,s) - \epsilon_{zz}(z,s)], \\ &2\sigma_{xx}(z,s) = sG_2(s)[2\epsilon_{xx}(z,s) + \epsilon_{zz}(z,s) - 3\alpha_o\theta(z,s)]. \end{aligned} \tag{4.10}$$

Eliminating $\epsilon_{zz}(z,s)$ in equation (4.10), one has

$$\sigma_{xx}(z,s) = 3\frac{G_1(s)G_2(s)}{2G_1(s)+G_2(s)}\, s\,[\epsilon_{xx}(z,s) - \alpha_o\,\theta(z,s)]. \tag{4.11}$$

Let

$$R(\psi) = L^{-1}\left(\frac{G_1(s)G_2(s)}{2G_1(s)+G_2(s)}\right). \tag{4.12}$$

Equation (4.11) becomes

$$\sigma_{xx}(z,\psi) = 3\int_0^{\psi} R(\psi-\psi')\frac{\partial}{\partial\psi'}[\epsilon_{xx}(z,\psi') - \alpha_o\,\theta(z,\psi')]d\psi'. \tag{4.13}$$

By changing variables from the reduced time ψ to the physical time t, equation (4.13) results in

$$\sigma_{xx}(z,t) = 3\int_0^{t} R(\xi(z,\lambda))\frac{\partial}{\partial\lambda}[\epsilon_{xx}(\lambda) - \alpha_o\,\theta(z,\lambda)]d\lambda, \tag{4.14}$$

where $\xi(z,\lambda)$ is defined as

$$\xi(z,\lambda) = \int_{\lambda}^{t}\phi(z,s)\,ds. \tag{4.15}$$

Free edge boundary conditions reveal the fact that

$$\int_0^{t}\sigma_{xx}(z,t)\,dz = 0. \tag{4.16}$$

The equilibrium condition of the moment of momentum is automatically satisfied

because of the symmetric nature of the plate. Equations (4.14) and (4.16) constitute coupled integral equations which lead to the solution for σ_{xx} and ϵ_{xx}. They were solved [23] by numerical finite-sum integration without determining an analytical expression for $\dot{\epsilon}_{xx}(\lambda)$. The analytical expression of $\dot{\epsilon}_{xx}(\lambda)$ is necessary if the stress is to be minimized by the method of variational calculus.

Combining these two equations gives

$$\int_0^l \int_0^t R(\xi(z,\lambda)) [\dot{\epsilon}_{xx}(\lambda) - \alpha_o \dot{\theta}(z,\lambda)] d\lambda \, dz = 0. \tag{4.17}$$

Exchanging the integrals and using the fact that $\dot{\epsilon}_{xx}$ is not a function of z, one arrives at

$$\int_0^t [\dot{\epsilon}_{xx}(\lambda) \int_0^l R(\xi(z,\lambda)) \, dz - \alpha_o \int_0^l R(\xi(z,\lambda)) \dot{\theta}(z,\lambda) \, dz] \, d\lambda = 0. \tag{4.18}$$

Equation (4.18) is valid for any t only if the integrand is zero.

$$\dot{\epsilon}_{xx}(\lambda) \int_0^l R(\xi(z,\lambda)) \, dz - \alpha_o \int_0^l R(\xi(z,\lambda)) \dot{\theta}(z,\lambda) \, dz = 0. \tag{4.19}$$

This leads to

$$\dot{\epsilon}_{xx}(\lambda) = \frac{\alpha_o \int_0^l R(\xi(z,\lambda)) \dot{\theta}(z,\lambda) \, dz}{\int_0^l R(\xi(z,\lambda)) \, dz}. \tag{4.20}$$

Therefore, the residual thermal stresses of the free plate can be expressed as

$$\sigma_{xx}(z,t_f) = 3\int_0^{t_f} R(\xi(z,t))\,[\dot{\epsilon}_{xx}(t) - \alpha_o\,\dot{\theta}(z,t)]\,dt, \tag{4.21}$$

where

$$\dot{\epsilon}_{xx}(t) = \frac{\alpha_o \int_0^l R(\xi(z,t))\,\dot{\theta}(z,t)\,dz}{\int_0^l R(\xi(z,t))\,dz}.$$

Since the analyses of thermal stresses in viscoelastic materials require the consideration of temperature dependent properties and the thermal contraction, the temperature field in the plate during the cooling should first be determined. For a step change in surface temperature from T_0 to T_w, the transient temperature distributions can be given as [12]

$$\frac{T-T_w}{T_0-T_w} = \frac{4}{\pi}\sum_{n=1}^{\infty}\frac{1}{n}\exp(-(\frac{n\pi}{2l})^2\,\alpha t)\sin(\frac{n\pi z}{2l}), \qquad n = 1, 3, 5, \cdots \tag{4.22}$$

where

$T_o = initial\ temperature,$

$T_w = surface\ temperature,$

$\alpha = thermal\ diffusivity,$

$2l = thickness\ of\ the\ plate.$

In the following mathematical operations, the terms on the right hand side can be regarded as $f(z,t)$ for simplicity.

$$\frac{T-T_w}{T_o-T_w} = f(z,t). \tag{4.23}$$

Equation (4.23) can be rearranged in the form of

$$\frac{\theta}{\theta_w} = \frac{T - T_o}{T_w - T_o} = 1 - f(z,t). \tag{4.24}$$

If θ_w varies over time, superposition requires that

$$\theta(z,t) = \int_0^t \theta_w(\lambda) \frac{\partial}{\partial \lambda} f(z, t-\lambda)\, d\lambda. \tag{4.25}$$

Taking the derivative of equation (4.25) with respect to t gives

$$\dot{\theta}(z,t) = \int_0^t \theta_w(\lambda) \frac{\partial^2}{\partial t \partial \lambda} f(z, t-\lambda)\, d\lambda - f(z,0)\, \theta_w(t). \tag{4.26}$$

The values of $\dot{\theta}(z,t)$ calculated from equation (4.26) are used in equation (4.21) to determine the transient and final thermal stress distributions. The influence of cooling rate on the final stress field can also be investigated.

For illustrative purposes, the parameters of this cooling problem took on the following typical values:

$$T_o = 200\ ^oC,\ T_w = 40\ ^oC,\ 2l = 0.6\ cm, \tag{4.27}$$
$$\alpha = \frac{k}{\rho c} = 7.676 \cdot 10^{-4}\ \ cm^2/sec.,\ \alpha_o = 1.0 \cdot 10^{-5}\ \ ^oC^{-1}.$$

The time-temperature shift factor $\phi(T)$ is given by W.L.F. equation [36].

$$\log(\phi(T)) = \frac{-17.44\,(T - T_g)}{51.6 + (T - T_g)}. \tag{4.28}$$

Muki and Sternberg [27] obtained the values of $R(\xi)$ for polymethyl methacrylate at 80 ^{o}C by using the asymptotic method for finding the inverse Laplace transform in equation (4.12). The expression of $R(\xi)$, which has separate approximate representations in different ranges of ξ, is given by

$$
\begin{aligned}
R(\xi) &= 10^{10.35}\{\,0.513 - 0.913\,[\,1 - \exp(-1.89\xi)\,] + 0.0234\xi \\
&\quad - 0.0476\xi^2 + 0.0465\xi^3 - 0.0301\xi^4\,\}, \quad (0 \le \xi \le 0.398), \\
R(\xi) &= 10^{10.35}\{\,0.366 - 0.121\log(\xi)\,\}, \\
&\quad (0.398 \le \xi \le 70.8), \\
R(\xi) &= 10^{10.35}\{\,6.66\cdot 10^{-4} + 1.33\xi^{-1/2} - 10.6\xi^{-3/2} + 114\xi^{-5/2} \\
&\quad - 951\xi^{-7/2}\,\}, \quad (70.8 \le \xi < \infty),
\end{aligned}
\tag{4.29}
$$

where ξ is in hours. A constant value of 0.35 was assumed for the poisson ratio ν. Figure 4-2 presents the plot of $R(\xi)$ in semilogarithmic scale.

The transient stress distributions of a free plate under rapid cooling from its surfaces are shown in Figure 4-3. The corresponding temperature distributions are presented in Figure 4-4. The initial cooling of the surface leads to the contraction of the surface which produces tensile stress near the surface balanced by the compressive stress in the core region. Most of these stresses relax while the plate is still hot. The subsequent cooling, and therefore contraction, in the core region creates compressive stress near the surface also balanced by the tensile stress in the core region. Most of these stresses remain while the plate is cold.

The remaining thermal stresses in the plate after the cooling, i.e. tension in the core region balanced by the compression near the surface, are regarded as residual stresses. These stress distributions are also influenced by the cooling rate since the stress relaxation is a strong function of temperature.

Figure 4-6 presents the final stress distributions subject to different cooling

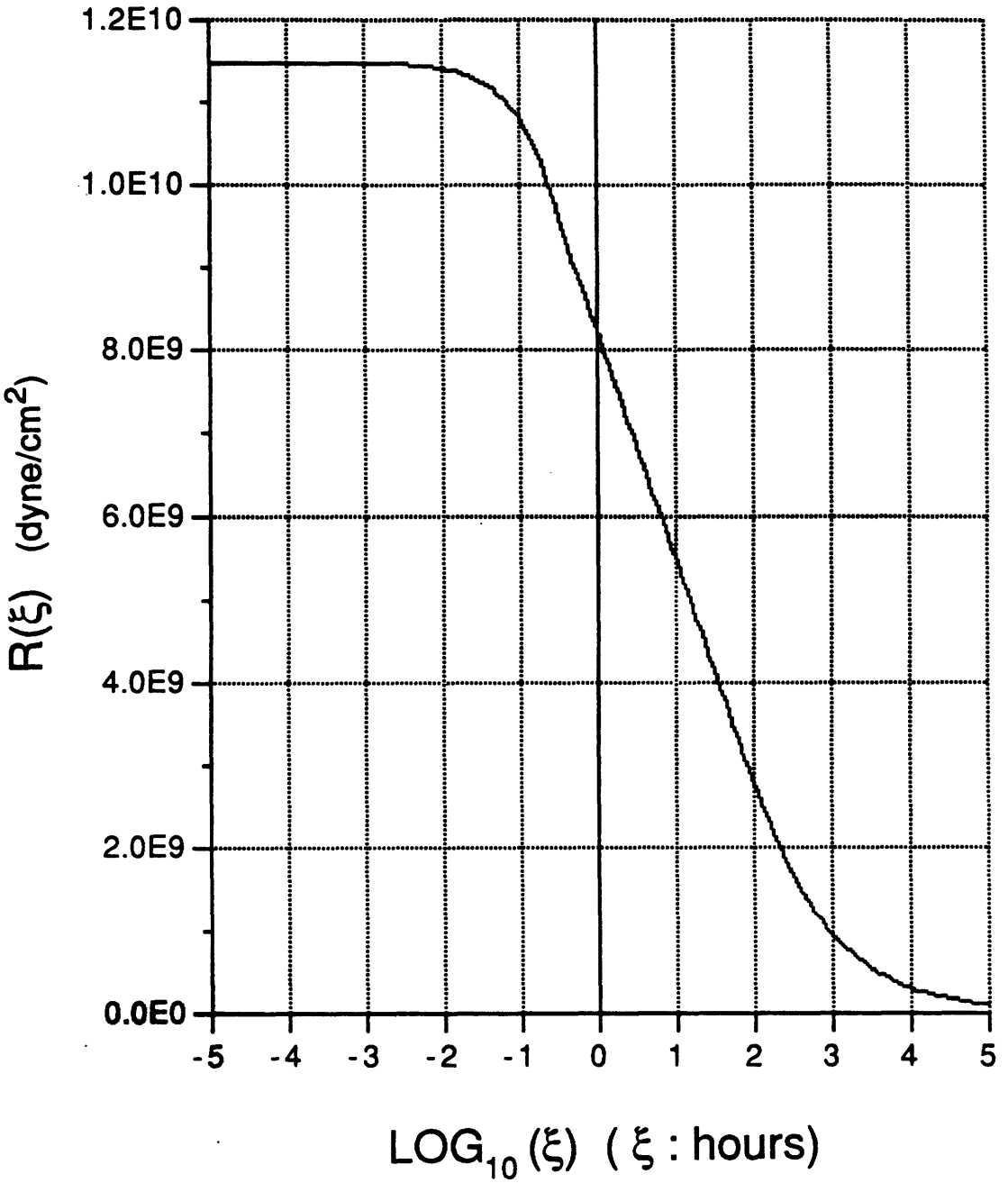

Figure 4-2: Values of $R(\xi)$ for polymethyl methacrylate at 80°C by Muki and Sternberg [27].

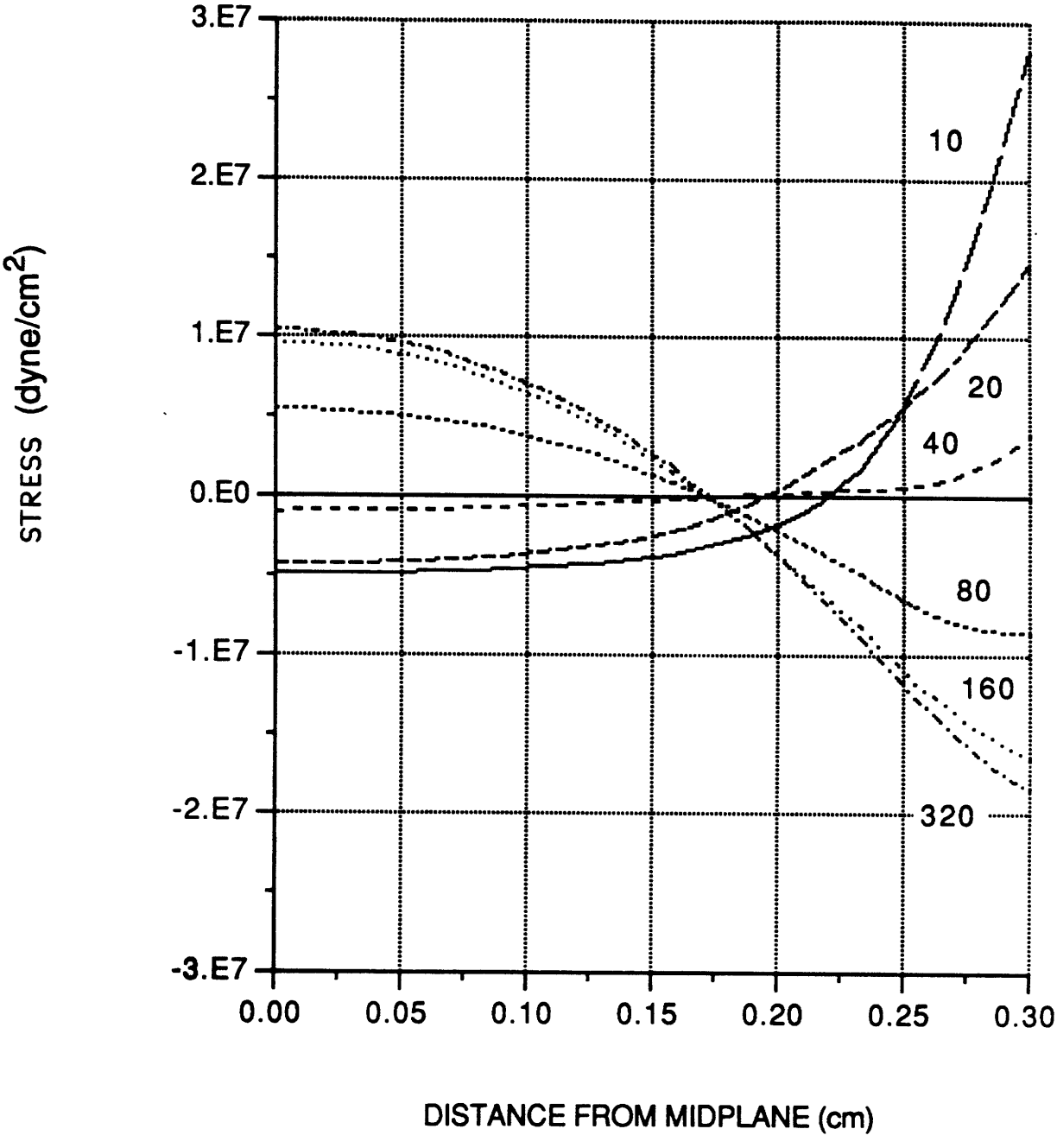

Figure 4-3: Transient Stress Distributions of a Free Plate under Rapid Cooling from Its Surfaces, 10 to 320 seconds.

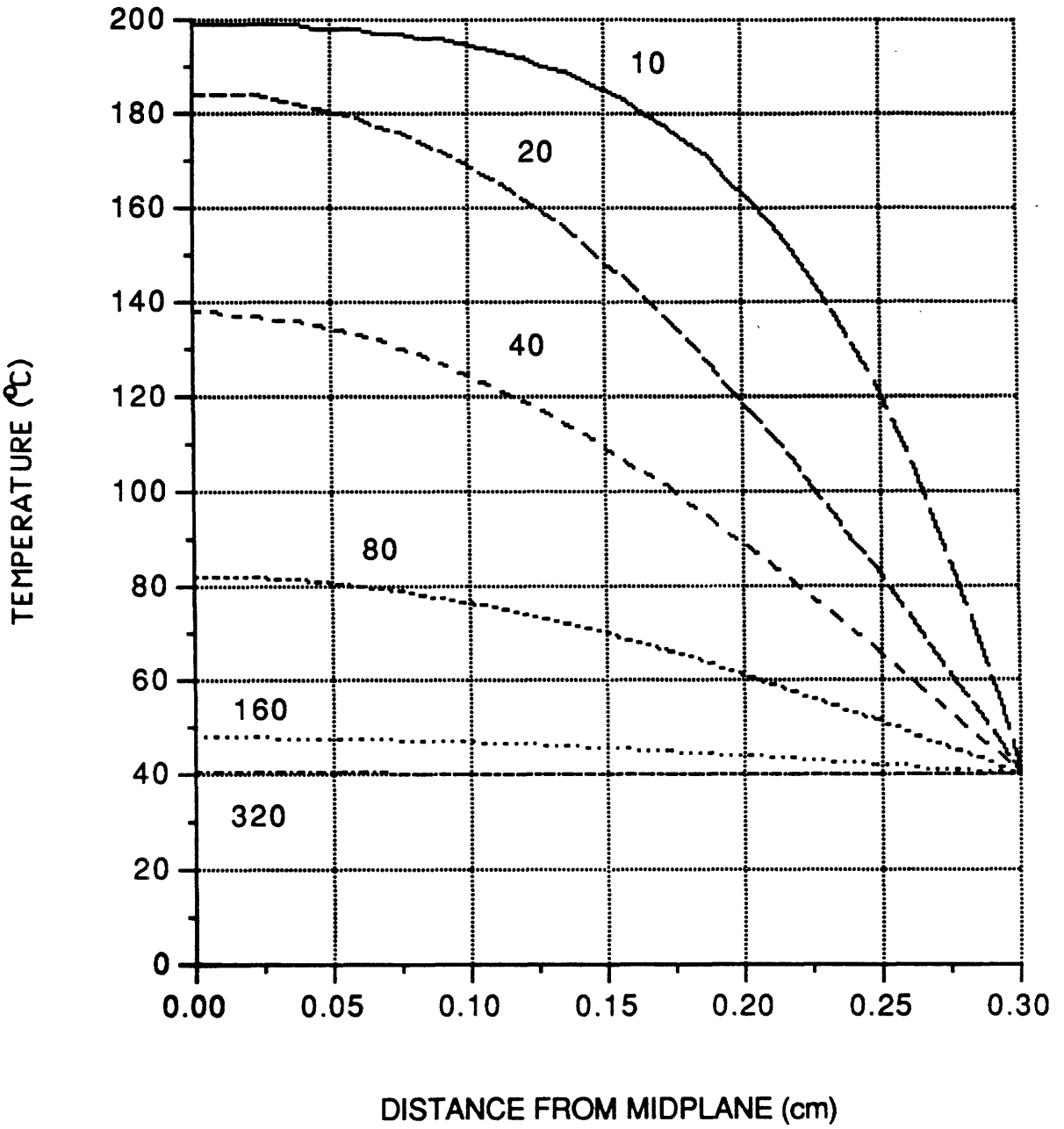

Figure 4-4: Transient Temperature Distributions of a Free Plate under Rapid Cooling from Its Surfaces, 10 to 320 seconds.

rates shown in Figure 4-5. It is clear that slower cooling results in smaller stresses because of the longer time for stress relaxation. Ideally, if the cooling time is infinite, the residual thermal stress will be zero. However, this is not possible in practice since the productivity will be greatly reduced. Therefore, finding an optimal cooling path within a specified time period is critical to both quality and productivity of injection molded parts.

4.2.2 A bounded plate

The thermal stresses of a bounded plate, which is shown in Figure 4-7, were also investigated by Muki and Sternberg [27]. Again, it is assumed that the lateral dimensions are much larger than the thickness and the lateral displacement is completely constrained.

The strain fields in the plate can then be given as

$$\epsilon_{xx} = \epsilon_{yy} = \epsilon_{xy} = \epsilon_{yz} = \epsilon_{zx} = 0, \quad \epsilon_{zz} = \frac{\partial u_z}{\partial z}. \tag{4.30}$$

The stress components in this case are

$$\sigma_{zz} = \sigma_{xy} = \sigma_{yz} = \sigma_{zx} = 0, \quad \sigma_{xx} = \sigma_{yy}. \tag{4.31}$$

The dilatational and the deviatoric strains can be given as

$$\begin{aligned} e_{xx} &= e_{yy} = -\frac{1}{3}\epsilon_{zz}, \qquad e_{zz} = \frac{2}{3}\epsilon_{zz}, \\ e_{xy} &= e_{yz} = e_{zx} = 0. \end{aligned} \tag{4.32}$$

Correspondingly, the stress components are

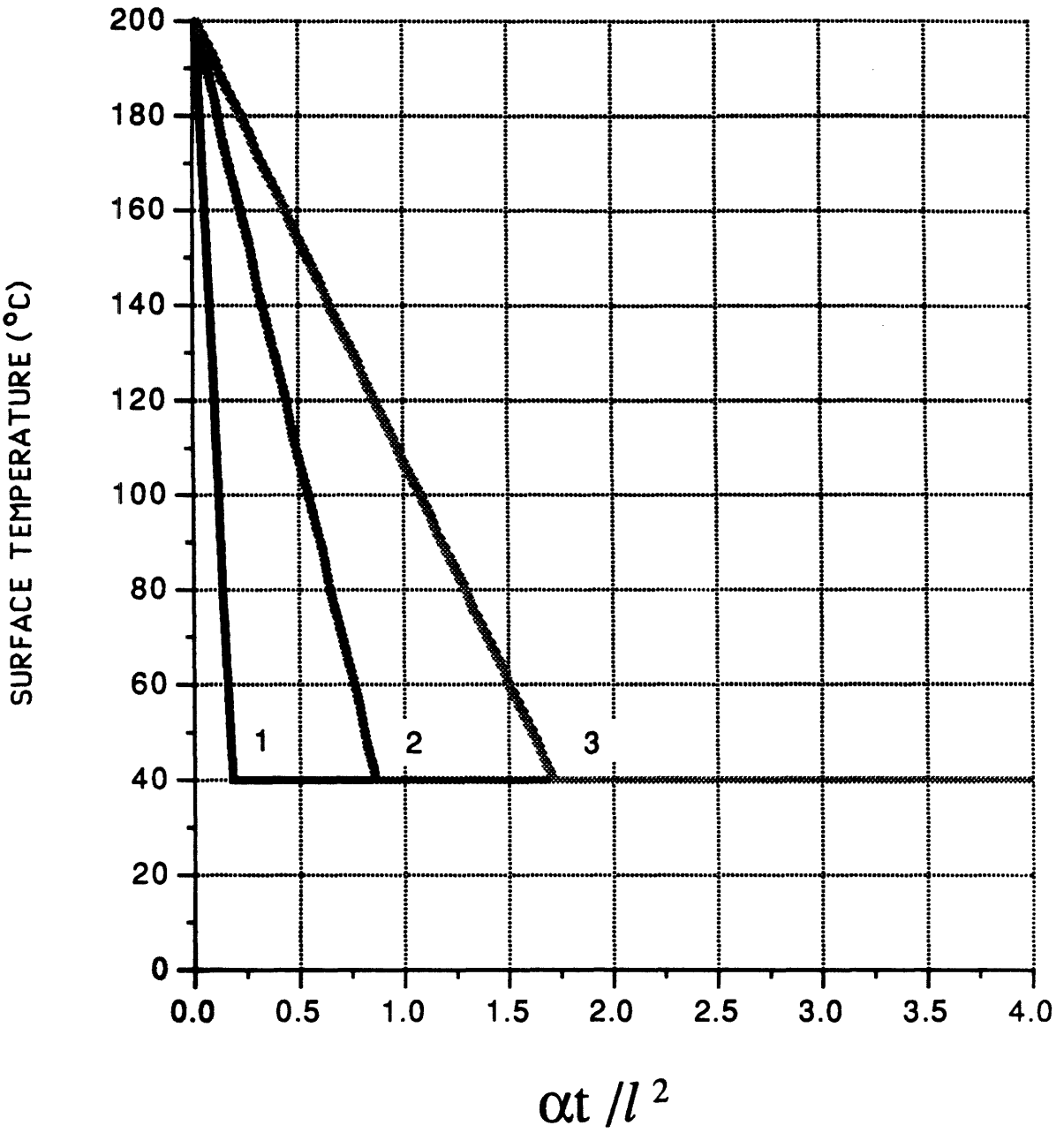

Figure 4-5: Surface Temperature Profiles of Different Cooling Rates.

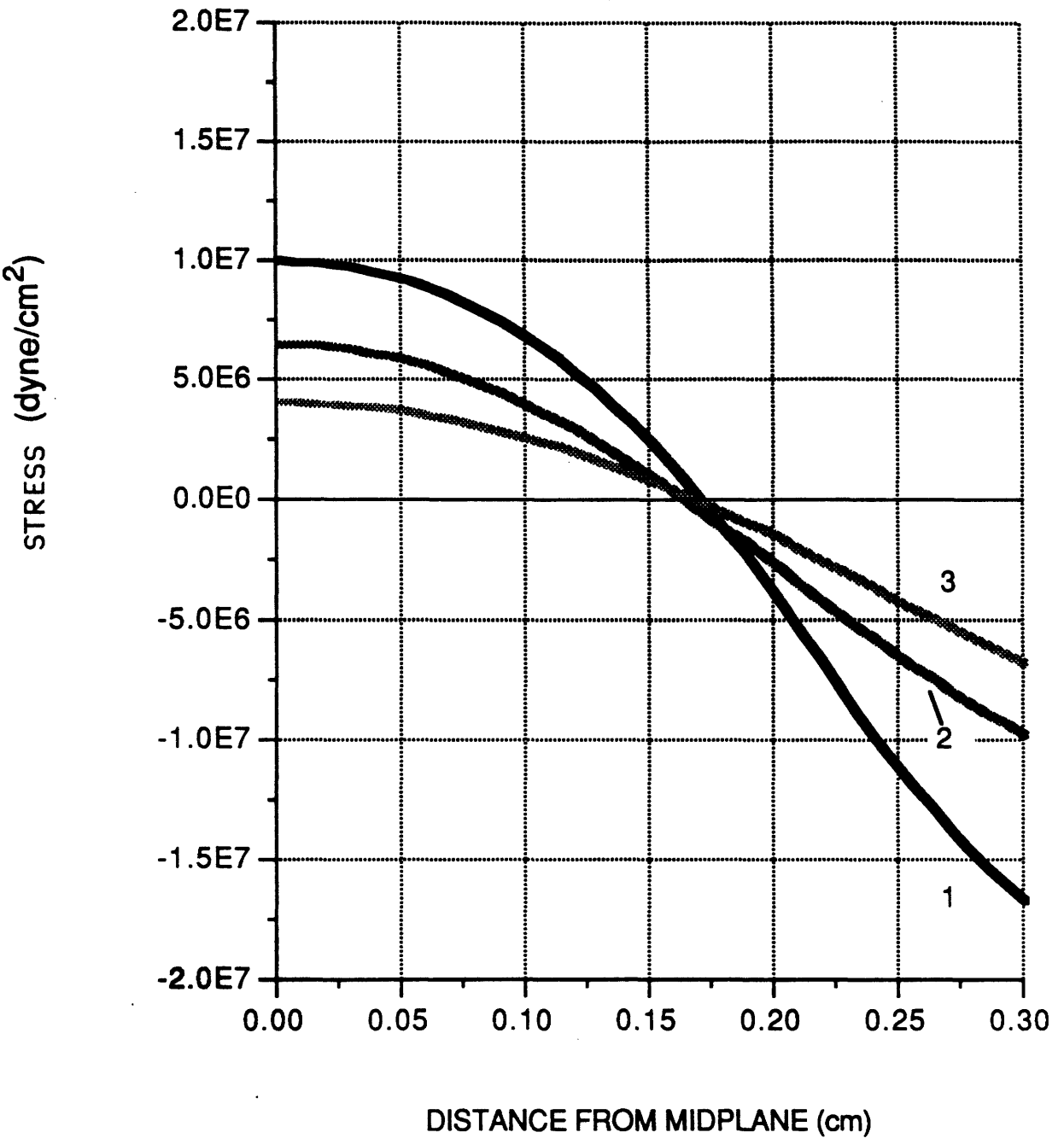

Figure 4-6: Residual Stress Distributions of a Free Plate Subject to Different Cooling Rates.

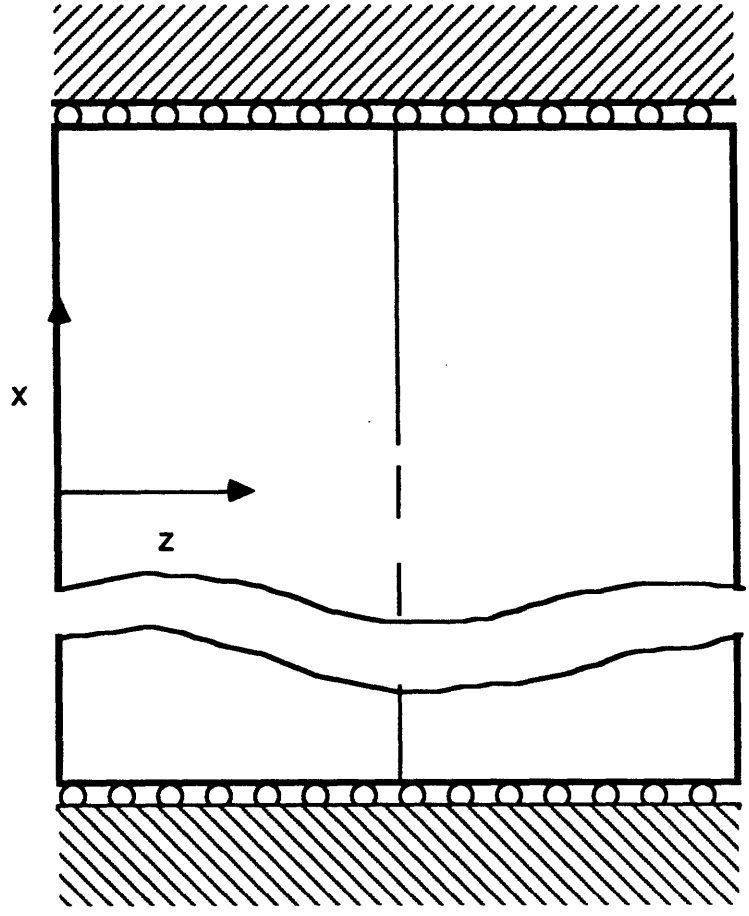

Figure 4-7: Schematic Diagram of a Bounded Plate.

$$s_{xx} = s_{yy} = \frac{1}{3}\sigma_{xx}, \qquad s_{zz} = -\frac{2}{3}\sigma_{xx},$$
$$s_{xy} = s_{yz} = s_{zx} = 0. \tag{4.33}$$

Substituting equations (4.32) and (4.33) into equation (4.1) yield the following pair of integral equations.

$$-\sigma_{xx}(z,\psi) = \int_0^{\psi} G_1(\psi-\psi')\frac{\partial}{\partial\psi'}[\epsilon_{zz}(z,\psi')]\, d\psi',$$
$$2\sigma_{xx}(z,\psi) = \int_0^{\psi} G_2(\psi-\psi')\frac{\partial}{\partial\psi'}[\epsilon_{zz}(z,\psi') - 3\alpha_o\theta(z,\psi')]\, d\psi'. \tag{4.34}$$

Applying the Laplace transform to Equation (4.34) and making use of the convolution theorem, one arrives at

$$\sigma_{xx}(z,s) = -sG_1(s)\epsilon_{zz}(z,s)$$
$$2\sigma_{xx}(z,s) = sG_2(s)[\epsilon_{zz}(z,s) - 3\alpha_o\theta(z,s)]. \tag{4.35}$$

Eliminating $\epsilon_{zz}(z,s)$ from equations (4.35), one has

$$\sigma_{xx}(z,s) = -3\alpha_o \frac{G_1(s)G_2(s)}{2G_1(s)+G_2(s)}\, s\,\theta(z,s). \tag{4.36}$$

As in the case of free plate, let

$$R(\psi) = L^{-1}\left(\frac{G_1(s)G_2(s)}{2G_1(s)+G_2(s)}\right). \tag{4.37}$$

Equation (4.36) becomes

$$\sigma_{xx}(z,\psi) = -3\alpha_o \int_0^{\psi} R(\psi - \psi')) \frac{\partial}{\partial \psi'} \theta(z,\psi')\, d\psi'. \tag{4.38}$$

By converting the reduced time ψ to physical time t, the final thermal stresses of a bounded plate can be shown as

$$\sigma_{xx}(z,t_f) = -3\alpha_o \int_0^{t_f} R(\xi(z,t)) \frac{\partial}{\partial t} \theta(z,t)\, dt, \tag{4.39}$$

$$where \quad \xi(z,t) = \int_t^{t_f} \phi(\theta(z,\lambda)\, d\lambda.$$

Another way to obtain equation (4.39) is to eliminate $\dot{\epsilon}_{xx}(t)$ from equation (4.21) since $\dot{\epsilon}_{xx}(t) = 0$ due to the mechanical constraints on the edges.

The values of $\dot{\theta}(z,t)$ calculated from equation (4.26) are used in equation (4.39) to determine the stress distributions. The functions of $\phi(\theta)$ and $R(\xi)$ used in the case of free plate are also utilized in this bounded plate.

The final stress distributions resulting from different cooling rates are shown in Figure 4-8. Figure 4-5 presents the corresponding surface temperature profiles. Tensile stresses exist across the thickness of the bounded plate because of the constraints on the edges of the plate. The surface cools the fastest and consequently has the least time for stress relaxation. Hence, the surface stress is the largest across the thickness. Slower cooling allows more stress relaxation and therefore leads to smaller stresses. However, it is not efficient to allow the cooling to last a long period of time. An optimal cooling profile within a specified time period is therefore strongly desired.

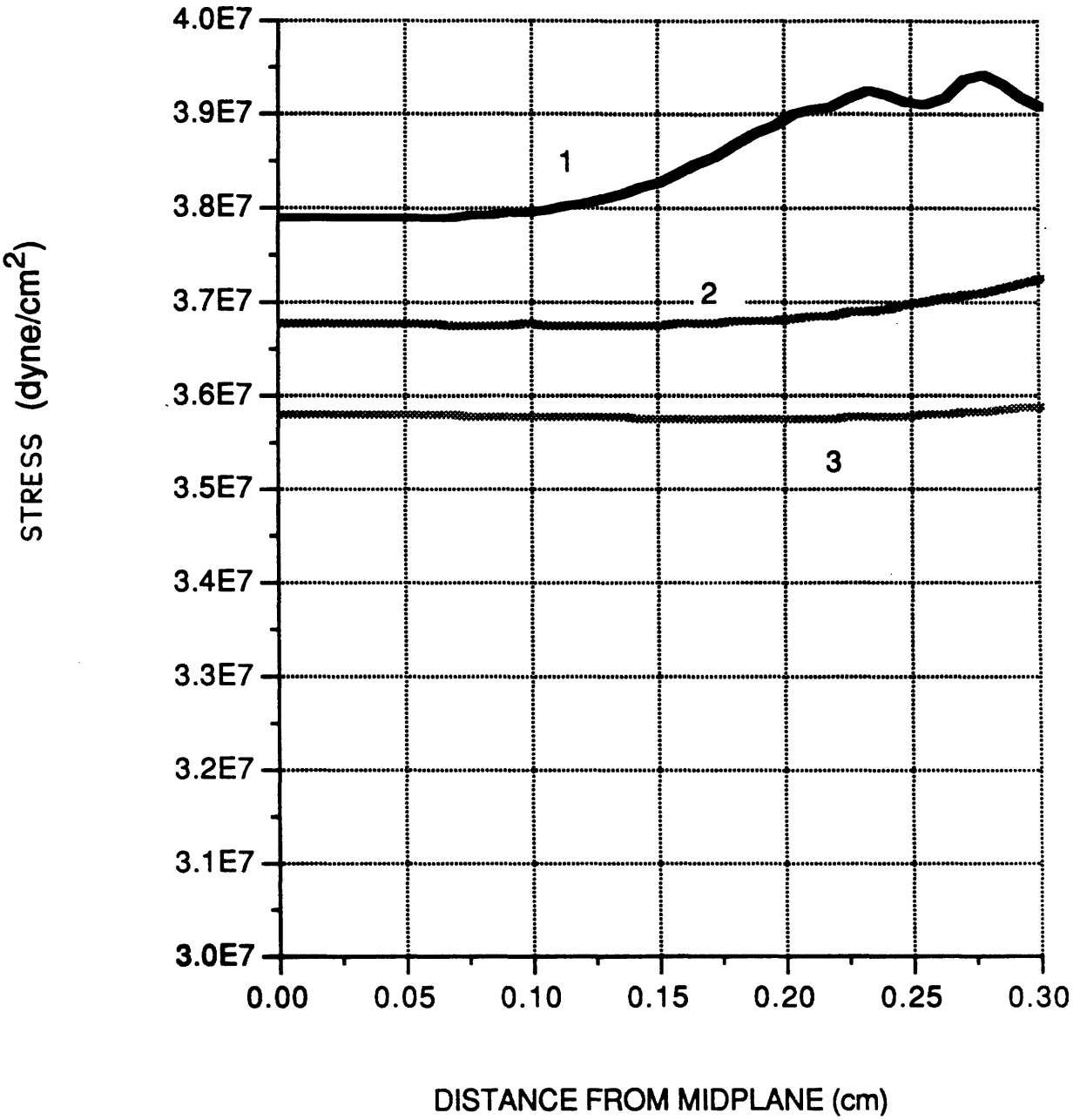

Figure 4-8: Final Stress Distributions of a Bounded Plate under Different Cooling Rates.

4.3 Optimal Cooling

When a plate of viscoelastic material is cooled symmetrically from both surfaces, the differential thermal contraction and stress relaxation produce residual thermal stresses. The thermal analyses in the previous section have shown that slower cooling led to smaller residual thermal stresses. However, slow cooling is not economically desired because it increases the cost and reduces the productivity.

Therefore, an optimal thermal history, which cools the plate from θ_o to θ_1 within a specified period $t=0$ to $t=t_f$ and results in minimal residual stresses at $t=t_f$, is critical to both the part quality and productivity. The work presents in the following assumes the temperature $\theta_w(t)$ on the surfaces of the plate can be varied as a function of time and determines the optimal thermal history of $\theta_w(t)$ for minimum residual thermal stresses.

4.3.1 A free plate

The cooling of a free plate produces compressive stresses on the surfaces and tensile stresses in the center [23, 28]. Since the stresses on the surfaces usually have the highest magnitude, it is reasonable to use the surface stress as the target for minimization in this particular analysis. However, for general case, the stress of concern is assumed to be at $z = z_o$.

The residual thermal stress at $z = z_o$ of a free plate can be obtained from equation (4.21) as

$$\sigma(z_o,t_f) = 3\int_0^{t_f} R(\xi(z_o,t))\,[\dot{\epsilon}(t) - \alpha_o\,\dot{\theta}(z_o,t)]\,dt, \tag{4.40}$$

where

α_o = *coefficient of thermal expansion,*

$\theta = T - T_o$, T_o = *initial temperature,*

$$\xi(z,t) = \int_t^{t_f} \phi(\theta(z,s))\,ds,$$

ϕ = *time–temperature shift factor,*

$$\dot{\epsilon}(t) = \frac{\alpha_o \int_0^l R(\xi(z,t))\,\dot{\theta}(z,t)\,dz}{\int_0^l R(\xi(z,t))\,dz}.$$

Equation (4.26) will be used as the system equation with the temperature as the state variables to determine the optimal cooling profile. The optimal control problem is to find an admissible control $\theta_w(t)$ that causes the system

$$\dot{\theta}(z,t) = \int_0^t \theta_w(\lambda)\frac{\partial^2}{\partial t\partial\lambda}\mathbf{f}(z,t-\lambda)\,d\lambda - \mathbf{f}(z,0)\,\theta_w(t). \tag{4.41}$$

to follow an admissible trajectory $\theta(z,t)$ which is prescribed at $t=0$ and $t=t_f$ and minimizes the residual stress expressed in equation (4.40). Half thickness of the plate is divided into n nodes and the temperatures of the nodes are the state variables. $\dot{\theta}(z,t)$, $\mathbf{f}$ and $\mathbf{f}(z,0)$ in equation (4.41), therefore, are in vector forms. A performance measure J is defined as the square of the stress at $z = z_o$ since the objective is to minimize the magnitude of the stress.

$$J = \{\int_0^{t_f} 3\,R(\xi(z_o,t))\,[\dot{\epsilon}(t) - \alpha_o\,\dot{\theta}(z_o,t)]\,\}^2. \tag{4.42}$$

The terminal constraints of this optimal control problem can be specified as

$$\theta(z,0) = 0, \quad \theta(z,t_f) = \theta_f \tag{4.43}$$

A terminal function in vector form, therefore, can be defined as

$$\mathbf{N}(\theta(z,t_f)) = \theta(z,t_f) - \theta_f = 0. \tag{4.44}$$

The difficulty of using the gradient method [3] to solve this problem is that a function $\theta(z,t)$ which satisfies equation (4.41) for an optimal $\theta_w(t)$ will not necessarily satisfy equation (4.44). In other words, the gradient method will not satisfy the boundary conditions. Thus we need to incorporate equation (4.44) directly in the gradient method. An augmented functional also in vector form, therefore, is formed as

$$\begin{aligned} \mathbf{N} &= \mathbf{N}(\theta(z,t_f)) \\ &+ \int_0^{t_f} \mathbf{Q}^T(z,t) \left[\int_0^t \theta_w(\lambda) \frac{\partial^2}{\partial t \partial \lambda} \mathbf{f}(z,t-\lambda)\, d\lambda \right. \\ &\left. - \mathbf{f}(z,0)\, \theta_w(t) - \dot{\theta}(z,t) \right] dt. \end{aligned} \tag{4.45}$$

This is accomplished by adjoining the system equation (4.41) to the N function with the Lagrange multipliers $\mathbf{Q}(z,t)$'s, where $\mathbf{Q}$ is an $n \times n$ matrix.

The approach of Bryson and Denham [3] separates the problems of minimizing J with the constraint equation (4.41), and satisfying both equation (4.41) and $\mathbf{N} = 0$ simultaneously. Applying variational calculus to these separated problems, we obtain

$$\delta J = 2\sigma \int_0^{t_f} H_u\, \delta\theta_w\, dt, \tag{4.46}$$

$$\delta \mathbf{N} = [\frac{d\mathbf{N}(\theta(z,t_f))}{d\theta(z,t_f)} - \mathbf{Q}(z,t_f)]^T \delta\theta(z,t_f)$$

$$+ \int_0^{t_f} \mathbf{G}_x{}^T \delta\theta(z,t)\, dt + \int_0^{t_f} \mathbf{G}_u\, \delta\theta_w\, dt, \tag{4.47}$$

where $\mathbf{G}_x$ is an $n \times n$ matrix and $\mathbf{G}_u$ is in vector form. The derivations of H_u,$\mathbf{G}_x$ and $\mathbf{G}_u$ are shown in Appendix A. If we let the coefficients of $\delta\theta(z,t_f)$ and $\delta\theta(z,t)$ equal zero, we have

$$\mathbf{Q}(z,t_f) = \frac{d\mathbf{N}(\theta(z,t_f))}{d\theta(z,t_f)}, \qquad \mathbf{G}_x = \dot{\mathbf{Q}}^T(z,t) = \mathbf{0}. \tag{4.48}$$

The values of $\mathbf{Q}(z,t)$ can then be determined from equation (4.48) by backward integration. $\mathbf{Q}(z,t)$ is then used in equation (A.31) to calculate $\mathbf{G}_u$. Equation (4.47) is then reduced to

$$\delta \mathbf{N} = \int_0^{t_f} \mathbf{G}_u\, \delta\theta_w\, dt. \tag{4.49}$$

Before every iteration in gradient method, values of δN are chosen so that $N(\theta(z,t_f))$ will be closer to zero after that iteration. In other words, values of $\theta(z,t_f)$ are expected to get closer to θ_f after every iteration. The values of $\delta\mathbf{N}$ may be chosen by $\delta\mathbf{N} = -\mu\,\mathbf{N}(\theta(t_f))$, $0 < \mu \leq 1$. Therefore in every iteration, $\delta\theta_w$ is expected to create a specified change of $\delta\mathbf{N}$ in equation (4.49) and also to have a minimum value of δJ in equation (4.46).

The minimization of δJ subject to constraints (4.49) can be achieved by adjoining (4.49) to (4.46) by Lagrange multipliers. However, since equations (4.46) and (4.49) are linear equations, there is no minimum for δJ subject to constraints on the size of $\delta\mathbf{N}$. A method for creating a minimum is to add a quadratic integral

penalty function in $\delta\theta_w$ to (4.46),

$$\delta J_1 = \delta J + \frac{1}{2}\int_0^{t_f} \delta\theta_w W\, \delta\theta_w\, dt, \tag{4.50}$$

where W is an arbitrary positive-definite weighting factor and is used to adjust the step size of every iteration. Therefore, adjoining (4.49) to (4.50) with constant Lagrange multipliers **S**, which is in vector form, results in

$$J_2 = \delta J_1 + \mathbf{S}^T\Big(\int_0^{t_f} \mathbf{G}_u\, \delta\theta_w\, dt - \delta\mathbf{N}\Big). \tag{4.51}$$

The first variation of equation (4.51) gives

$$\delta J_2 = \int_0^{t_f} [2\,\sigma\, H_u + \delta\theta_w W + \mathbf{S}^T\mathbf{G}_u]\,\delta(\delta\theta_w)\, dt. \tag{4.52}$$

A minimum of δJ_2 occurs if

$$2\,\sigma\, H_u + \delta\theta_w W + \mathbf{S}^T\mathbf{G}_u = 0. \tag{4.53}$$

Rearranging equation (4.53) for $\delta\theta_w$ leads to

$$\delta\theta_w = -\,W^{-1}\,(2\,\sigma\, H_u + \mathbf{S}^T\mathbf{G}_u). \tag{4.54}$$

Equation (4.54) gives the values of $\delta\theta_w$ for every numerical iteration in

$$\theta_w^{\,i+1} = \theta_w^{\,i} + \delta\theta_w(t) \tag{4.55}$$

The weighting factor $W(t)$ is obviously used to adjust the step size in every iteration. The values of the vector $\mathbf{S}$ in equation (4.54) are yet to be determined. Substituting (4.54) into (4.49) leads to

$$\delta \mathbf{N} = -\mathbf{K}_{GH} - \mathbf{K}_{GG}\,\mathbf{S}, \tag{4.56}$$

where $\mathbf{K}_{GH}$, a vector, and $\mathbf{K}_{GG}$, an $n \times n$ matrix, are defined as

$$\mathbf{K}_{GH} = \int_0^{t_f} (2\sigma H_u)\, W^{-1}\, (\mathbf{G}_u)\, dt,$$

$$\mathbf{K}_{GG} = \int_0^{t_f} (\mathbf{G}_u)\, W^{-1}\, (\mathbf{G}_u)^T\, dt. \tag{4.57}$$

If $\mathbf{K}_{GG}$ is not singular, equation (4.56) can be solved for the required value of $\mathbf{S}$.

$$\mathbf{S} = -\mathbf{K}_{GG}^{-1}(\,\delta \mathbf{N} + \mathbf{K}_{GH}\,). \tag{4.58}$$

Finally, δJ can be found by substituting (4.54) and (4.58) into (4.46), which gives

$$\delta J = -(\,K_{HH} - \mathbf{K}_{HG}\,\mathbf{K}_{GG}^{-1}\mathbf{K}_{HG}^{T}\,) + \mathbf{K}_{HG}\,\mathbf{K}_{GG}^{-1}\,\delta \mathbf{N}. \tag{4.59}$$

where K_{HH}, in scalar form, is defined as

$$K_{HH} = \int_0^{t_f} (2\sigma H_u)\, W^{-1}\, (2\sigma H_u)\, dt. \tag{4.60}$$

The first and second terms on the right hand side of equation (4.59) should equal zero to the desired degree of accuracy when the optimal condition is reached. The choice of $W(t)$ in equation (4.54) should be made by comparing the actual values of $\delta \mathbf{N}$ and δJ with the predicted values from equations (4.56) and (4.59). If the

differences are too large, W should be increased, or vice versa.

The numerical procedure of the first-order gradient algorithm for solving this opimal cooling problem can be summarized in the block diagram given in Table 4-I. The numerical iteration begins with making an initial guess for $\theta_w(t)$, $0 \leq \theta_w(t) \leq t_f$. The thermal field $\theta(z,t)$ is then determined by integrating the system equations (4.41) with the initial condition $\theta(z,0) = 0$. The shift factor $\phi(\theta(z,t))$, reduced time ξ and relaxation modulus $R(\xi)$ are computed from equations (4.28), (4.40) and (4.29) respectively.

Subsequently, the values of $\mathbf{N}(\theta(z,t_f))$ are calculated by equation (4.44). At the same time, $\mathbf{Q}(z,t)$ can be determined from (4.48) by backward integration. The values of $\mathbf{Q}(z,t)$ are then used to calculate $\mathbf{G}_u$ in equation (A.31). H_u is obtained from equation (A.23). Values of $\mathbf{K}_{HG}$, $\mathbf{K}_{GG}$ and $\mathbf{K}_{HH}$ are then computed from equations (4.57) and (4.60).

The desired values of δN in every iteration are chosen by $\delta\mathbf{N} = -\mu\,\mathbf{N}(\theta(z,t_f))$, $0 < \mu \leq 1$. Once values of $\delta\mathbf{N}$ are specified, $\mathbf{S}$ is then calculated using equation (4.58). Finally, $\delta\theta_w(t)$ is determined from equation (4.54), and used to correct the value of θ_w by $\theta_w^{\,i+1} = \theta_w^{\,i} + \delta\theta_w(t)$. $\theta_w^{\,i+1}$ is then used as the new guess to repeat the numerical iterations until the first and second terms of equation (4.59) equal zero to the desired degree of accuracy.

Figure 4-9 shows the initial guess of the surface temperature history and the optimal cooling path obtained from the numerical iterations for minimum surface stress. The surface temperature had to drop the final temperature well before the final time to allow the temperature inside the plate to reach the final temperature at the final time. The final stress distributions which result from these two thermal histories are presented in Figure 4-10. In this particular case, the magnitude of surface stress is used as the target of minimization because it is always the largest

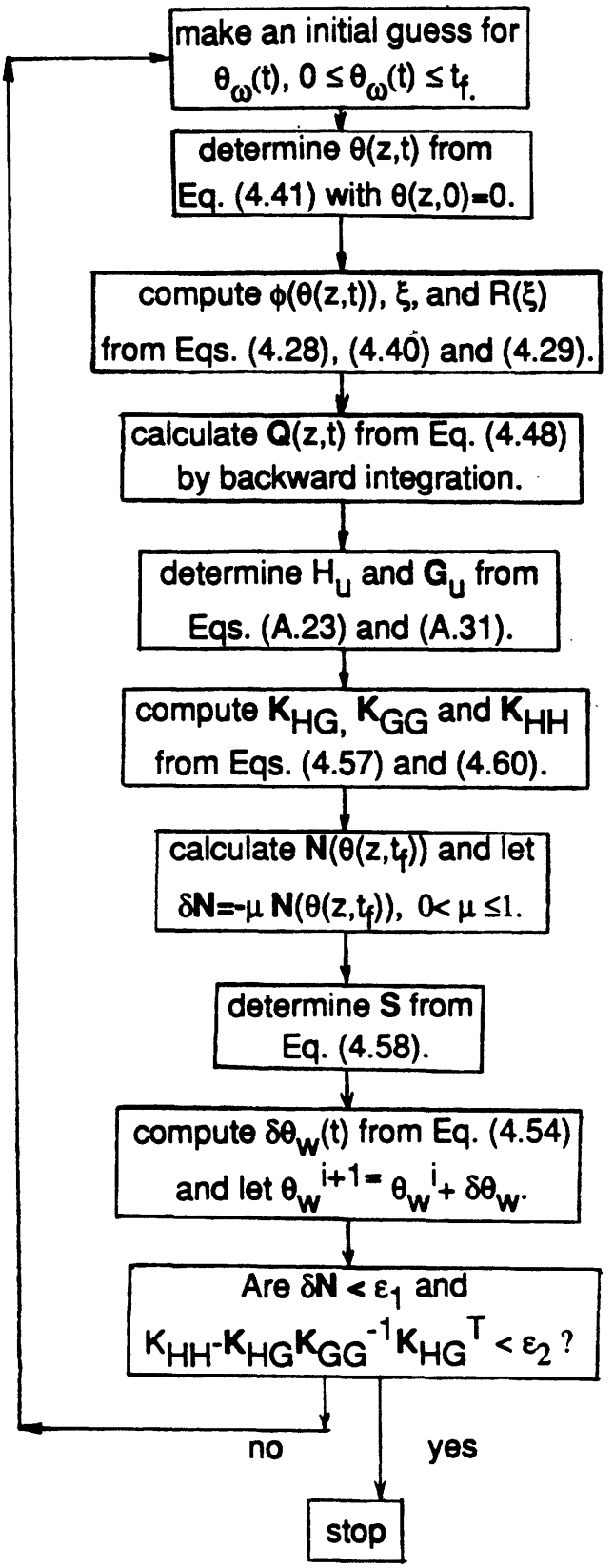

Table 4-I: Block Diagram of the Numerical Iterations.

across the thickness and is critical to the surface dimensions. The optimal cooling profile reduces the magnitude of surface stress significantly as compared with the stress resulting from very rapid cooling (Figure 4-6).

The physical insights of this optimal cooling profile are explained as follows. When the cooling has proceeded to near the final stage, the stress state is tensile in the core region and compressive on the surface. A short term surface reheating expands the surface and produces an even larger compressive stress. Larger compressive stress allows more stress relaxation because the stress relaxation for viscoelastic materials follows roughly an exponential decay.

The surface reheating also raises the surface temperature and consequently allows faster stress relaxation. The effects of higher temperature and larger amount of stress allow more and faster stress relaxation, and therefore reduce the surface stress to a minimum. The extent of the surface reheating is also critical to the final stress magnitude. Too much reheating will also raise the temperature in the core region while insufficient reheating will result in larger compressive stress on the surface.

This optimal cooling path is initial-guess dependent. If a different initial guess of surface temperature profile (Figure 4-11) is given instead, the optimal temperature path obtained from the numerical iteration will be different. This alternative can also reduce the surface stress significantly (Figure 4-12). Therefore, many local minimums exist in this particular problem and nearly every minimum can reduce the surface stress significantly. This occurs because the plate is free to contract during the cooling process. No mechanical constraint exists on its edges and the target of minimization is the stress magnitude at a given point across the thickness only. In general, the characteristics of the optimal cooling path for minimizing the surface stress of a free plate presents a short period of surface reheating.

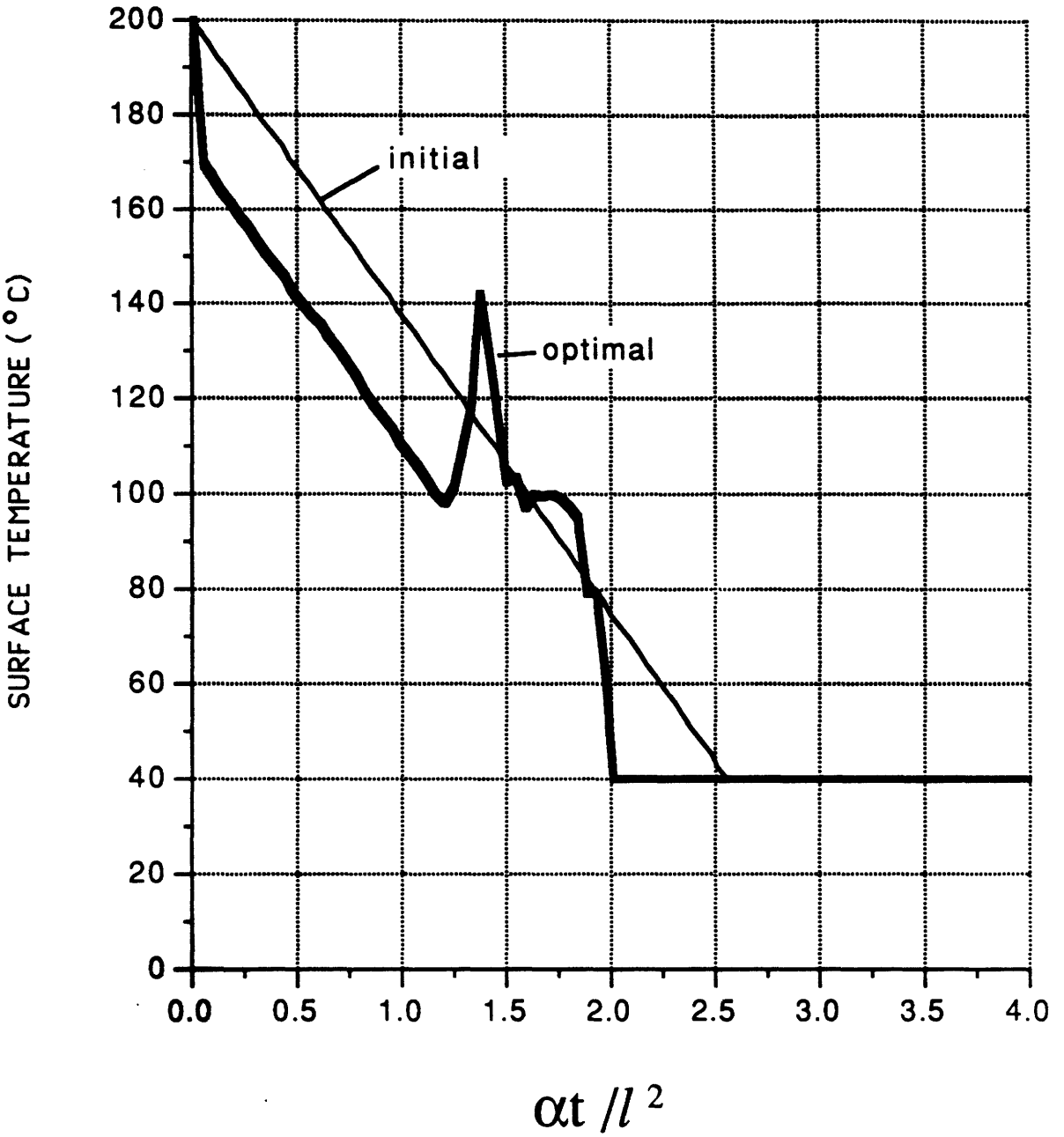

Figure 4-9: The Initial Guess of Surface Temperature and the Optimal Cooling Path Resulting from Numerical Iterations.

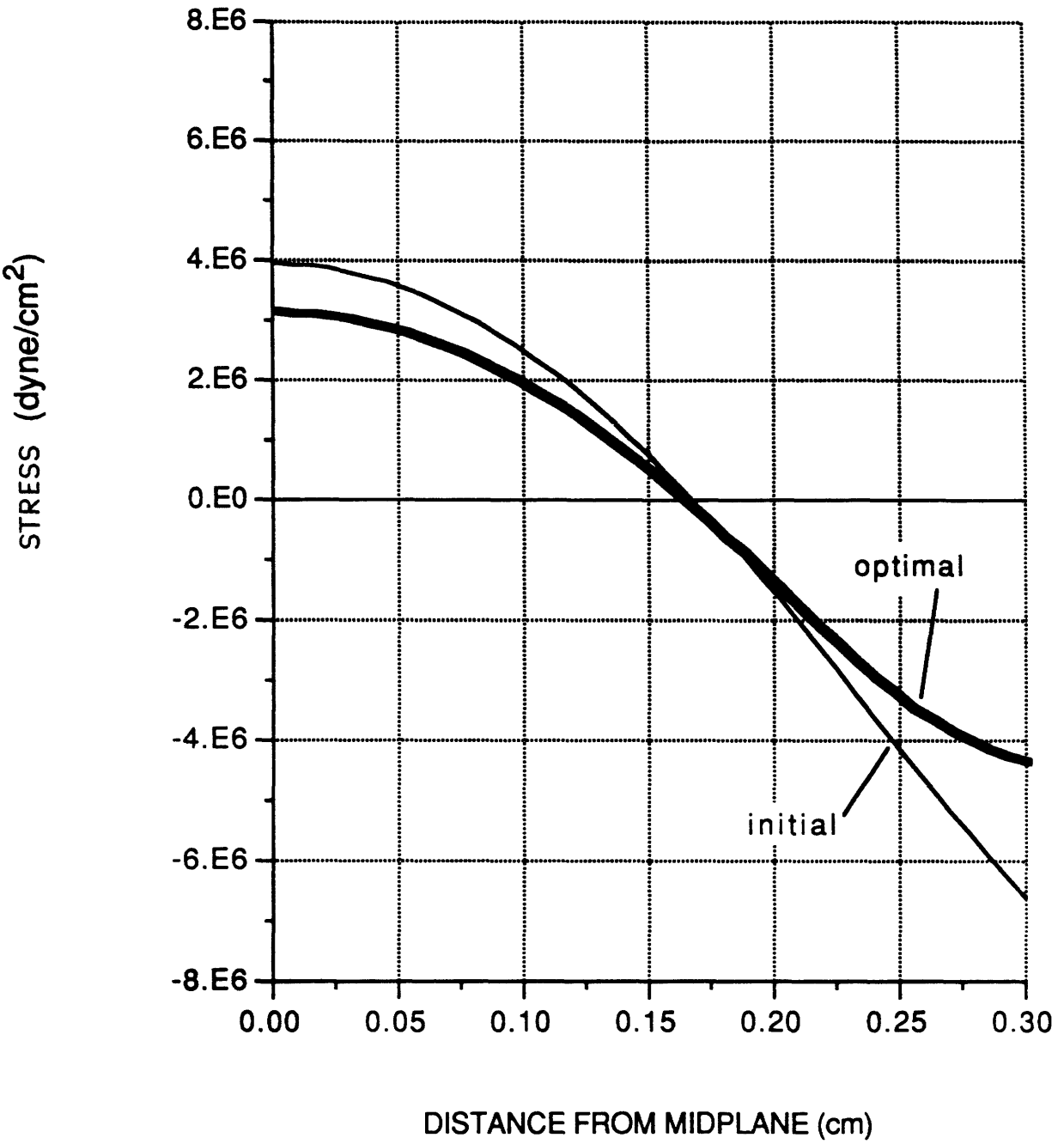

Figure 4-10: The Final Stress Distributions Resulting from the Thermal Histories in Figure 4-9.

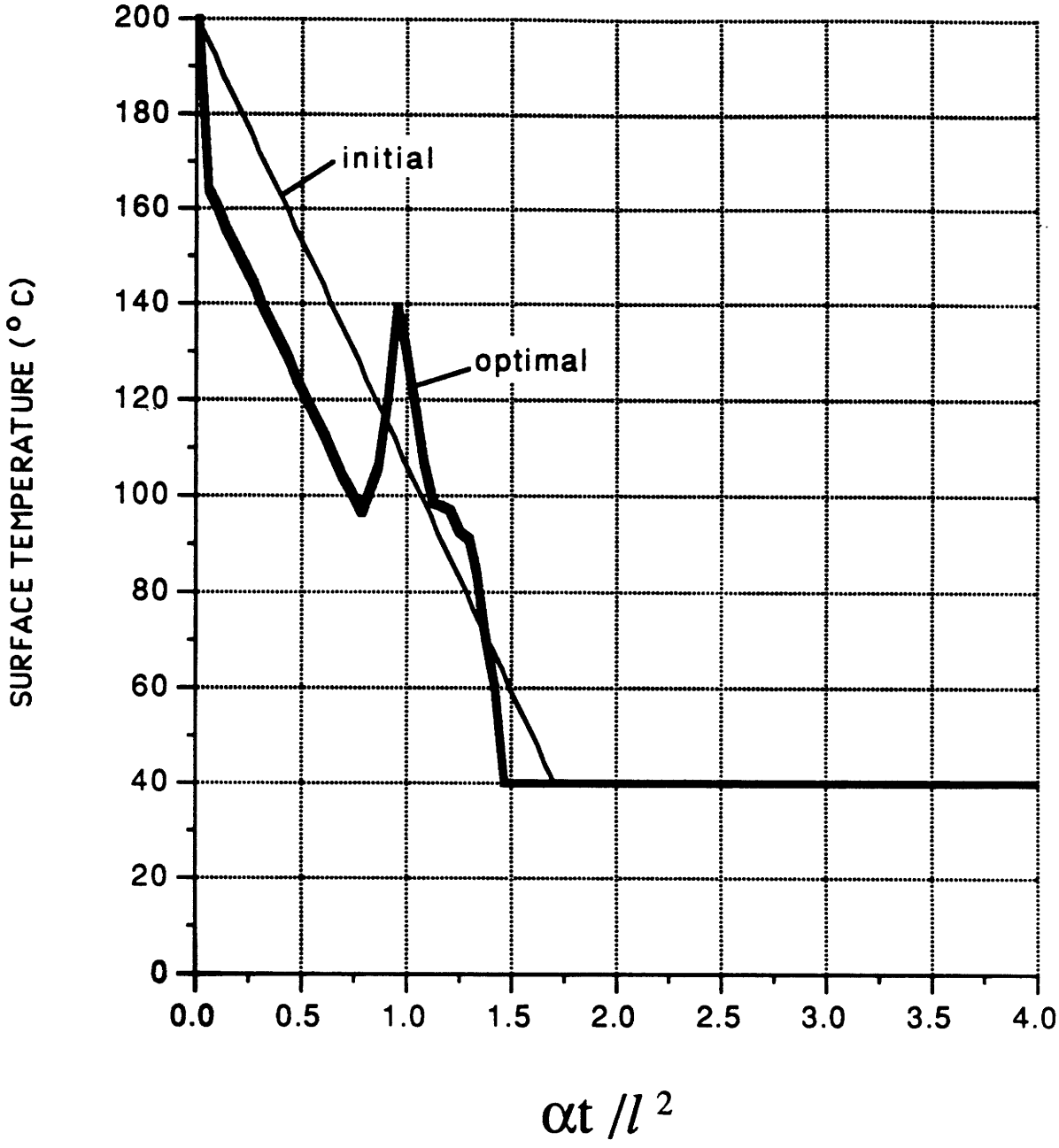

Figure 4-11: The Initial Guess of Surface Temperature and the Optimal Cooling Path Resulting from Numerical Iterations.

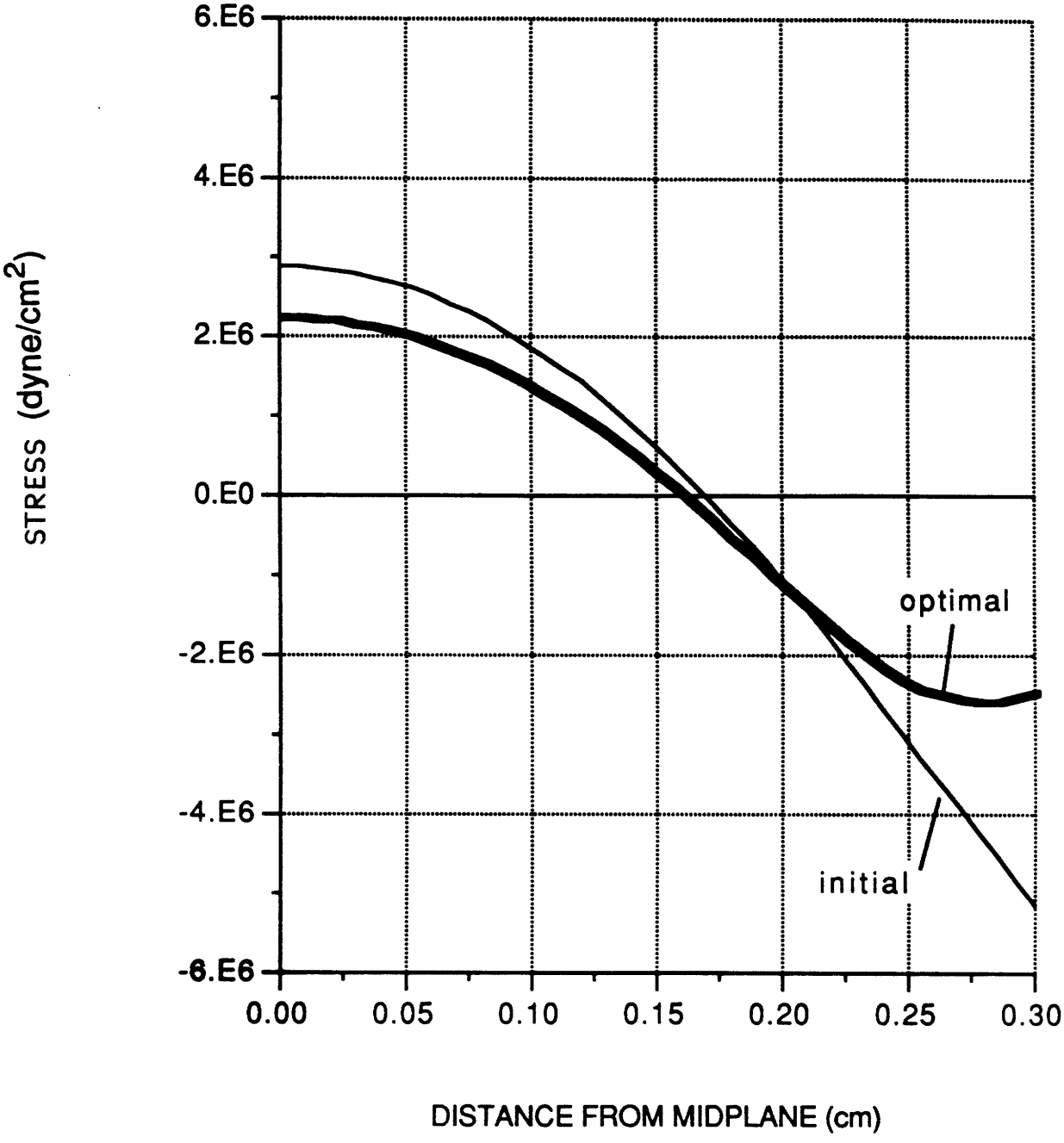

Figure 4-12: The Final Stress Distributions Resulting from the Thermal Histories in Figure 4-11.

The optimal cooling profile for minimizing the entire stress field rather than the stress at a given point should also be investigated. In this case, the summation of the stress magnitude at every node across the thickness is defined as the performance measure J. Therefore, the optimal cooling profile for minimizing the entire stress field would be the superposition of the optimal profile for minimizing the stress at every point across the plate.

In order to obtain a smooth profile from superposition, the number of nodes across the thickness should be substantially increased and the time step should be decreased. However, the computing time to determine H_u is increased by orders of magnitude due to the multiple integrals in H_u and the newly-defined performance measure J. This study is left as the future work using much faster computing machine.

4.3.2 A bounded plate

The final thermal stress at $z = z_o$ of a bounded plate can be rewritten from equation (4.39) as

$$\sigma(z_o,t_f) = -3\alpha_o \int_0^{t_f} R(\xi(z_o,t))\,\theta(z_o,t)\,dt, \tag{4.61}$$

where

α_o = *coefficient of thermal expansion,*

$\theta = T - T_o$, T_o = *initial temperature,*

$\xi(z_o,t) = \int_t^{t_f} \phi(\theta(z_o,s))\,ds,$

ϕ = *time–temperature shift factor.*

Since the material on the surface cools the fastest, which implies the least stress

relaxation, the final thermal stress on the surface is expected to be the largest across the thickness of the plate. Therefore, it is reasonable to choose the final stresses on the surface as the target for minimization.

Since the magnitude of stress is to be minimized, a performance measure I is defined as the square of the stress at the target $z = z_o$.

$$I = \{-3\alpha_o \int_0^{t_f} R(\xi(z_o,t))\,\theta(z_o,t)\,dt\}^2. \tag{4.62}$$

The same system equation for temperature which was used in the case of free plate will also be used here.

$$\theta(z,t) = \int_0^t \theta_w(\lambda) \frac{\partial^2}{\partial t \partial \lambda} \mathbf{f}(z,t-\lambda)\,d\lambda - \mathbf{f}(z,0)\,\theta_w(t). \tag{4.63}$$

The initial state is $\theta(z,0) = 0$, while the final state is given by $\theta(z,t_f) = \theta_f$. As in the free plate, a terminal function can also be defined as

$$\mathbf{N}(\theta(z,t_f)) = \theta(z,t_f) - \theta_f = 0. \tag{4.64}$$

Furthermore, an augmented functional $\mathbf{N}$ should also be formed.

$$\begin{aligned}\mathbf{N} &= \mathbf{N}(\theta(z,t_f)) \\ &+ \int_0^{t_f} \mathbf{Q}^T(z,t)\,[\int_0^t \theta_w(\lambda) \frac{\partial^2}{\partial t \partial \lambda} \mathbf{f}(z,t-\lambda)\,d\lambda - \mathbf{f}(z,0)\,\theta_w(t) \\ &- \dot{\theta}(z,t)\,]\,dt.\end{aligned} \tag{4.65}$$

The first variation of equations (4.62) and (4.65) gives

$$\delta J = 2\sigma \int_0^{t_f} F_u\,\delta\theta_w\,dt. \tag{4.66}$$

$$\delta \mathbf{N} = \left[\frac{d\mathbf{N}(\theta(z,t_f))}{d\theta(z,t_f)} - \mathbf{Q}(z,t_f) \right]^T \delta\theta(z,t_f)$$

$$+ \int_0^{t_f} \mathbf{G}_x{}^T \delta\theta(z,t)\, dt + \int_0^{t_f} \mathbf{G}_u\, \delta\theta_w\, dt. \qquad (4.67)$$

Note that equation (4.67) is identical to equation (4.47). Moreover, by comparing equations (4.42) and (4.62), it is clear that the only difference is in the $\dot{\epsilon}(t)$ term. Therefore, F_u is given by the first three terms of H_u presented in equation (A.23) of Appendix A. G_x and G_u are also shown in Appendix A. With F_u, G_x and G_u known, the same algorithm used in the solution of free plate can be employed to iterate the optimal cooling path.

Figure 4-13 shows the final thermal stress distributions across half the plate resulting from quenching, linear and optimal coolings. The corresponding temperature profiles are given in Figure 4-14. In this case, the surface stress was minimized. Quenching produces the largest surface stress while the optimal cooling gives the smallest stress on the surface.

The optimal cooling profile presents an initial rapid cooling followed by a slower cooling for most of the cooling period. Since every node across the thickness should reach the final temperature θ_f at $t = t_f$, θ_w should reach θ_f well before t_f. Although the final temperature jump would produce surface stress that cannot relax, the optimal cooling still produces minimum final stress.

The optimal cooling profile for minimizing the entire stress field across the thickness, rather than the stress at a given point, is presented in Figure 4-16. In other words, the summation of the stress at every node across the thickness is defined as the performance measure J. The initial jump of the surface temperature is larger in this case than that in Figure 4-14 in order for the average temperature across the thickness to follow the same profile shown in Figure 4-14 because the

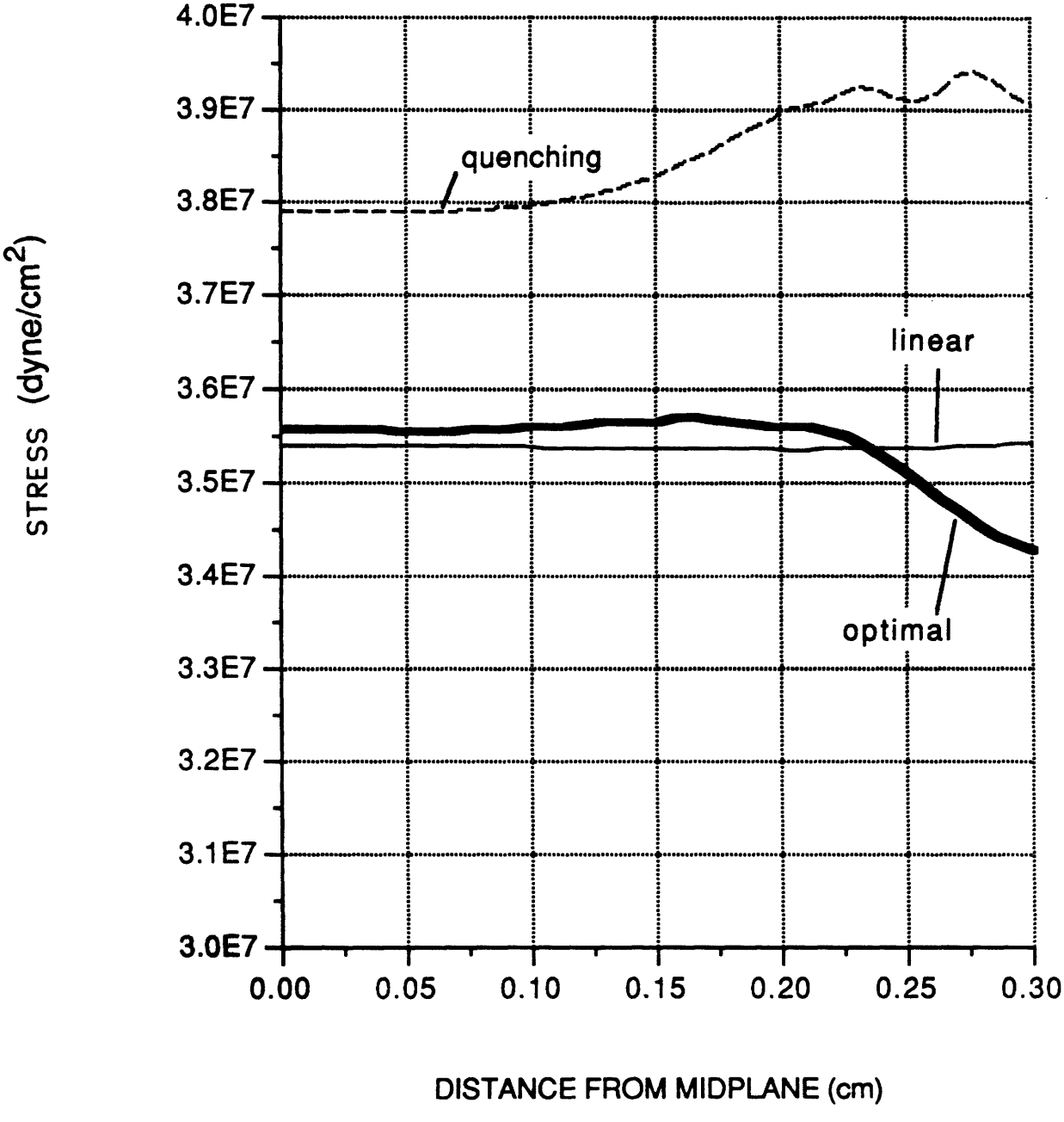

Figure 4-13: Final Thermal Stresses from Quenching, Linear and Optimal Coolings for Minimum Surface Stress.

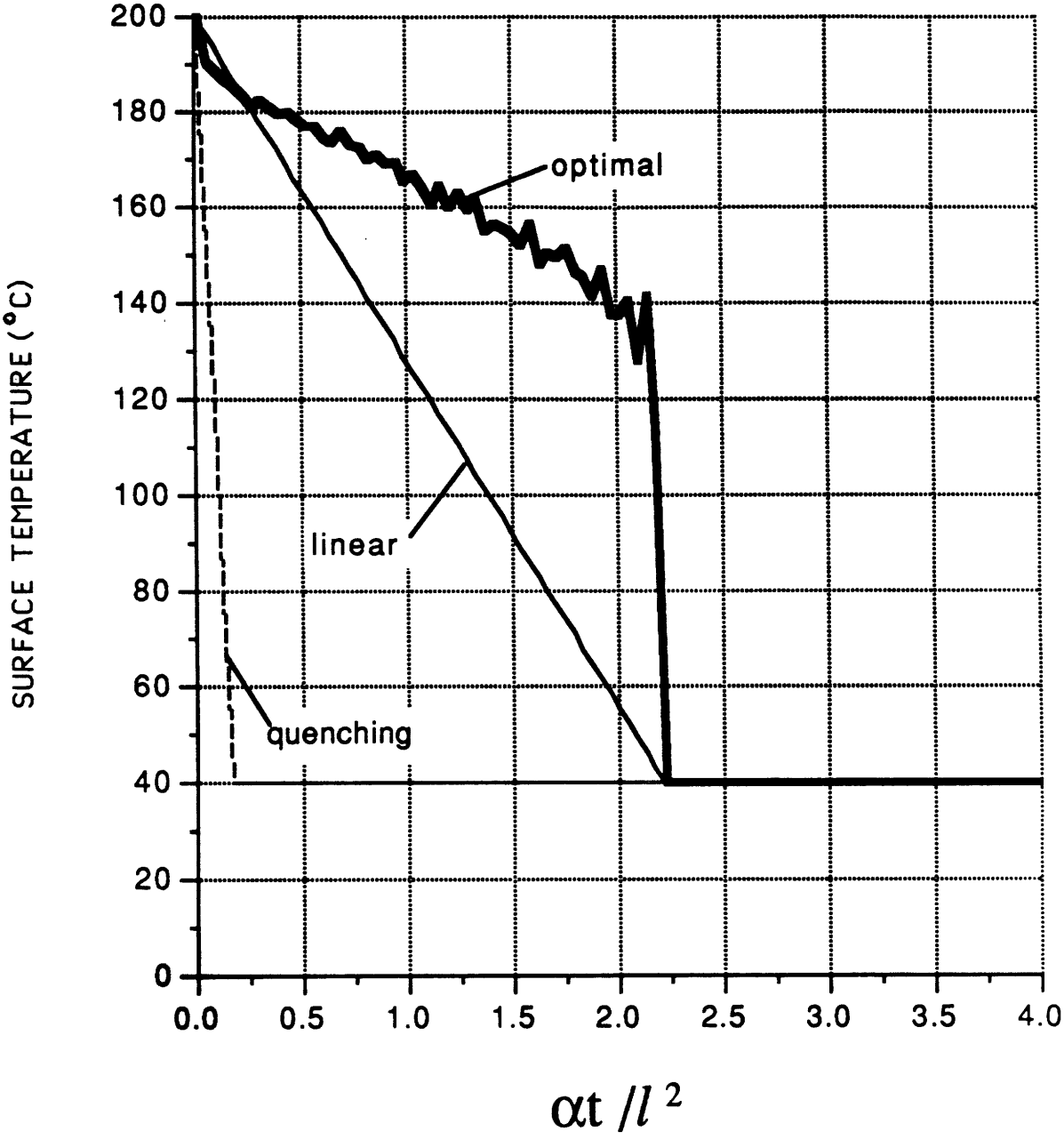

Figure 4-14: Temperature Profiles of Quenching, Linear and Optimal Coolings for Minimum Surface Stress.

entire stress field is minimized.

The resulting stress distribution is given in Figure 4-15. Obviously, the entire stress field is smaller than that in Figure 4-13 since it is the target of minimization. However, the surface stress is larger than that in Figure 4-13 because the surface stress rather that the entire stress field is minimized in Figure 4-13. The focus of minimization in Figure 4-13 is the surface stress while that in Figure 4-15 is the summation of stress across the thickness.

The physical insight of the optimal cooling is explained in the following. Since the initial and final temperatures are fixed, the total thermal strain resulting from the cooling of a bounded plate is constant. In order to have minimum final thermal stress, maximum stress relaxation should be achieved during the cooling cycle, which is constrained from t_o to t_f. Since the period of cooling is also fixed, producing more strain and therefore more stress in the very early stage would allow a longer period for stress relaxation. Therefore, a rapid cooling in the very beginning is desired.

The degree of the temperature jump in the initial cooling also affects the relaxation because relaxation time constant increases with decreasing temperature. If the surface of the plate is cooled quickly to the final temperature in the beginning, only a small amount of stress will relax because of the low temperature. Although this has produced more stress in the beginning and left a longer period for stress relaxation, the stress remains frozen in.

On the other hand, if the initial jump is small, the small stress resulting from this small thermal strain would relax quickly due to the high temperature. However, the large stress resulting from the final temperature jump would not have time to relax. The trade-off between thermal strain and temperature has led to the optimal temperature path that the surface should follow during most of the cooling

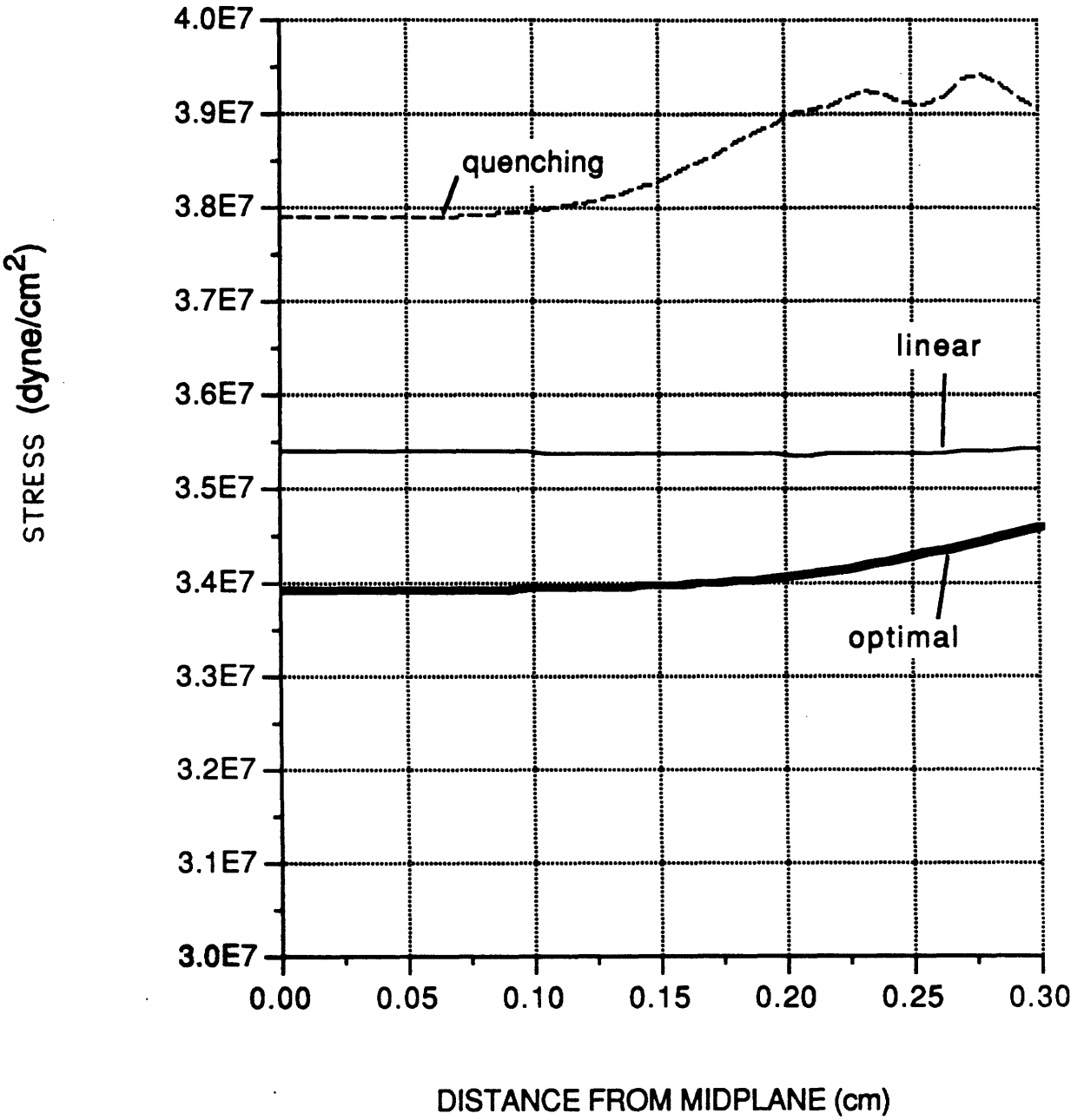

Figure 4-15: Final Thermal Stresses from Quenching, Linear and Optimal Coolings for Minimum Entire Stress Field.

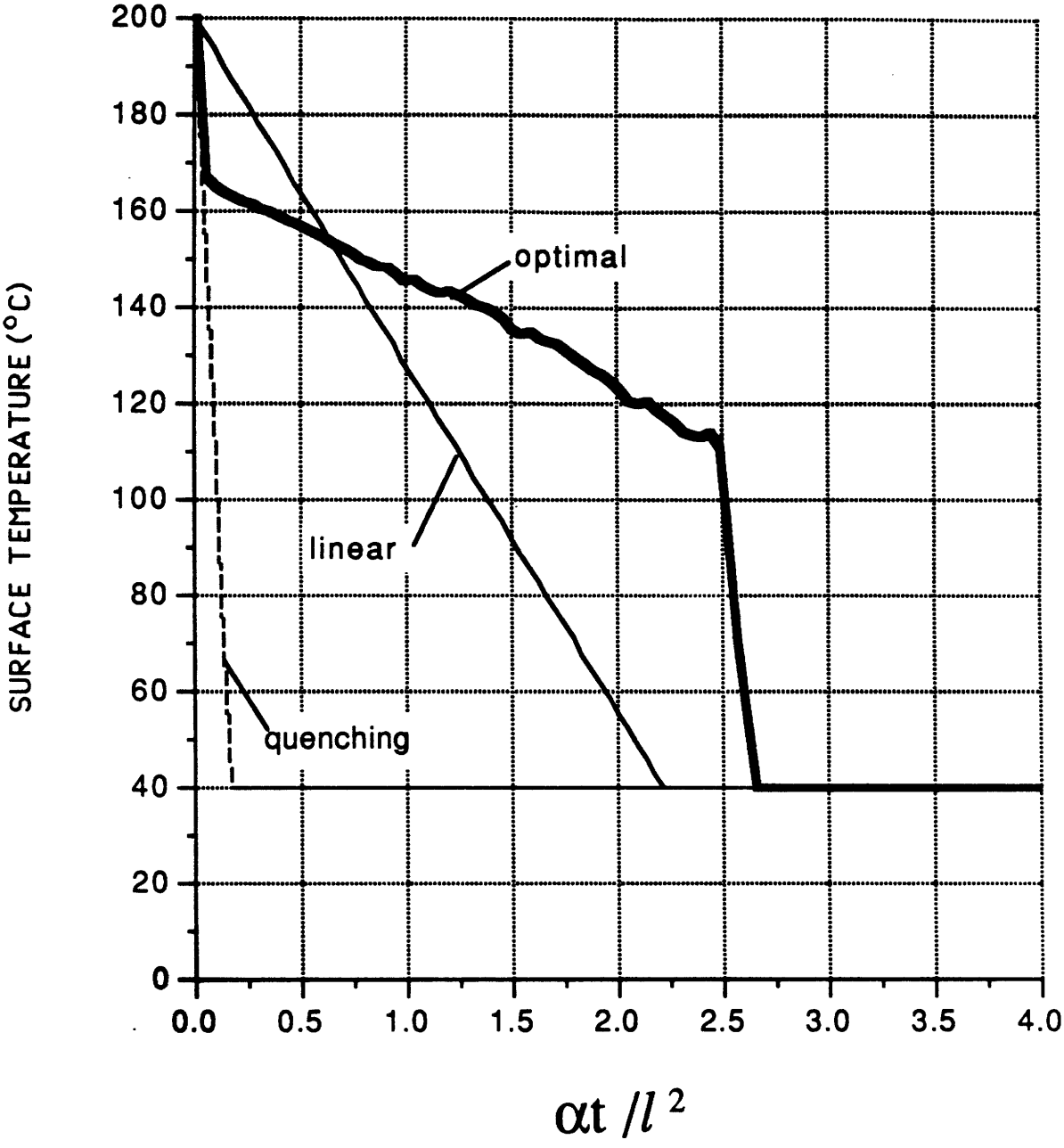

Figure 4-16: Temperature Profiles of Quenching, Linear and Optimal Coolings for Minimum Entire Stress Field.

cycle for maximum stress relaxation.

Gurtin and Murphy [9] studied the interface residual stresses of a fiber-reinforced viscoelastic plate which was cooled from cure temperature to room temperature. The differential coefficients of thermal expansion between the matrix and fibers create the interface residual stresses. They assumed uniform temperature in the reinforced part and derived an optimal cooling path for minimum residual stresses at the interface between the fibers and the matrix. The matrix was assumed to be a viscoelastic material while the fibers were assumed not to deform. The residual stress at time t_f is given by

$$\sigma(t_f) = -\int_0^{t_f} G(\xi(t))\,\dot{\theta}(t)\,dt, \tag{4.68}$$

where

$$\xi(t) = \int_t^{t_f} \phi(\theta(s))\,ds,$$

$$G = 2\left(\frac{1+\nu}{1-\nu}\right)(\alpha_m - \alpha_f)\,G_1,$$

$\theta(t) = temperature,$

$\nu = Poisson\ ratio\ of\ matrix,$

$G_1 = shear\ relaxation\ function\ of\ matrix,$

$\alpha_m = coefficient\ of\ thermal\ expansion\ of\ matrix,$

$\alpha_f = coefficient\ of\ thermal\ expansion\ of\ fiber.$

This equation and the method of variational calculus were then used to obtain an optimal temperature path [9], which is given by,

$$\dot{\theta}(t) = \frac{G''(\xi(t))\,\phi(\theta(t))^2\,\phi'(\theta(t))}{G'(\xi(t))\,[2\,\phi'(\theta(t))^2 - \phi(\theta(t))\,\phi''(\theta(t))]}, \tag{4.69}$$

with an initial discontinuity given by

$$\theta_o - \theta(0) = \frac{\phi(\theta(0))}{\phi'(\theta(0))}, \tag{4.70}$$

where

θ_o = *initial temperature,*

$\theta(0)$ = *temperature at* $t = 0$.

Equation (4.68) is similar to equation (4.61) in the sense that the integrands are the product of $\dot{\theta}$ and a relaxation function. By assuming simple exponential forms for the function of shift factor ϕ and the relaxation function, the analytical solutions (equations (4.69) and (4.70)) may be used to verify the solution (Figure 4-14) obtained from the numerical iterations.

By comparing equations (4.61) and (4.68), G and ϕ can take the following exponential forms

$$G(\xi) = 3\,\alpha_o\,R(\xi) = 3{\cdot}10^5 \cdot \exp(-\xi/2.24{\cdot}10^5),$$

$$\phi(\theta) = \begin{cases} \exp(0.1533\,(\theta - \theta_g)), & \theta \geq \theta_g, \\ 1, & \theta < \theta_g \end{cases} \tag{4.71}$$

where

$$\xi(t) = \int_t^t f\,\phi(\theta(s))\,ds,$$

θ_g = *glass transition temperature.*

Substituting G and ϕ into equations (4.69) and (4.70) gives

$$\dot{\theta} = \frac{-\exp(0.1533(\theta - \theta_g))}{2.24 \cdot 10^5 \cdot 0.1533},$$

$$\theta_o - \theta(0) = 6.5. \tag{4.72}$$

Solving the first order differential equation gives

$$\theta = \theta_g - \frac{1}{0.1533} \ln\left(\frac{t}{2.24 \cdot 10^5} + \exp(-0.1533(\theta(0) - \theta_g))\right). \tag{4.73}$$

The optimal temperature path given by equation (4.73) is plotted in Figure 4-17. At the same time, using these exponential forms of R and ϕ in the optimal cooling of the bounded plate, the optimal temperature profile from the first gradient algorithm is obtained and also shown in Figure 4-17. By comparing these two curves, the solution from the first gradient algorithm is verified.

The surface temperature of the bounded plate jumps to the final temperature well before the final time to allow the temperature inside the plate to reach the final temperature at the end of the cooling period. This is because a temperature gradient is considered in the bounded plate while the reinforced plate [9] assumes uniform temperature in the plate.

4.4 Summary

The objective of this study was to find an optimal thermal history within a specified time period for minimizing residual thermal stresses in the cooling processes of viscoelastic materials.

The development of the thermal stresses caused by the temperature gradient

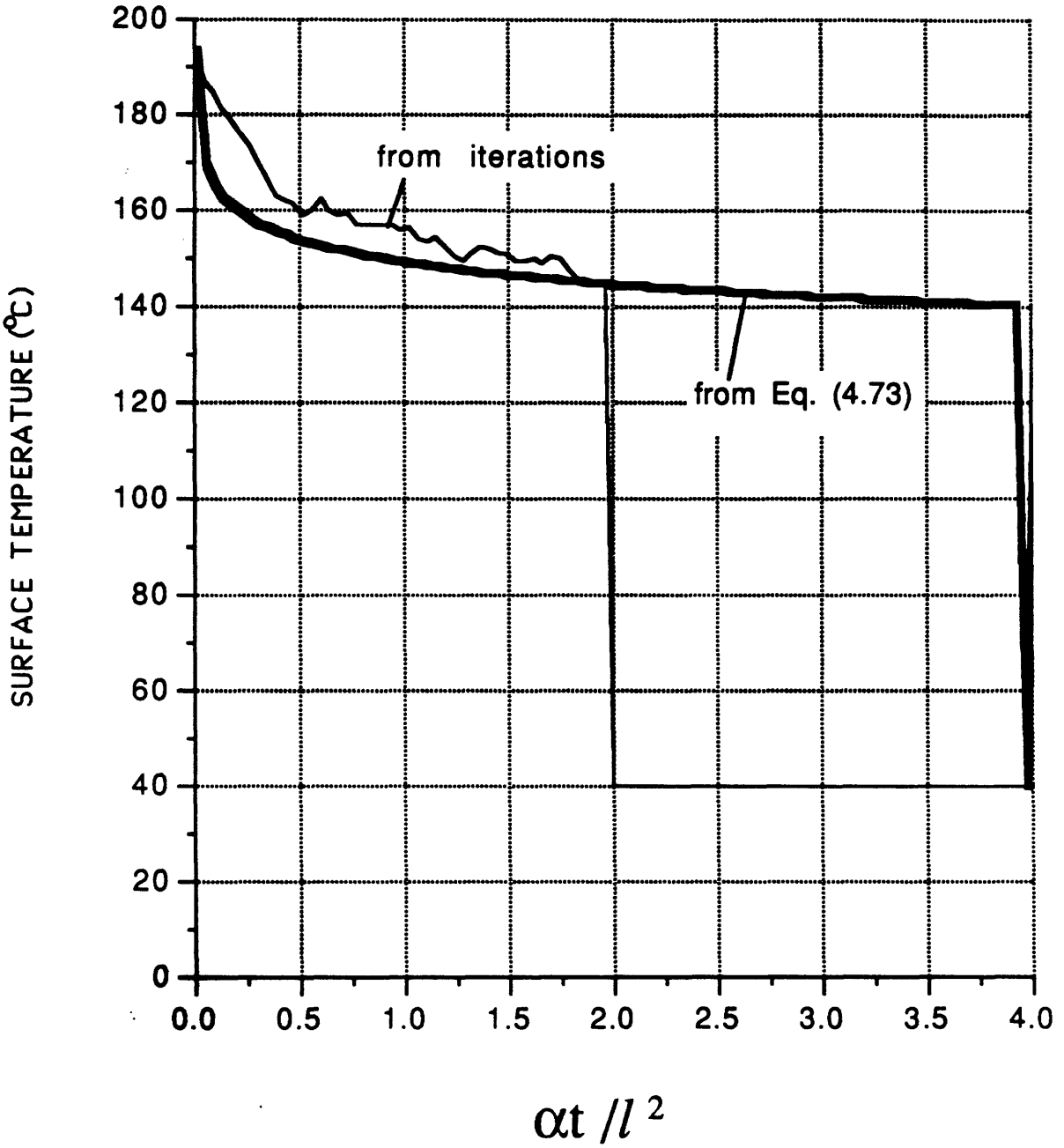

Figure 4-17: Optimal Temperature Profiles Given by equation (4.73) and First Gradient Algorithm.

during the cooling was first analyzed. The temperature gradient developed during the cooling results in differential thermal contraction and stress relaxation, which consequently lead to the thermal stresses in the parts.

Both free and bounded plates with temperature gradients across their thicknesses were investigated. The surface temperature of each plate was chosen as the control variable. The node temperatures across the thickness represented the state variables. Since the magnitude of the stress was minimized, the square of the stress at the location of minimization was defined as the performance measure *J*. Euler-Lagrange equations were solved with first gradient numerical iteration to obtain the optimal cooling profile.

The optimal cooling profile of a free plate shows a short period of surface reheating near the end of the cooling if the surface stress is minimized. The physical meaning of the surface reheating has also been interpreted. The optimal cooling profile changes when the target of minimization is varied. This path is initial-guess dependent. If a different initial guess of surface temperature profile is chosen, the optimal temperature path obtained from the numerical iteration will be different.

Many local minimums exist in this particular optimal control problem and nearly every minimum can reduce the surface stress significantly. This is because the plate is free to contract during the cooing process. There is no mechanical constraint on its edges and the target of minimization is the stress magnitude at one point across the thickness only. In general, the characteristics of the optimal cooling path for minimizing the surface stress of a free plate presents a short period of surface reheating.

The optimal cooling profile for minimizing the entire stress field rather than the stress at a given point in the free plate should also be investigated. In this

case, the optimal cooling profile for minimizing the entire stress field would be the superposition of the optimal profile for minimizing the stress at every point across the plate.

In order to obtain a smooth profile from superposition, the number of nodes across the thickness should be substantially increased and the time step should be decreased. However, the computing time to determine H_u is increased by orders of magnitude due to the multiple integrals in H_u and the newly-defined performance measure J. This study is left as the future work using much faster computing machine.

The optimal cooling profile of a bounded plate presents an initial rapid cooling followed by a slower cooling for most of the cooling period. The surface temperature stays on the optimal cooling path until the time that the surface temperature has to drop to the final temperature so that the temperature inside the plate can reach the final temperature at the final time. Although the final temperature jump would produce stress on the surface that cannot relax, the total stress is still a minimum. A physical interpretation of the optimal cooling profile has also been given.

The optimal cooling profile for minimizing the entire stress field across the thickness, rather than the stress at a given point, was also investigated. The summation of the stress at every node across the thickness is defined as the performance measure J. The initial jump of the surface temperature is larger in this case than the profile of minimizing surface stress in order for the average temperature across the thickness to follow the profile of minimizing surface stress because the entire stress field is minimized.

The analytical expression of residual thermal stress between the fiber and the matrix in fiber-reinforced composite is similar to that of the bounded plate if the

fibers are assumed rigid. Therefore, the optimal cooling profile of the composite for minimum residual stresses at the interface could also be given by the solution of the bounded plate.

Chapter 5

Conclusions and Recommendations

5.1 Conclusions

Two approaches have been studied in this thesis to minimize the residual stresses in molded parts through optimization of the thermal history of the process.

The first approach is to apply a passive insulation layer with low thermal inertia on the cavity surface to decouple the processes of material flow and cooling. The passive insulation layer prevents the polymer melt from freezing during filling of the mold and allows the flow-induced stresses to relax after filling. The cavity surface attains high temperature during filling and subsequently cools down to low temperature due to heat transfer to the mold. The layer provides a hot cavity surface during the filling and a cold cavity surface during the cooling. This allows the flow-induced stresses to relax immediately after the filling and the injected polymer in the cavity to quickly solidify and be ejected from the mold.

Two simple criteria for the optimal thermal properties and required thickness of the layer have also been presented. The first criterion tells us that the smaller the value of $k\rho c$ of the layer, the higher is the interface temperature. The second criterion allows us to calculate the required minimum thickness for the layer so that the flow-induced stress can relax after the filling and the increase of subsequent cooling time is kept to a minimum.

In addition to the required thermal properties and thickness for the layer, the materials used for the layer should also satisfy the requirements of good wear resistance, high melting point, good bonding strength to the cavity and smooth surface finish. A material for the layer which meets all these requirements and

have low $k\rho c$ is yet to be developed.

A numerical simulation model for the molding cycle has also been developed in order to understand the process and evaluate this approach. This model utilized the Leonov constitutive equation to account for the time- and temperature-dependent stress relaxation. The results show that the stresses inside the parts relax completely while those near the surface relax only partially or not at all. Most of the relaxation occurs in the first half second after the filling when the polymer is still at a relatively high temperature. The maximum stresses exist not on the surface but near the surface. This is due to the fact that the frozen layer on the surface does not accumulate any more strain during the filling, since the strain rate is zero in the frozen layer.

By comparing the results from coated and uncoated cavities, the insulation layer raises the cavity temperature during the filling, and subsequently allows the flow-induced stresses to relax immediately after the filling. Both simulation and experimental results show that the final stresses in the molded parts are reduced by at least 40% with the use of insulation layer. The cooling time is increased by less than 20 % and the total cycle time should be increased by a smaller percentage. The required injection pressure is also reduced because the polymer has a higher temperature and therefore a lower viscosity during the filling. A smaller injection molding machine can be used to inject the same shot size.

A typical molding process includes a material flow and a cooling process. The parts start to cool before the process of material flow is completed. The technique presented in this thesis decouples the processes of material flow and cooling in order to relax the flow-induced stresses after the flow.

This idea can be applied to not only the injection molding process but also all the molding processes, including the molding of metals. Its effects are particularly

significant in the molding of metals because the values of $k\rho c$ for metals are much larger than those of polymers. An insulation layer like ceramic can easily raise the interface temperature to a higher level if metals are to be molded instead of polymers.

The second approach, an active control of the surface temperature, is to find an optimal thermal history within a specified time period for minimizing residual thermal stresses in viscoelastic materials. This technique can be applied to the annealing process of large structural molded parts as well as the molding of fiber-reinforced polymeric composites. The annealing process is usually necessary to reduce the flow-induced and thermally-induced stresses which result from the molding process. However, the annealing process itself would also create thermally-induced stresses in the parts because of the temperature gradient during the cooling process.

The temperature gradient leads to differential thermal contraction and relaxation, which subsequently results in residual thermal stresses in the parts. Therefore, the annealing process should be very slow, usually taking days, in order to reduce the temperature gradient and have a uniform cooling. As a result, an optimal cooling profile within a specified time period for minimum residual thermal stresses is critical to both quality and productivity of the molded parts.

Plates with and without mechanical constraints on their edges were investigated. The surface temperature of the plate was chosen as the control variable and temperature gradient inside the plate was considered. Euler-Lagrange equations were solved with first gradient algorithm to iterate the solutions. The optimal cooling profile of a free plate shows a short period of surface reheating near the end of the cooling if the surface stress is minimized. The physical meaning of the surface reheating has also been presented. The optimal cooling profile changes when the target of minimization is varied. This path is initial-guess

dependent. If a different initial guess of surface temperature profile is chosen, the optimal temperature path obtained from the numerical iteration will be different.

Many local minimums exist in this particular optimal control problem and nearly every minimum can reduce the surface stress significantly. This occurs because the plate is free to contract during the cooling process. No mechanical constraint exists on its edges, and the target of minimization is the stress magnitude at one point across the thickness only. In general, the characteristics of the optimal cooling path for minimizing the surface stress of a free plate presents a short period of surface reheating.

The optimal cooling profile for minimizing the entire stress field rather than the stress at a given point should also be investigated. However, the computing time in determining H_u is increased by orders of magnitude due to the multiple integrals involved in H_u and the newly-defined performance measure J. This study is left as the future work using much faster computing machine.

The optimal cooling profile of a bounded plate presents an initial rapid cooling followed by a slower cooling for most of the cooling period. The surface temperature stays on this path until the time that it has to drop to the final temperature so that the temperature inside the plate can reach the final temperature at the final time. Although the final temperature jump produces stress that cannot relax, the total stress is still a minimum. A physical interpretation of the optimal cooling profile has also been given.

The optimal cooling profile for minimizing the entire stress field across the thickness of the bounded plate, rather than the stress at a given point, was also investigated. The summation of the stress at every node across the thickness is defined as the performance measure J. The initial jump of the surface temperature is larger in this case than the profile of minimizing surface stress in order for the

average temperature across the thickness to follow the profile of minimizing surface stress because the entire stress field is minimized.

The analytical expression of residual thermal stress between the fiber and the matrix in fiber-reinforced composite is similar to that of the bounded plate if the fibers are assumed rigid. Therefore, the optimal cooling profile of the composite for minimum residual stresses at the interface is also given by the solution of the bounded plate.

5.2 Recommendations

1. Materials for the insulation layer on the cavity surface need to be developed.

2. Fountain flow (elongational flow) should also be considered in the model in addition to shear flow.

3. The stresses due to packing and cooling should be included in the simulation of the molding cycle.

4. Minimizing the entire stress field in the free plate, i.e. the integration of stress magnitude across the thickness, should also be investigated.

5. The optimal thermal history in the whole injection molding cycle should be determined using the low thermal inertia mold.

6. The optimal temperature profile should be verified by experiments.

References

[1] Aggarwala, B.D. and Saibel, E.
Tempering Stresses in an Infinite Glass Plate.
Phys. Chem. Glasses 2(5):137-140, 1961.

[2] Bathe, K.J.
Finite Element Procedures in Engineering Analysis.
Prentice-Hall, Inc., 1982.

[3] Bryson, A.E. and Denham, W.F.
A Steepest-Ascent Method for Solving Optimum Programming Problems.
Journal of Applied Mechanics :247-257, June, 1962.

[4] Chung, T. S. and Ryan, M. E.
Analysis of the Packing Stage in Injection Molding.
Polymer Engineering and Science 21(5):271-275, 1981.

[5] Wang, K.K., et al.
Computer Aided Injection Molding System.
Technical Report 2-10, Cornell Injection Molding Program, 1974-1983.

[6] Dietz, W., White, J. L. and Clark, E. S.
Orientation Development and Relaxation in Injection Molding of Amorphous Polymers.
Polymer Engineering and Science 18(4):273-281, 1978.

[7] Greener, J.
Generalized Criteria for Packing in Injection Molding.
SPE 43th ANTEC :822-825, 1985.

[8] Greener, J. and Pearson, G. H.
Orientation Residual Stresses and Birefringence in Injection Molding.
Journal of Rheology 27(2):115-134, 1983.

[9] Gurtin, M.E. and Murphy, L.F.
On Optimal Temperature Paths for Thermorheologically Simple Viscoelastic Materials.
Quarterly of Applied Mathematics :179-189, 1980.

[10] Harry, D. H. and Parrott, R. G.
Numerical Simulation of Injection Mold Filling.
Polymer Engineering and Science 10(4):209-214, 1970.

[11] Hertzberg, R.W.
Deformation and Fracture Mechanics of Engineering Materials.
John Wiley & Sons, .

[12] Holman, J.P.
Heat Transfer.
McGraw-Hill, Inc., 1976.

[13] Isayev, A.I.
Orientation Development in the Injection Molding of Amorphous Polymers.
Polymer Engineering and Science 23(5):271-284, 1983.

[14] Isayev, A.I. and Hieber, C.A.
Toward a Viscoelastic Modelling of the Injection Molding of Polymers.
Rheol. Acta 19:168-182, 1980.

[15] John, L. I.
Strain-Free Injection Molding.
Modern Plastics 40:111, 1963.

[16] Kamal, M. R. and Kenig, S.
The Injection Molding of Thermoplastics, Part I: Theoretical Model.
Polymer Engineering and Science 12(4):294-301, 1972.

[17] Kim, B.H.
Low Thermal Inertia Injection Molding.
PhD thesis, Massachusetts Institute of Technology, 1983.

[18] Kim, S.G.
Knowledge-Based Synthesis System for Injection Molding.
PhD thesis, Massachusetts Institute of Technology, 1985.

[19] Kuo, Y. and Kamal, M.R.
Flows of Thermoplastics in the Filling and Packing Stages of Injection Molding.
In *Proceedings of International Conference on Polymer Processing.* MIT, Cambridge, MA., August, 1977.

[20] Leonov, A.I., Lipkina,E.H., Paskhin, E.D. and Prokunin, A.N.
Theoretical and Experimental Investigation of Shearing in Elastic Polymer Liquids.
Rheol. Acta 15:411-426, 1976.

[21] Leonov, A.I.
Nonequilibrium Thermodynamics and Rheology of Viscoelastic Polymer Media.
Rheol. Acta 15:85-98, 1976.

[22] Lee, E.H. and Rogers, T.G.
Solution of Viscoelastic Stress Analysis Problems Using Measured Creep or Relaxation Functions.
Journal of Applied Mechanics :127-133, 1963.

[23] Lee, E.H., Rogers, T.G. and Woo, T.C.
Residual Stresses in a Glass Plate Cooled Symmetrically from Both Surfaces.
Journal of The American Ceramic Society 48(9):480-487, 1965.

[24] Acierno, D., La Mantia, F. P., Marrucci, G. and Titomanlio, G.
A Non-Linear Viscoelastic Model with Structure-Dependent Relaxation Times.
J. of Non-Newtonian Fluid Mechanics 1:125-146, 1976.

[25] Menges, G. and Wubken, G.
Influence of Processing Conditions on Molecular Orientation in Injection Moldings.
SPE 31st ANTEC' , 1973.

[26] Morland, L.W. and Lee, E.H.
Stress Analysis for Linear Viscoelastic Materials with Temperature Variation.
Trans. Soc. Rheol. 4:233, 1960.

[27] Muki, R. and Sternberg, E.
On Transient Thermal Stresses in Viscoelastic Materials with Temperature Dependent Properties.
Journal of Applied Mechanics 28:193, 1961.

[28] Narayanaswamy, O.S. and Gardon, R.
Calculation of Residual Stresses in Glass.
Journal of The American Ceramic Society 52(10):554-558, 1970.

[29] Oda, K., White, J. L. and Clark E. S.
Influence of Melt Deformation History on Orientation in Vitrified Polymers.
Polymer Engineering and Science 18(1):53-59, 1978.

[30] Rubin, I.I.
Injection Molding of Plastics.
John Wiley and Sons, Inc., 1973.

[31] Schwarzl, F. and Staverman, A.J.
Time-Temperature Dependence of Linear Viscoelastic Behavior.
Journal of Applied Physics 23(8):838-843, 1952.

[32] Siegmann, A., Buchman, A. and Kenig, S.
Residual Stresses in Polymers III: The Influence of Injection-Molding Process Conditions.
Polymer Engineering and Science 22(9):560-568, 1982.

[33] Tadmor, Z.
Molecular Orientation in Injection Molding.
Journal of Applied Polymer Science 18:1753-1772, 1974.

[34] White, J. L. and Dietz, W.
Some Relationships Between Injection Molding Conditions and the Characteristics of Vitrified Molded Parts.
Polymer Engineering and Science 19(15):1081-1091, 1979.

[35] White, J.
Fluid Mechanical Analysis of Injection Mold Filling.
Polymer Engineering and Science 15(1), 1975.

[36] Williams, M.L., Landel, R.F. and Ferry, J.D.
The Temperature Dependence of Relaxation Mechanisms in Amorphous Polymers and Other Glass-forming Liquids.
Journal of American Chemical Society 77:3701, 1955.

[37] Wu, P.C., Huang, C.F. and Gogos, C.G.
Simulation of the Mold Filling Process.
Polymer Engineering and Science 14(3), 1974.

Appendix A
Derivation of H_u, G_x and G_u

Equation (4.42) is rewritten as

$$J = \{ \int_0^{t_f} 3\, R(\xi(z_o,t))\, [\dot{\epsilon}(t) - \alpha_o\, \dot{\theta}(z_o,t)]\, dt \}^2, \tag{A.1}$$

where

$$\xi(z,t) = \int_t^{t_f} \phi(\theta(z,s))\, ds. \tag{A.2}$$

$$\theta(z_o,t) = \int_0^t \theta_w(\lambda) \frac{\partial}{\partial \lambda} f(z_o,t-\lambda)\, d\lambda, \tag{A.3}$$

$$\dot{\theta}(z_o,t) = \int_0^t \theta_w(\lambda) \frac{\partial^2}{\partial t \partial \lambda} f(z_o,t-\lambda)\, d\lambda - f(z_o,0)\, \theta_w(t), \tag{A.4}$$

$$\dot{\epsilon}(t) = \frac{\alpha_o \int_0^l R(\xi(z,t))\, \dot{\theta}(z,t)\, dz}{\int_0^l R(\xi(z,t))\, dz}. \tag{A.5}$$

The first variation of equation (A.1) gives

$$\delta J = -6\sigma\alpha_o \int_0^{t_f} \{R(\xi(z_o,t)) \cdot \tag{A.6}$$

$$\left[\int_0^t \frac{\partial^2}{\partial t \partial \lambda} f(z_o, t-\lambda)\, \delta\theta_w(\lambda)\, d\lambda - f(z_o,0)\, \delta\theta_w(t)\right]$$

$$+ \dot{\theta}(z_o,t)\, R'(\xi(z_o,t)) \cdot$$

$$\int_t^{t_f} \phi'(\theta(z_o,s)) \int_0^s \frac{\partial}{\partial \lambda} f(z_o, s-\lambda)\, \delta\theta_w(\lambda)\, d\lambda\, ds\}\, dt$$

$$+ 6\sigma \int_0^{t_f} R'(\xi(z_o,t)) \int_t^{t_f} \phi'(\theta(z_o,\lambda))\, \delta\theta_w(\lambda)\, d\lambda\, \dot{\epsilon}(t)\, dt$$

$$+ 6\sigma\alpha_o \int_0^{t_f} \frac{R(\xi(z_o,t))}{\left(\int_0^l R(\xi(z,t))\, dz\right)^2} \cdot$$

$$\{\left[\int_0^l R(\xi(z,t))\, dz\right] \cdot$$

$$\left[\int_0^l R'(\xi(z,t)) \int_t^{t_f} \phi'(\theta(z,s)) \int_0^s \frac{\partial}{\partial \lambda} f(z, s-\lambda)\, \delta\theta_w(\lambda)\, d\lambda\, ds\ \dot{\theta}(z,t)\, dz\right.$$

$$\left. + \int_0^l R(\xi(z,t)) \left(\int_0^t \frac{\partial^2}{\partial t \partial \lambda} f(z, t-\lambda)\, \delta\theta_w(\lambda)\, d\lambda - f(z,0)\, \delta\theta_w(t)\right) dz\right]$$

$$- \left[\int_0^l R(\xi(z,t))\, \dot{\theta}(z,t)\, dz\right] \cdot$$

$$\left[\int_0^l R'(\xi(z,t)) \int_t^{t_f} \phi'(\theta(z,s)) \int_0^s \frac{\partial}{\partial \lambda} f(z, s-\lambda)\, \delta\theta_w(\lambda)\, d\lambda\, ds\, dz\right]\}\, dt$$

In order to have a form like

$$\delta J = 2\sigma \int_0^{t_f} H_u\, \delta\theta_w\, dt, \tag{A.7}$$

$\delta\theta_w$ in equation (A.6) should be relocated outside some of the integrals. This can be

demonstrated with one of the most complicated terms

$$6\,\sigma\,\alpha_o \int_0^{t_f} \frac{R(\xi(z_o,t))}{\int_0^l R(\xi(z,t))\,dz} \int_0^l R'(\xi(z,t)) \int_t^{t_f} \phi'(\theta(z,s)) \int_0^s \frac{\partial}{\partial\lambda} f(z,s-\lambda)\,\delta\theta_w(\lambda)\,d\lambda\,ds\;\dot{\theta}(z,t)\,dz\,dt. \tag{A.8}$$

It can also be written as

$$6\,\sigma\,\alpha_o \int_0^l \int_0^{t_f} \frac{R(\xi(z_o,t))\,R'(\xi(z,t))\,\dot{\theta}(z,t)}{\int_0^l R(\xi(z,t))\,dz} \int_t^{t_f} \phi'(\theta(z,s)) \int_0^s \frac{\partial}{\partial\lambda} f(z,s-\lambda)\,\delta\theta_w(\lambda)\,d\lambda\,ds\,dt\,dz. \tag{A.9}$$

If we let

$$A(z,t) = \frac{R(\xi(z_o,t))\,R'(\xi(z,t))\,\dot{\theta}(z,t)}{\int_0^l R(\xi(z,t))\,dz}, \tag{A.10}$$

$A(z,t)$ can then be expressed as

$$A(z,t) = \int_0^t \frac{R(\xi(z_o,s))\,R'(\xi(z,s))\,\dot{\theta}(z,s)}{\int_0^l R(\xi(z,s))\,dz}\,ds. \tag{A.11}$$

Integrating (A.9) by parts gives

$$6\,\sigma\,\alpha_o \int_0^l \Big\{ \Big[A(z,t) \int_t^{t_f} \phi'(\theta(z,s)) \int_0^s \frac{\partial}{\partial\lambda} f(z,s-\lambda)\,\delta\theta_w(\lambda)\,d\lambda\,ds \Big]_0^{t_f} - \int_0^{t_f} A(z,t)\,(-\phi'(\theta(z,t))) \int_0^t \frac{\partial}{\partial\lambda} f(z,t-\lambda)\,\delta\theta_w(\lambda)\,d\lambda\,dt \Big\}\,dz. \tag{A.12}$$

The first term is clearly zero while the second term can be shown as

$$6\,\sigma\,\alpha_o \int_0^l \int_0^t f\, A(z,t)\,\phi'(\theta(z,t)) \int_0^t \sum_{n=1}^{\infty} f_{1n}(z,t)\, f_{2n}(\lambda)\cdot$$

$$\delta\theta_w(\lambda)\, d\lambda\, dt\, dz, \quad n = 1, 3, 5, \cdots \tag{A.13}$$

where

$$\frac{\partial}{\partial\lambda} f(z,t-\lambda) = \sum_{n=1}^{\infty} f_{1n}(z,t)\, f_{2n}(\lambda), \quad n = 1, 3, 5, \cdots$$

$$f_{1n}(z,t) = \frac{\alpha\pi n}{l^2} \exp\left(-\left(\frac{n\pi}{2l}\right)^2 \alpha\, t\right) \sin\left(\frac{n\pi z}{2l}\right), \tag{A.14}$$

$$f_{2n}(\lambda) = \exp\left(\left(\frac{n\pi}{2l}\right)^2 \alpha\,\lambda\right).$$

Equation (A.14) was derived from equation (4.22). Equation (A.13) can also be rearranged as

$$6\,\sigma\,\alpha_o \int_0^l \sum_{n=1}^{\infty} \int_0^t f\, A(z,t)\,\phi'(\theta(z,t))\, f_{1n}(z,t) \int_0^t f_{2n}(\lambda)\cdot$$

$$\delta\theta_w(\lambda)\, d\lambda\, dt\, dz, \quad n = 1, 3, 5, \cdots \tag{A.15}$$

Again, let

$$B_n(z,t) = A(z,t)\,\phi'(\theta(z,t))\, f_{1n}(z,t), \tag{A.16}$$

then

$$B_n(z,t) = \int_t^{t_f} - A(z,\lambda)\,\phi'(\theta(z,\lambda))\,f_{1n}(z,\lambda)\,d\lambda. \tag{A.17}$$

Integration by parts of (A.15) also gives

$$6\,\sigma\,\alpha_o \int_0^l \sum_{n=1}^{\infty} \{\,[B_n(z,t) \int_0^t f_{2n}(\lambda)\,\delta\theta_w(\lambda)\,d\lambda\,]_0^{t_f}$$

$$- \int_0^{t_f} B_n(z,t)\,f_{2n}(t)\,\delta\theta_w(t)\,dt\,\}\,dz, \quad n = 1, 3, 5, \cdots \tag{A.18}$$

Again, it is obvious that the first term is zero. Substituting $B_n(z,t)$ in (A.18) by equations (A.17) and (A.11) gives

$$6\,\sigma\,\alpha_o \int_0^l \sum_{n=1}^{\infty} \{- \int_0^{t_f} \int_t^{t_f} - \int_0^{\lambda} \frac{R(\xi(z_o,s))\,R'(\xi(z,s))\,\dot{\theta}(z,s)}{\int_0^l R(\xi(z,s))\,dz}\,ds \cdot$$

$$\phi'(\theta(z,\lambda))\,f_{1n}(z,\lambda)\,d\lambda\,f_{2n}(t)\,\delta\theta_w(t)\,dt\,\}\,dz, \quad n = 1, 3, 5, \cdots \tag{A.19}$$

Rearranging (A.19) results in

$$6\,\sigma\,\alpha_o \int_0^{t_f} \int_0^l \int_t^{t_f} \sum_{n=1}^{\infty} f_{1n}(z,\lambda)\,f_{2n}(t)\,\phi'(\theta(z,\lambda)) \int_0^{\lambda}$$

$$\frac{R(\xi(z_o,s))\,R'(\xi(z,s))\,\dot{\theta}(z,s)}{\int_0^l R(\xi(z,s))\,dz}\,ds\,d\lambda\,dz\,\delta\theta_w(t)\,dt, \quad n = 1, 3, 5, \cdots \tag{A.20}$$

which leads to

$$6\sigma\alpha_o \int_0^{t_f} \int_0^{l} \int_t^{t_f} -\frac{\partial}{\partial\lambda} f(z,\lambda-t)\,\phi'(\theta(z,\lambda)) \int_0^{\lambda} \frac{R(\xi(z_o,s))\,R'(\xi(z,s))\,\dot{\theta}(z,s)}{\int_0^{l} R(\xi(z,s))\,dz}\,ds\,d\lambda\,dz\,\delta\theta_w(t)\,dt. \tag{A.21}$$

With similar procedures applied to other terms, equation (A.6) can be expressed as

$$\delta J = \int_0^t 6\,\alpha_o\,\sigma\,\{\int_t^t \frac{\partial^2}{\partial\lambda^2} f(z_o,\lambda-t)\,R(\xi(z_o,\lambda))\,d\lambda \qquad (A.22)$$

$$+ R(\xi(z_o,t))f(z_o,0)$$

$$+ \int_t^t \frac{\partial}{\partial\lambda} f(z_o,\lambda-t)\,\phi'(\theta(z_o,\lambda))\int_0^\lambda R'(\xi(z_o,s))\,\dot{\theta}(z_o,s)\,ds\,d\lambda$$

$$+ \phi'(\theta(z_o,t))\int_0^t R'(\xi(z_o,\lambda))\frac{\dot{\epsilon}(\lambda)}{\alpha_o}\,d\lambda$$

$$- \int_0^l \int_t^t \frac{\partial}{\partial\lambda} f(z,\lambda-t)\,\phi'(\theta(z,\lambda))\cdot$$

$$\int_0^\lambda \frac{R(\xi(z_o,s))\,R'(\xi(z,s))\,\dot{\theta}(z,s)}{\int_0^l R(\xi(z,s))\,dz}\,ds\,d\lambda\,dz$$

$$- \int_0^l \int_t^t \frac{\partial^2}{\partial\lambda^2} f(z,\lambda-t)\frac{R(\xi(z_o,\lambda))\,R(\xi(z,\lambda))}{\int_0^l R(\xi(z,\lambda))\,dz}\,d\lambda\,dz$$

$$- R(\xi(z_o,t))\frac{\int_0^l R(\xi(z,t))\,f(z,0)\,dz}{\int_0^l R(\xi(z,t))\,dz}$$

$$+ \int_0^l \int_t^t \frac{\partial}{\partial\lambda} f(z,\lambda-t)\,\phi'(\theta(z,\lambda))\cdot$$

$$\int_0^\lambda \frac{R(\xi(z_o,s))\,R'(\xi(z,s))\,\dot{\epsilon}(s)}{\int_0^l R(\xi(z,s))\,dz\,\alpha_o}\,ds\,d\lambda\,dz\,\}\,\delta\theta_w\,dt.$$

H_u can then be easily obtained from the integrand of equation (A.22) as

$$H_u = 3\,\alpha_o \{ \int_t^{t_f} \frac{\partial^2}{\partial\lambda^2} f(z_o,\lambda-t)\, R(\xi(z_o,\lambda))\, d\lambda \qquad (A.23)$$

$$+ R(\xi(z_o,t))\, f(z_o,0)$$

$$+ \int_t^{t_f} \frac{\partial}{\partial\lambda} f(z_o,\lambda-t)\, \phi'(\theta(z_o,\lambda)) \int_0^{\lambda} R'(\xi(z_o,s))\, \dot{\theta}(z_o,s)\, ds\, d\lambda$$

$$+ \phi'(\theta(z_o,t)) \int_0^{t} R'(\xi(z_o,\lambda)) \frac{\dot{\epsilon}(\lambda)}{\alpha_o}\, d\lambda$$

$$- \int_0^{l} \int_t^{t_f} \frac{\partial}{\partial\lambda} f(z,\lambda-t)\, \phi'(\theta(z,\lambda)) \cdot$$

$$\int_0^{\lambda} \frac{R(\xi(z_o,s))\, R'(\xi(z,s))\, \dot{\theta}(z,s)}{\int_0^{l} R(\xi(z,s))\, dz}\, ds\, d\lambda\, dz$$

$$- \int_0^{l} \int_t^{t_f} \frac{\partial^2}{\partial\lambda^2} f(z,\lambda-t) \frac{R(\xi(z_o,\lambda))\, R(\xi(z,\lambda))}{\int_0^{l} R(\xi(z,\lambda))\, dz}\, d\lambda\, dz$$

$$- R(\xi(z_o,t)) \frac{\int_0^{l} R(\xi(z,t))\, \dot{f}(z,0)\, dz}{\int_0^{l} R(\xi(z,t))\, dz}$$

$$+ \int_0^{l} \int_t^{t_f} \frac{\partial}{\partial\lambda} f(z,\lambda-t)\, \phi'(\theta(z,\lambda)) \cdot$$

$$\int_0^{\lambda} \frac{R(\xi(z_o,s))\, R'(\xi(z,s))\, \dot{\epsilon}(s)}{\int_0^{l} R(\xi(z,s))\, dz\, \alpha_o}\, ds\, d\lambda\, dz \}.$$

To derive $\mathbf{G}_u$, equation (4.45) is rewritten here as

$$\mathbf{N} = \mathbf{N}(\theta(z,t_f))$$

$$+ \int_0^{t_f} \mathbf{Q}^T(z,t) \left[\int_0^t \theta_w(\lambda) \frac{\partial^2}{\partial t \partial \lambda} \mathbf{f}(z,t-\lambda)\, d\lambda \right.$$

$$\left. - \mathbf{f}(z,0)\, \theta_w(t) - \theta(z,t) \right] dt. \qquad (A.24)$$

Since $\mathbf{N}$ is a differentiable function, we can write

$$\mathbf{N} = \int_0^{t_f} \frac{d}{dt} \mathbf{N}(\theta(z,t))\, dt + \mathbf{N}(\theta(z,0))$$

$$+ \int_0^{t_f} \mathbf{Q}^T(z,t) \left[\int_0^t \theta_w(\lambda) \frac{\partial^2}{\partial t \partial \lambda} \mathbf{f}(z,t-\lambda)\, d\lambda \right.$$

$$\left. - \mathbf{f}(z,0)\, \theta_w(t) - \theta(z,t) \right] dt. \qquad (A.25)$$

The minimization does not affect $\mathbf{N}(\theta(z,0))$ because $\theta(z,0)$ is fixed. Therefore, we can exclude it from the functional. Applying the chain rule to $d\mathbf{N}/dt$ gives

$$\mathbf{N} = \int_0^{t_f} \left[\frac{d\mathbf{N}}{d\theta} \right]^T \theta(z,t)\, dt$$

$$+ \int_0^{t_f} \mathbf{Q}^T(z,t) \left[\int_0^t \theta_w(\lambda) \frac{\partial^2}{\partial t \partial \lambda} \mathbf{f}(z,t-\lambda)\, d\lambda \right.$$

$$\left. - \mathbf{f}(z,0)\, \theta_w(t) - \theta(z,t) \right] dt. \qquad (A.26)$$

The first variation of equation (A.26) gives

$$\delta\mathbf{N} = \int_0^{t_f} \left[\frac{d\mathbf{N}(\theta(z,t))}{d\theta(z,t)} - \mathbf{Q}(z,t) \right]^T \delta\theta(z,t)\, dt$$

$$+ \int_0^{t_f} \mathbf{Q}^T(z,t) \left[\int_0^t \frac{\partial^2}{\partial t \partial \lambda} \mathbf{f}(z,t-\lambda)\, \delta\theta_w(\lambda)\, d\lambda - \mathbf{f}(z,0)\, \delta\theta_w(t) \right] dt. \qquad (A.27)$$

Integrating the first term by parts gives

$$\delta\mathbf{N} = [\frac{d\mathbf{N}(\theta(z,t_f))}{d\theta(z,t_f)} - \mathbf{Q}(z,t_f)]^T \delta\theta(z,t_f)$$

$$+ \int_0^{t_f} \mathbf{Q}^T(z,t)\,\delta\theta(z,t)\,dt$$

$$+ \int_0^{t_f} \mathbf{Q}^T(z,t)\,[\int_0^t \frac{\partial^2}{\partial t\partial\lambda}\mathbf{f}(z,t-\lambda)\,\delta\theta_w(\lambda)\,d\lambda - \mathbf{f}(z,0)\,\delta\theta_w(t)]\,dt. \qquad (A.28)$$

Applying the same procedure as before to relocate $\delta\theta_w$ out of the integral $\int_0^t$ in the second term, one arrives at

$$\delta\mathbf{N} = [\frac{d\mathbf{N}(\theta(z,t_f))}{d\theta(z,t_f)} - \mathbf{Q}(z,t_f)]^T \delta\theta(z,t_f)$$

$$+ \int_0^{t_f} \mathbf{Q}^T(z,t)\,\delta\theta(z,t)\,dt$$

$$+ \int_0^{t_f} [-\mathbf{Q}^T(z,t)\,f(z,0) \qquad (A.29)$$

$$- \int_t^{t_f} \mathbf{Q}^T(z,\lambda)\frac{\partial^2}{\partial\lambda^2}\mathbf{f}(z,\lambda-t)\,d\lambda]\,\delta\theta_w(t)\,dt.$$

$\mathbf{G}_x$ and $\mathbf{G}_u$ can then be given as

$$\mathbf{G}_x = \mathbf{Q}^T(z,t), \qquad (A.30)$$

$$\mathbf{G}_u = -[\mathbf{Q}^T(z,t)\,f(z,0) + \int_t^{t_f} \mathbf{Q}^T(z,\lambda)\frac{\partial^2}{\partial\lambda^2}\mathbf{f}(z,\lambda-t)\,d\lambda]. \qquad (A.31)$$

Appendix B
Derivation of Interface Temperature

Consider two semi-infinite bodies that are initially at temperature T_i and 0 respectively. The two bodies are in contact at $t>0$. The temperature at the interface is to be analyzed.

The formulation of this problem is

$$\frac{\partial T_1}{\partial t} = \alpha_1 \frac{\partial^2 T_1}{\partial z^2},$$
$$\frac{\partial T_2}{\partial t} = \alpha_2 \frac{\partial^2 T_2}{\partial z^2}. \qquad (B.1)$$

$$where\ \alpha_1 = \frac{k_1}{\rho_1 c_1}, \quad \alpha_2 = \frac{k_2}{\rho_2 c_2}.$$

subject to the following boundary conditions.

$$T_1 = T_i \qquad at\ z = -\infty,$$
$$T_1 = T_2 \qquad at\ z = 0,$$
$$k_1 \frac{\partial T_1}{\partial z} = k_2 \frac{\partial T_2}{\partial z} \qquad at\ z = 0, \qquad (B.2)$$
$$T_2 = 0 \qquad at\ z = \infty.$$

We may write the Laplace transform of equation (B.1) in time

$$\frac{d^2T_1(s)}{dz^2} - q_1{}^2T_1(s) = -\frac{T_i}{\rho_1},$$

$$\frac{d^2T_2(s)}{dz^2} - q_2{}^2T_2(s) = 0, \tag{B.3}$$

$$\text{where } q_1{}^2 = \frac{s}{\alpha_1}, \quad q_2{}^2 = \frac{s}{\alpha_2},$$

and the transform of equation (B.2)

$$T_1(s) = \frac{T_i}{s} \qquad at\ z = -\infty,$$

$$T_1(s) = T_2(s) \qquad at\ z = 0,$$

$$k_1 \frac{dT_1(s)}{dz} = k_2 \frac{dT_2(s)}{dz} \qquad at\ z = 0, \tag{B.4}$$

$$T_2(s) = 0 \qquad at\ z = \infty.$$

The general solutions of equation (B.3), expressed in terms of exponentials are

$$T_1(s) = \frac{T_i}{\alpha_1} + A\ \exp(-q_1 z) + B\ \exp(q_1 z),$$

$$T_2(s) = C\ \exp(-q_2 z) + D\ \exp(q_2 z). \tag{B.5}$$

The constants A, B, C and D can be determined by considering equation (B.4).

$$A=0, \qquad B=\frac{T_i/s}{1+\left(\frac{(k\rho c)_1}{(k\rho c)_2}\right)^{1/2}},$$
$$C=\frac{T_i/s}{1+\left(\frac{(k\rho c)_2}{(k\rho c)_1}\right)^{1/2}}, \qquad D=0. \tag{B.6}$$

This leads to

$$T_2(s)=\frac{T_i}{1+\left(\frac{(k\rho c)_2}{(k\rho c)_1}\right)^{1/2}}\left(\frac{\exp(-q_2 z)}{s}\right). \tag{B.7}$$

Inversion of the Laplace transform allows us to arrive at

$$T_2=\frac{T_i}{1+\left(\frac{(k\rho c)_2}{(k\rho c)_1}\right)^{1/2}} erfc\left(\frac{z}{2\sqrt{\alpha_2 t}}\right). \tag{B.8}$$

The temperature at the interface is given by

$$(T_2)_{z=0}=\frac{T_i}{1+\left(\frac{(k\rho c)_2}{(k\rho c)_1}\right)^{1/2}}. \tag{B.9}$$

The temperature drop of body 1 at the interface is

$$(\Delta T_1)_{z=0}=T_i-(T_2)_{z=0}=\frac{T_i\left(\frac{(k\rho c)_2}{(k\rho c)_1}\right)^{1/2}}{1+\left(\frac{(k\rho c)_2}{(k\rho c)_1}\right)^{1/2}}. \tag{B.10}$$

Therefore, from equation (B.9) and (B.10),

$$\left(\frac{\Delta T_1}{T_2}\right)_{z=0}=\left(\frac{(k\rho c)_2}{(k\rho c)_1}\right)^{1/2}. \tag{B.11}$$

Appendix C
Temperature Dependence of Elastic Modulus of Rubber

This appendix demonstrates [11] that the elastic modulus of rubber should increase with increasing temperature by the laws of thermodynamics. The first law of thermodynamics gives

$$dU = dQ + dW. \tag{C.1}$$

where
dU = *change in internal energy,*
dQ = *change in heat absorbed or released,*
dW = *work done on the system.*

From the second law of thermodynamics, for a reversible process,

$$dQ = T \cdot dS, \tag{C.2}$$

where
T = *temperature,*
dS = *change in entropy.*

If an elastomeric rod of length l is extended by an amount dl due to a tensile load F, the work done on the rod is $F \cdot dl$. Therefore, equation (C.1) can be expressed as

$$dU = T \cdot dS + F \cdot dl. \tag{C.3}$$

At constant temperature, equation (C.3) can be rearranged as

$$F = \left(\frac{\partial U}{\partial l}\right)_T - T\left(\frac{\partial S}{\partial l}\right)_T \qquad (C.4)$$

where

$\left(\frac{\partial U}{\partial l}\right)_T$ = *change in strain energy,*

$\left(\frac{\partial S}{\partial l}\right)_T$ = *change in entropy.*

Since polymer chains prefer a random configuration, their unloaded degree of order is low and entropy is high. When a tensile force is applied, the entropy decreases as the chains become straightened and aligned. Therefore, $\left(\frac{\partial S}{\partial l}\right)_T$ is negative, which means the force F required to extend the rubber rod increases with increasing temperature T which can be seen from equation (C.4). This leads to the conclusion that the elastic modulus of rubber, or polymer in the rubbery state, increases with increasing temperature.